Transmission / Reflection and Short-Circuit Line Permittivity Measurements

James Baker-Jarvis

Electromagnetic Fields Division
Center for Electronics and Electrical Engineering
National Engineering Laboratory
National Institute of Standards and Technology
Boulder, Colorado 80303-3328

U.S. DEPARTMENT OF COMMERCE, Robert A. Mosbacher, Secretary
NATIONAL INSTITUTE OF STANDARDS AND TECHNOLOGY, John W. Lyons, Director
Issued July 1990

Contents

Contents(cont.)

Abstract

The transmission/reflection and short-circuit line methods for measuring complex permittivity are examined. Equations for permittivity are developed from first principles. New robust algorithms that eliminate the ill- behaved nature of the commonly used transmission/reflection method at frequencies corresponding to integral multiples of one-half wavelength in the sample are presented. These allow measurements to be made on samples of any length. An uncertainty analysis is presented which yields estimates of the errors incurred due to the uncertainty in scattering parameters, length measurement and reference plane position. The equations derived here indicate that the minimum uncertainty for transmission/reflection measurements of nonmagnetic materials occurs at integral multiples of one-half wavelength in the material. In addition, new equations for determining complex permittivity independent of reference plane position and sample length are derived. New equations are derived for permittivity determination using the short-circuit line allow positioning the sample arbitrarily in the sample holder.

Key words: calibration; coaxial line; dielectric constant; loss factor; microwave measurements; permeability measurement; permittivity measurement; reflection method; short- circuit; transmission; uncertainty; wave guide.

Chapter 1

Introduction

Broadband measurements of complex dielectric constants are required for a multitude of applications. Due to their relative simplicity, the transmission/reflection (TR) and short-circuit line (SCL) methods are presently widely used broadband measurement techniques. In these methods a sample is placed in a section of waveguide or coaxial line and the scattering parameters are measured, preferably by an automatic network analyzer [ANA]. The relevant scattering equations relate the measured scattering parameters to the permittivity and permeability of the material.

For the TR measurement method, the system of equations contains as variables the complex permittivity and permeability, the two reference plane positions, and, in some applications, the sample length. In the TR procedure we have more data at our disposal than in SCL measurements since we have all four of the scattering parameters. The system of equations is generally overdetermined and therefore can be solved in various ways.

In SCL measurements the variables are complex permittivity and permeability, sample length, distance from sample to short-circuit and reference plane positions. However, in most problems we know the sample length, reference plane position, and distance from short-circuit plane position to sample. In these cases we have four unknown quantities (complex permittivity and permeability) and therefore require four independent real equations to solve for these variables. These equations can be generated by taking reflection coefficient data at two positions in the transmission line, thus yielding the equivalent of four real equations for the four unknown quantities.

Measurements are said to have a high precision if there is a small random uncertainty, whereas measurements are said to have a high accuracy if the systematic uncertainty is small. Measurement uncertainty is a combination of the random and systematic errors. It is possible to correct for some systematic errors. The uncertainties and corrections of a set of measurements is of paramount importance. The uncertainties yield an estimate of the deviation of the mean of a set of sample measurements from the true value. The literature lacks a comprehensive summary of the uncertainties for the TR and SCL methods.

In addition there are corrections which can be made to measurements. For example, correction formulas exist that take into account the gap that exists around a sample in a waveguide. A summary of corrections is presented in this report.

With the advent of modern ANA systems there is generally no paucity of data, and thus efficient numerical algorithms for the reduction of the scattering data are of paramount importance. To accommodate modern ANA systems, Nicolson and Ross [1] and Weir [2] introduced procedures for obtaining broadband measurements, both in the time and frequency domains. In the Nicolson-Ross-Weir (NRW) procedure the equations for the scattering parameters are combined in such a fashion that the system of equations can be decoupled, so that this procedure yields an explicit equation for the permittivity and permeability as a function of the scattering parameters. This solution has formed the basis of the commonly used technique for obtaining permittivity and permeability from scattering measurements [3], [4], [5]. The compact form of these equations, while elegant, is not well-behaved for low-loss materials at frequencies corresponding to integral multiples of one-half wavelength in the sample. In fact the Nicolson-Ross-Weir equations are divergent, due to large phase uncertainties, for very low-loss materials at integral multiples of one-half wavelength in the material. Many researchers avoid this problem by measuring samples which are less than one-half wavelength in length at the highest measurement frequency. However, this approach, as shown later in the report, severely limits the viability of the TR method since short samples increase measurement uncertainty. Stuchly and Matuszewski [6] presented a slightly different derivation than Nicolson and Ross and obtained two explicit equations for the permittivity.

Ligthardt [7], in a detailed analysis, presented a method for determining permittivity by solving the scattering equations for the permittivity over

a calculated uncertainty region and then averaged the results. Ligthardt's equations are useful for high-loss materials, but for low-loss materials they suffer the same pathologies as the Nicolson-Ross [1], Weir [2], and Stuchly [6] equations at multiples of one-half wavelength. In this report I present a procedure for obtaining complex permittivity from the scattering equations which is stable over the frequency spectrum. This procedure minimizes instabilities in determination of permittivity by setting the permeability to unity. This new procedure thus allows measurements to be taken on samples of arbitrary length.

Another problem encountered is the transformation of S-parameter measurements at the calibration reference planes to the plane of the sample. This transformation requires knowledge of the position of the sample in the sample holder. However this information may be limited in many applications. The port extension and gating features of network analyzers are of some help in determining reference plane position, but does not completely solve the problem. Equations that are independent of reference plane positions are desirable. Also, equations that are independent of sample length are useful for high temperature applications. In the past other authors, for example, Altschuler [8], Harris [9], Scott [10], addressed the problem of either reference plane invariance or sample length invariance, but the problem of combined reference plane and sample length invariance remains to be resolved.

The goal of this report is threefold: first, to examine the scattering equations in detail for the TR and SCL methods and to present an improved method for solving the equations in an iterative fashion with application to permittivity measurements; second, to derive scattering equations that are invariant to the position of the reference planes and sample lengths; and third, to present an uncertainty analysis for this new solution.

Chapter 2

Transmission/Reflection Method

2.1 Theory

In the TR measurement, a sample is inserted into either a waveguide or coaxial line and the sample is subjected to an incident electromagnetic field [see figure 2.1]. The scattering equations are found from an analysis of the electric field at the sample interfaces. If we assume electric fields E_I, E_{II}, and, E_{III} in either the *TEM* mode in a coaxial line or the TE_{10} mode in a waveguide, (with a time dependence of $\exp(j\omega t)$) in the regions I, II, and III, we can write the spatial distribution of the electric field for an incident field normalized to 1:

$$E_I = \exp(-\gamma_o x) + C_1 \exp(\gamma_o x) \ , \tag{2.1}$$

$$E_{II} = C_2 \exp(-\gamma x) + C_3 \exp(\gamma x), \tag{2.2}$$

$$E_{III} = C_4 \exp(-\gamma_o x), \tag{2.3}$$

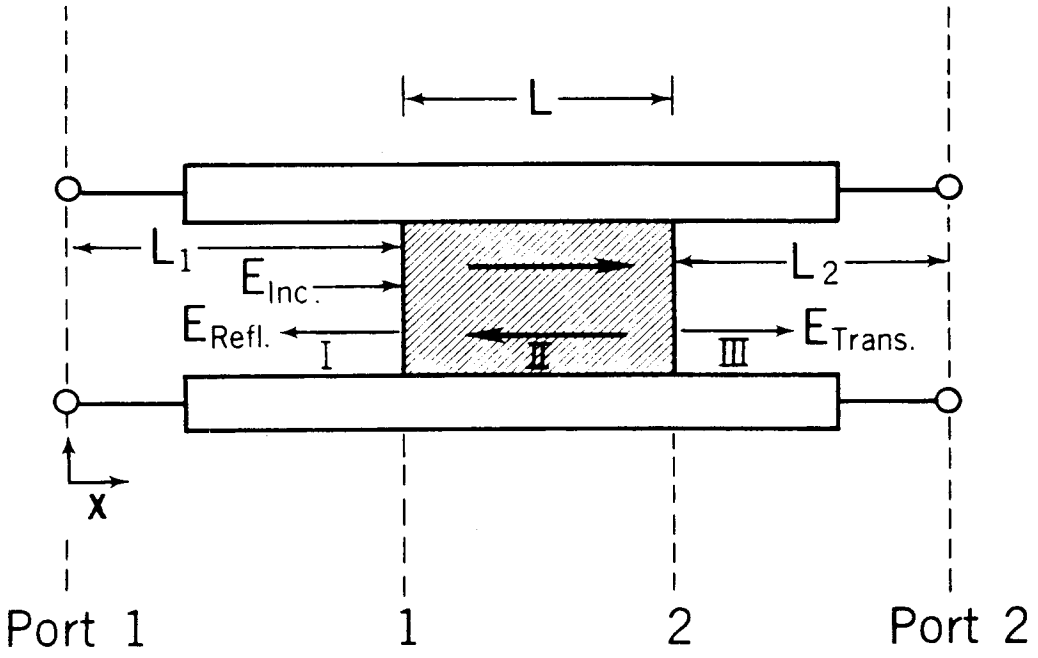

Figure 2.1: A dielectric sample in a transmission line and the incident(inc) and reflected (refl) electric field distributions in the regions I, II, and III. Port 1 and port 2 denote calibration reference plane positions.

where

$$\gamma = j\sqrt{\frac{\omega^2 \mu_R^* \epsilon_R^*}{c_{vac}^2} - \left(\frac{2\pi}{\lambda_c}\right)^2}, \tag{2.4}$$

$$\gamma_o = j\sqrt{\left(\frac{\omega}{c_{lab}}\right)^2 - \left(\frac{2\pi}{\lambda_c}\right)^2}, \tag{2.5}$$

$$\epsilon = [\epsilon_R' - j\epsilon_R'']\epsilon_o = \epsilon_R^* \epsilon_o, \tag{2.6}$$

$$\mu = [\mu_R' - j\mu_R'']\mu_o = \mu_R^* \mu_o. \tag{2.7}$$

Here $j = \sqrt{-1}$, c_{vac} and c_{lab} are the speed of light in vacuum and laboratory, ω is the angular frequency, λ_c is the cutoff wavelength, ϵ_o and μ_o are the permittivity and permeability of vacuum, ϵ_R^* and μ_R^* are the complex permittivity and permeability relative to a vacuum, and γ_o, γ are the propagation constants in vacuum and material respectively. The constants C_i are determined from the boundary conditions. The boundary condition on the electric field is the continuity of the tangential component at the interfaces. The tangential component can be calculated from Maxwell's equations given an electric field with only a radial component.

$$E_I(x = L_1) = E_{II}(x = L_1), \tag{2.8}$$

$$E_{II}(x = L_1 + L) = E_{III}(x = L_1 + L), \tag{2.9}$$

where $L_{air} = L_1 + L_2 + L$ is the length of the air line, L_1 and L_2 are the distances from the respective ports to sample faces, and L is the sample length. The boundary condition on the magnetic field requires the additional assumption that no surface currents are generated. If this condition holds, then the tangential component of the magnetic field is continuous across the interface. The tangential component can be calculated from Maxwell's equations for an electric field with only a radial component.

$$\frac{1}{\mu_o}\frac{\partial E_I}{\partial x}(x = L_1) = \frac{1}{\mu}\frac{\partial E_{II}}{\partial x}(x = L_1), \tag{2.10}$$

$$\frac{1}{\mu}\frac{\partial E_{II}}{\partial x}(x = L_1 + L) = \frac{1}{\mu_o}\frac{\partial E_{III}}{\partial x}(x = L_1 + L). \tag{2.11}$$

For a two-port device the expressions for the measured scattering parameters are obtained by solving eqs (2.1)– (2.3) subject to the boundary conditions. We assume that $S_{12} = S_{21}$. The explicit expressions are given by

$$S_{11} = R_1^2 \left[\frac{\Gamma(1-z^2)}{1-\Gamma^2 z^2} \right], \tag{2.12}$$

$$S_{22} = R_2^2 \left[\frac{\Gamma(1-z^2)}{1-\Gamma^2 z^2} \right], \tag{2.13}$$

$$S_{21} = R_1 R_2 \left[\frac{z(1-\Gamma^2)}{1-\Gamma^2 z^2} \right], \tag{2.14}$$

where

$$R_1 = \exp(-\gamma_o L_1), \tag{2.15}$$

$$R_2 = \exp(-\gamma_o L_2), \tag{2.16}$$

where L_1 and L_2 are the distances from the calibration reference planes to the sample ends, and R_1 and R_2 are the respective reference plane transformation expressions. Eqs (2.12)–(2.14) are not new and are derived in detail elsewhere [1], [11]. We also have an expression for z, the transmission coefficient,

$$z = \exp(-\gamma L). \tag{2.17}$$

We define the reflection coefficient by

$$\Gamma = \frac{\frac{\gamma_o}{\mu_o} - \frac{\gamma}{\mu}}{\frac{\gamma_o}{\mu_o} + \frac{\gamma}{\mu}}. \tag{2.18}$$

For coaxial line the cutoff frequency approaches 0, ($\omega_c \to 0$) and therefore Γ reduces to

$$\Gamma = \frac{\frac{c_{vac}}{c_{lab}} \sqrt{\frac{\mu_R^*}{\epsilon_R^*}} - 1}{\frac{c_{vac}}{c_{lab}} \sqrt{\frac{\mu_R^*}{\epsilon_R^*}} + 1}. \tag{2.19}$$

Additionally, S_{21} for the empty sample holder is

$$S_{21}^{o} = R_1 R_2 \exp(-\gamma_o L). \tag{2.20}$$

For nonmagnetic materials, eqs (2.12), (2.13), (2.14) contain ϵ_R', ϵ_R'', L, and the reference plane transformations R_1, R_2 as unknown quantities. Since the equations for S_{12} and S_{21} are equivalent for isotropic materials, we have four complex equations, eqs (2.12), (2.13), (2.14), (2.20), plus the equation for the length of the air line, or equivalently, nine real equations for the five unknowns. Additionally, in many applications we know the sample length. For magnetic materials we have seven unknowns. Thus, the system of equations is overdetermined, and it is possible to solve the equations in various combinations. As an example, in nonmagnetic materials if the position of the reference planes is not known accurately, then L_1 and L_2 can be eliminated from the equations to obtain equations that are reference plane invariant. A whole family of reference plane independent equations exists, but only the most useful are given below as examples:

$$|S_{11}| = \left| \frac{\Gamma(1 - z^2)}{1 - z^2\Gamma^2} \right|, \tag{2.21}$$

$$|S_{21}| = \left| \frac{z(1 - \Gamma^2)}{1 - z^2\Gamma^2} \right|, \tag{2.22}$$

$$\frac{S_{11}S_{22}}{S_{12}S_{21}} = \frac{(1 - \frac{\epsilon_R^*}{\mu_R^*})^2}{\frac{4\epsilon_R^*}{\mu_R^*}} \sinh^2 \gamma L, \tag{2.23}$$

$$\frac{S_{21}}{S_{21}^{o}} = \exp(\gamma_o L) \frac{z[1 - \Gamma^2]}{1 - z^2\Gamma^2}, \tag{2.24}$$

$$S_{21}S_{12} - S_{11}S_{22} = \exp[(-2\gamma_o)(L_{air} - L)] \frac{z^2 - \Gamma^2}{1 - z^2\Gamma^2}, \tag{2.25}$$

where the vertical bar denotes the magnitude of the complex expression. Equation (2.23) is valid only for coaxial line.

Nicolson and Ross [1], and Weir [2] combined the equations for S_{11} and S_{21} and discovered a formula for the permittivity and permeability. This procedure works well at frequencies where the sample length is not a multiple of one-half wavelength in the material. At these latter frequencies, however,

the solution procedure completely breaks down. In the Nicolson- Ross-Weir algorithm the reflection coefficient

$$\Gamma_1 = X \pm \sqrt{X^2 - 1}, \tag{2.26}$$

is given explicitly in terms of the scattering parameters where

$$X = \frac{1 - V_1 V_2}{V_1 - V_2}, \tag{2.27}$$

and

$$V_1 = S_{21} + S_{11}, \tag{2.28}$$

$$V_2 = S_{21} - S_{11}. \tag{2.29}$$

The correct root is chosen in eq (2.26) by requiring $|\Gamma_1| \leq 1$. The transmission coefficient, z_1, for the Nicolson-Ross-Weir procedure is given by

$$z_1 = \frac{S_{11} + S_{21} - \Gamma_1}{1 - (S_{11} + S_{21})\Gamma_1}, \tag{2.30}$$

and the permeability is given by

$$\mu_R^* = \frac{1 + \Gamma_1}{(1 - \Gamma_1)\Lambda\sqrt{\frac{1}{\lambda_0^2} - \frac{1}{\lambda_c^2}}}, \tag{2.31}$$

where λ_0 is the free space wavelength and λ_c is the cutoff wavelength. In this report $\mu_R^* = 1$ (this removes the ambiguity in the logarithm branch). The permittivity is given by

$$\frac{1}{\Lambda^2} = -[\frac{1}{2\pi L}\ln(\frac{1}{z_1})]^2, \tag{2.32}$$

$$\epsilon_R^* = \frac{\lambda_0^2}{\mu_R^*}[\frac{1}{\lambda_c^2} - [\frac{1}{2\pi L}\ln(\frac{1}{z_1})]^2]. \tag{2.33}$$

Equation (2.32) has an infinite number of roots for magnetic materials, since the logarithm of a complex number is multi-valued. In order to pick out the correct root it is necessary to compare the measured group delay to the calculated group delay. The calculated group delay is related to the change of the wave number, k, with respect to angular frequency

$$\tau_{calc.group} = L\frac{d}{df}\sqrt{\frac{\epsilon_R^*\mu_R^*}{\lambda_0^2} - \frac{1}{\lambda_c^2}}. \tag{2.34}$$

The measured group delay is

$$\tau_{meas.group} = -\frac{1}{2\pi}\frac{d\phi}{df}, \tag{2.35}$$

where ϕ is the measured phase. To determine the correct root, the calculated group delays are found from eq (2.35) for various values of n in the logarithm term in eq (2.32), using $\ln z = \ln|z| + j(\theta + 2\pi n)$, where $n = 0, \pm 1, \pm 2...$, and compared to the measured value from eq (2.35). The comparison yields the correct value of n. Many researchers think of the Nicolson-Ross-Weir solution as an explicit solution; however, due to the phase ambiguity, it is not.

In the limit of no loss, the Nicolson-Ross-Weir solution is divergent at integral multiples of one-half wavelength in the sample. This singular behavior can be minimized in cases which permeability is known *a priori*. An stable algorithm will be developed in the next section.

In figure 2.2, a typical plot utilizing the NRW [1] equations is displayed. At points corresponding to one-half wavelength the scattering parameter $\mid S_{11} \mid$ gets very small. Also, for small $\mid S_{11} \mid$ the uncertainty in the measurement of the phase of S_{11} on a network analyzer is very large. Thus, this uncertainty dominates the solution at these frequencies. To bypass this problem many researchers resort to short sample lengths. Use of short samples lowers the measurement sensitivity, however. In fact, as will be shown later in the report that when minimizing the uncertainty for low-loss, low permittivity materials, a relatively long sample is preferred.

Another interesting result can be obtained if we assume that ϵ_R^* and the measured value of an S-parameter are known at a single angular frequency, ω_k. In this case we can solve either (2.15) or (2.16) for the reference positions and then substitute this length into eqs (2.12)–(2.14) to obtain relations for the reference plane positions at other frequencies. This length is the equivalent electrical length of the section of line. If we let m denote "measured value"then we can obtain a relation for the reference plane rotation term at an angular frequency of ω_i

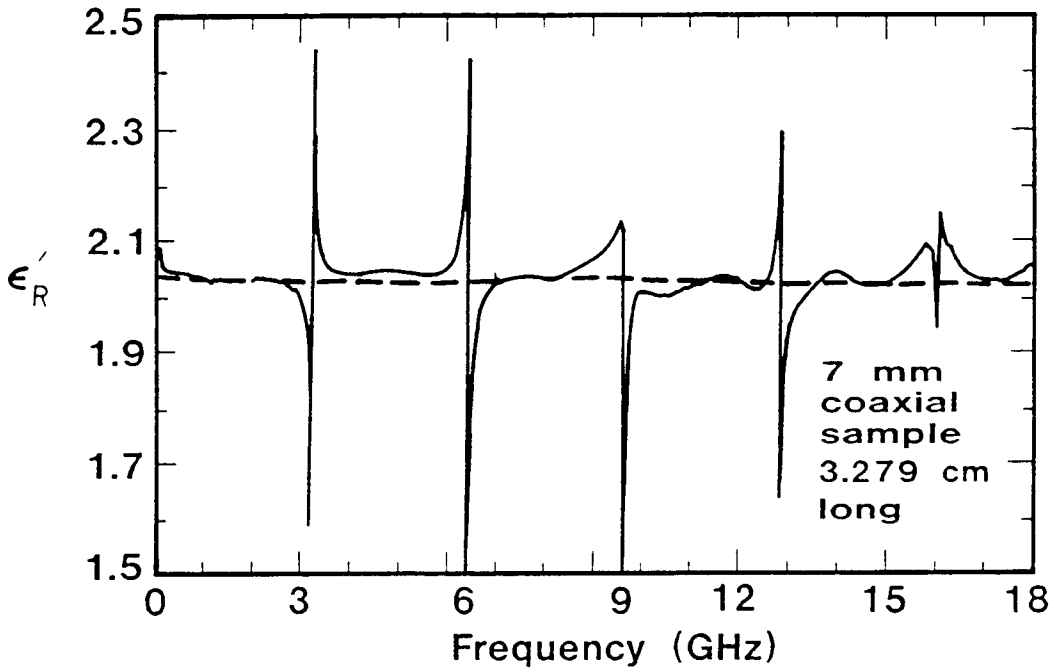

Figure 2.2: The determination of the permittivity of a polytetrafluoroethylene sample as a function of frequency using the Nicolson and Ross equations (solid line) and the iteration procedure (dashed line).

$$R_1^2(\omega_i) = [S_{11}(\omega_k)]_m^{(\frac{\gamma_i}{\gamma_k})} \left[\frac{1 - z^2\Gamma^2}{\Gamma(1 - z^2)}\right]^{(\frac{\gamma_i}{\gamma_k})}, \tag{2.36}$$

$$R_1(\omega_i)R_2(\omega_i) = [S_{21}(\omega_k)]_m^{(\frac{\gamma_i}{\gamma_k})} \left[\frac{1 - z^2\Gamma^2}{z(1 - \Gamma^2)}\right]^{(\frac{\gamma_i}{\gamma_k})}. \tag{2.37}$$

Thus, we can determine the reference plane positions in terms of $\epsilon_R^*(\omega_k)$ and the measured value of the scattering parameter at ω_k. Equations (2.36), (2.37) may be very useful for problems where other methods have produced an accurate measurement of ϵ_R^* at a single frequency.

2.2 Numerical Determination of Permittivity

There are various ways of solving the scattering equations depending on the information available to the experimenter. In cases where the sample length and reference plane positions are known to high accuracy taking various linear combinations of the scattering equations and solving the equations in an iterative fashion yields a very stable solution on samples of arbitrary length. A useful combination is

$$\frac{1}{2}\{[S_{12} + S_{21}] + \beta[S_{11} + S_{22}]\} = \frac{z(1 - \Gamma^2) + \beta\Gamma(1 - z^2)}{1 - z^2\Gamma^2}. \tag{2.38}$$

In eq (2.38) the S-parameters to be used need to be transformed from the calibration plane to the sample face by use of eq (2.15), (2.16). Here β is a constant which varies as a function of the sample length, uncertainty in scattering parameters and loss characteristics of the material. The constant β is a weighting function for the S- parameters. For low-loss materials, the S_{21} signal is strong and so we can set $\beta = 0$, whereas for materials of high loss S_{11} dominates and a large value of β is appropriate. A general relation for β is given by the ratio of the uncertainty in S_{21} divided by the uncertainty in S_{11}. In figure 2.2 the iterative solution of eq (2.38) (in the dashed line) is compared to the Nicolson-Ross procedure for a sample of

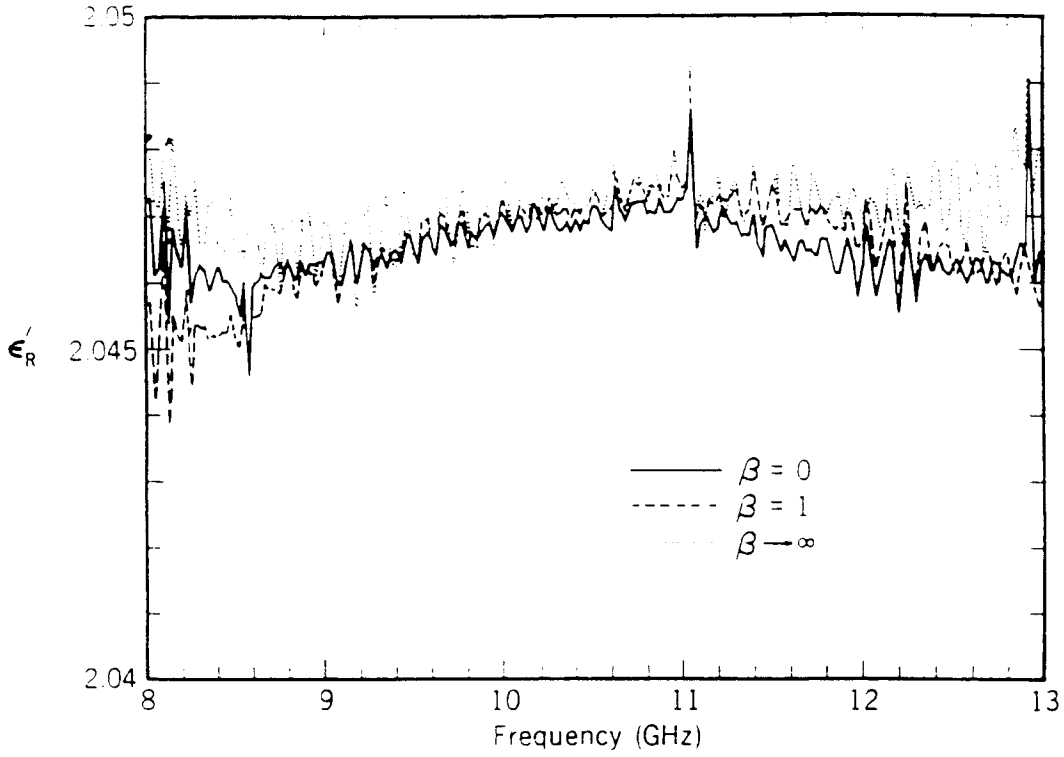

Figure 2.3 The real part of the permittivity obtained from eq (2.38) for various values of β. The dotted line is for $\beta \to \infty$, the solid line for $\beta = 0$ and the dashed line for $\beta = 1$.

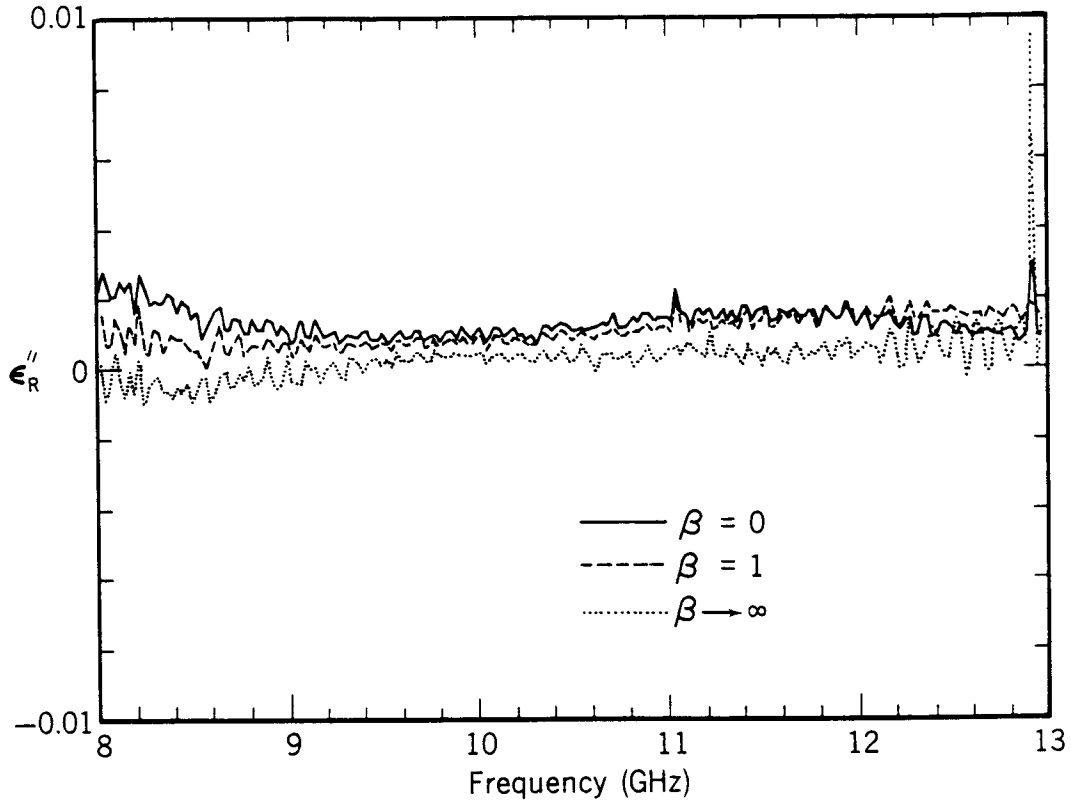

Figure 2.4 The imaginary part of the permittivity obtained from eq (2.38) for various values of β. The dotted line is for $\beta \to \infty$, the solid line for $\beta = 0$ and the dashed line for $\beta = 1$.

polytetrafluoroethylene (PTFE) in 7 mm coaxial line. The iterative solution process is summarized in appendix E. A striking contrast is seen between the solutions. In figure 2.3 and 2.4 data for PTFE in an X-band waveguide is reduced for permittivity while varying the parameter β. In the case of PTFE, which has low loss and relatively low ϵ'_R, the best results are produced by using only S_{21} and S_{12} data. One requirement for an iterative technique is the selection of the initial guess for the permittivity. As an initial guess we use the solutions to the Nicolson-Ross-Weir equations as a starting value and then use the previously obtained permittivity at one frequency as the initial guess for the next frequency.

For cases when the reference plane positions are uncertain, we find that eq (2.25) is robust. When we use eq (2.25), no reference plane transformation need be performed since it has been eliminated by use of the relation $L_{air} = L_1 + L_2 + L$. Equation (2.25) works well for both low-loss and high-loss materials. If eq (2.25) is solved in tandem with any one of eqs (2.21)–(2.24) the measurement can become independent of reference plane position and sample length. That is, we have four real equations for the four unknowns: ϵ'_R, ϵ''_R, L, L_{air}.

For magnetic materials, four independent real equations are required (or two independent complex equations). Since in this case there are seven unknowns and nine real equations, (eqs (2.12)– (2.14), (2.20) and the equation for length of sample holder) it is possible to use various combinations of the basic equations. When permeability is included for materials with both low-loss magnetic and dielectric properties, the solutions for both permittivity and permeability will be unstable at integral multiples of one-half wavelength in the material.

2.3 Corrections to Data

Once a set of measurements is obtained it is necessary to correct the data taking into account correctable, systematic uncertainties. These known uncertainty sources include air gaps around samples, waveguide wall imperfections, imperfect short-circuits, and waveguide losses. Air gaps are particularly important for coaxial samples; in particular, the gap near the center conductor is important since the electric field is higher in this region. In order to make corrections it is necessary to obtain precise measurements of

both the sample and the sample holder; air gauging equipment is useful for these measurements.

2.3.1 Gaps Between Sample and Holder

Air gaps around samples affect measured value of permittivity. In waveguide the air gap along the wide side of the guide has the primary influence on the calculated permittivity since this region has a higher electric field. For the same reason in coaxial line the gap near the center conductor contributes more than a gap of the same thickness near the outer conductor. See appendix C for gap correction formulas [12], [13], [14]. These correction formulas are approximate and generally undercorrect for the effects of the air gap. Imperfect waveguide or coaxial line walls have been studied by Hill [15] and the results from this work are summarized in appendix C. Waveguide and coaxial line losses can be probed by measuring the scattering parameters of the empty waveguide.

2.3.2 Attenuation Due to Imperfect Conductivity of Sample Holders

Since no waveguide is perfectly conducting, all propagating modes are attenuated to some degree. The finite conductivity of waveguide walls promotes power loss in the guide.

The power flow down the waveguide is given by

$$P = \frac{1}{2}\int_s Re[\vec{E} \times \vec{H^*}] \cdot d\vec{S} = \frac{Z}{2}\int_s |\vec{H}_t|^2 dS, \tag{2.39}$$

where Z is the wave impedance and $(_t)$ denotes the tangential component [16]. The power loss in the guide is

$$P_L = \int_c \frac{R_s}{2}|\vec{J}_z|^2 ds = \frac{R_s}{2}\int_c |\vec{H}_t|^2 ds, \tag{2.40}$$

where $R_s = \sqrt{\pi f \frac{\mu}{\sigma}}$ is the effective surface resistance, σ is the conductivity, and c is a closed path. The effective attenuation constant can be defined as

Table 2.1 Cutoff Frequencies.

EIA WR()	Band	Cutoff frequency(GHz)
650	L	0.908
430	W	1.372
284	S	2.078
187	C	3.152
90	X	6.557
42	K	14.047
22	Q	26.342

$$\alpha = \frac{P_L}{2P}. \tag{2.41}$$

For rectangular waveguide the integrals in eq (2.40) can be performed to obtain [16]

$$\alpha_{TE_{mn}} = \frac{2R_s}{b\eta\sqrt{1-(\frac{f_c}{f})^2}}\left[(1+\frac{b}{a})(\frac{f_c}{f})^2 + (1-(\frac{f_c}{f})^2)\frac{\frac{b}{a}(m^2(\frac{b}{a})+n^2)}{m^2(\frac{b}{a})^2+n^2}\right], \tag{2.42}$$

where a and b are the guide dimensions, f_c is the cutoff frequency, $m, n =$ 0,1,2,. . . and η is the impedance of free space. For $n = 0$ the attenuation is:

$$(\alpha)_{TE_{m0}} = \frac{R_s}{b\eta\sqrt{1-(f_c/f)^2}}[1+\frac{2b}{a}(\frac{f_c}{f})^2]. \tag{2.43}$$

Waveguides can be used over only a band of frequencies, so the selection of a waveguide depends on the frequencies to be measured. The cutoff frequency is a lower bound on frequencies that can be transmitted in the guide without introducing evanescent modes. A list of cutoff frequencies for various waveguide sizes is given in table (2.1). The cutoff frequency for either TE or TM waves in rectangular waveguide is given by

$$(f_c)_{mn} = \frac{1}{2\sqrt{\mu'\epsilon'}}\sqrt{(\frac{m}{a})^2+(\frac{n}{b})^2}, \tag{2.44}$$

where a is the long dimension of the guide, b is the short dimension of the guide and $m, n = 0, 1, 2....$ For the TE_{10} mode the cutoff frequency is:

$$(f_c)_{mn} = \frac{1}{2\sqrt{\mu'\epsilon'}a} = \frac{c}{2a}. \tag{2.45}$$

Rectangular waveguide operated in the TE_{10} mode becomes overmoded at twice the cutoff frequency. Operating frequencies and waveguide dimensions are given in tables (2.1) and (2.2).

For a circular waveguide of radius a the attenuation is given by [16]

$$\alpha_{TM_{mn}} = \frac{R_s}{a\eta} \frac{1}{\sqrt{1 - (\frac{f_c}{f})^2}}, \tag{2.46}$$

$$\alpha_{TE_{mn}} = \frac{R_s}{a\eta} \frac{1}{\sqrt{1 - (\frac{f_c}{f})^2}} \left[(\frac{f_c}{f})^2 + \frac{m^2}{(p'_{mn})^2 - m^2} \right], \tag{2.47}$$

where p'_{mn} are the roots of $J'_m(p'_{mn}) = 0$.

The cutoff frequencies in circular waveguide are given for TM_{mn} by

$$(f_c)_{mn} = \frac{p_{mn}}{\sqrt{\epsilon\mu}2\pi a}, \tag{2.48}$$

where p_{mn} are the nth root of $J_m(p_{mn}) = 0$. For TE_{mn} waves we have:

$$(f_c)_{mn} = \frac{p'_{mn}}{\sqrt{\epsilon\mu}2\pi a}, \tag{2.49}$$

where p'_{mn} are the nth roots of $J'_m(p'_{mn}) = 0$.

Coaxial line has the distinct advantage of having no cutoff frequency, however, coaxial line becomes multi-moded above a certain frequency. These multi-modes are due to bead resonance which couples in the TE_{11} and higher modes. The approximate upper frequency limit due to bead resonance is given in table (2.3).

Also, the propagation of the TE and TM modes in the cable in addition to the TEM mode is possible at higher frequencies. The cutoff wave numbers for higher TM waves in coaxial line are given by the roots of the equation [16],

$$\frac{N_n(k_c r_i)}{J_n(k_c r_i)} - \frac{N_n(k_c r_o)}{J_n(k_c r_o)} = 0, \tag{2.50}$$

Table 2.2 Rectangular waveguide dimensions and operating frequencies in air.

EIA WR	Band	a (cm)	b (cm)	TE_{10} Operating Frequency(GHz)
650	L	16.510	8.255	1.12 - 1.7
430	W	10.922	5.461	1.7 - 2.6
284	S	7.710	3.403	2.6 - 3.95
187	C	4.754	2.214	3.95 - 5.85
90	X	2.286	1.016	8.2 - 12.4
42	K	1.067	0.432	18 - 26.5
22	Q	0.569	0.284	33 - 50

Table 2.3 Air-filled coaxial cable operating frequencies.

Coaxial Cable Dimensions (mm)	Useful Operating Frequency (GHz)
3.5	0 - 34.5
7.0	0 - 18.2
14.0	0 - 08.6

and for TE waves in coaxial line by

$$\frac{N_n'(k_c r_i)}{J_n'(k_c r_i)} - \frac{N_n'(k_c r_o)}{J_n'(k_c r_o)} = 0, \tag{2.51}$$

where J and N denote the Bessel functions of the first and second kind, and r_i and r_o are the inner and outer radii, respectively [16]. The cutoff wavelengths are given approximately by

$$\lambda_c \approx \frac{2}{q}(r_o - r_i) \ , \ q = 1, 2, 3, ... \tag{2.52}$$

For example, the TM mode cutoff frequency in 7 mm coaxial line for eq (2.52) is approximately 34 GHz. For beadless air line it is possible to exceed the frequencies given in table 2.3

2.4 Instrumentation

The following apparatus is needed for broadband TR measurements:

- Automated network analyzer
- Data acquisition and analysis systems
- Precision waveguide or coaxial line

Network analyzers are rapidly becoming the preferred data acquisition system for many researchers. Network analyzer systems have various error sources. These include [17]:

- Imperfect matching at connectors
- Imperfect calibration standards
- Nonlinearity of mixers, gain and phase drifts in IF amplifiers, noise introduced by the analogue to digital converter
- Imperfect tracking in dual channel systems

Generally, the manufacturer furnishes the specification of its own system. The choice of network analyzer is crucial for good phase data; the ANA which is best suited for the frequency band of interest should be chosen.

2.4.1 ANA Calibration

Coaxial Line Calibration

Various components of the ANA introduce phase and magnitude uncertainties. Examples of these uncertainty sources are frequency response, various mismatches and radio frequency (r.f.) leakage. Calibration of the ANA removes the systematic uncertainties in a measurement of a set of standards, for example, shielded open circuit, reflect or load. Information on the difference between a specific measurement of these standards and the expected values (stored in ANA system) generates a set of error correction coefficients. The calibration coefficients are determined from solving a set of simultaneous

equations generated from the linear fractional transformation. After calibration, when the system is operated with *correction on* mode, the measurements are corrected by the calibration information.

The 7 mm line calibration kit contains the following standards:

- open-circuit
- short-circuit
- low and high frequency loads
- sliding load

The Waveguide Calibration Kit

For calibration of a given waveguide it is necessary to construct a calibration kit for the ANA. The TRL calibration consists of measuring a *thru*, a *reflect*, and a section of *line*. The length of line to be used as the *thru* is calculated as follows: the phase delay (ϕ) in waveguide is related to line length (ℓ) and guided wavelength (λ_g) by

$$\ell = \frac{\phi \lambda_g}{2\pi}, \tag{2.53}$$

where the guided wavelength is related to the free-space wavelength by:

$$\lambda_g = \frac{\lambda}{\sqrt{1 - (\frac{\lambda}{\lambda_c})^2}}. \tag{2.54}$$

The procedure for the calculation of the *line* length is to calculate ℓ for a phase delay of 20° at the lowest frequency of interest, and again for a phase delay of 160° at the highest frequency of interest, and then choose a line length between these extreme values, typically, $\lambda/4$ at geometric center frequency ($f_{center} = \sqrt{f_{min} f_{max}}$).

When using waveguide for measurements it is necessary to insert sections of waveguide, each approximately two wavelengths in length, between the coax-to-waveguide adapter and the sample holder. The function of the waveguide sections is to damp out any evanescent modes. The X-band calibration kit contains the following items:

- coax to waveguide adapters
- short-circuit
- a section of waveguide line to be used as a sample holder
- a section of calibration "line"
- two lengths of X-band waveguide approximately two wavelengths long
- loads

2.4.2 Sample Holder Specifications

The sample holder for TR measurements should consist of high precision waveguide or coaxial line. There should be a length of waveguide between the waveguide-to-coaxial line adapter and sample holder to damp out evanescent waves generated at these discontinuities. The length of the sample holder should be measured with a high degree of precision. Nicks and other abrasions in the sample holder will, of course, degrade performance. When 7 mm coaxial beadless air line is used, APC-7 connectors are usually preferred. The sample holder should be treated with extreme care and stored in a protected area.

The impedance of coaxial line is given by

$$Z_o = \sqrt{\frac{(R + j\omega L)}{(G + j\omega C)}} \tag{2.55}$$

where R = resistance, C = capacitance, L = inductance, and G = conductance (all per unit length). The surface impedance determines the loss in the line and is given by

$$Z_s = \frac{1+j}{\pi}\left[\frac{1}{D(\sigma\delta)_{oc}} + \frac{1}{d(\sigma\delta)_{ic}}\right], \tag{2.56}$$

where D is inner diameter of outer conductor, d is outer diameter of inner conductor, σ and $\delta = 1/\sqrt{\pi f \mu \sigma}$ are the conductivity and skin depth respectively [18].

Table 2.4 Connector directivity repeatability

Connector Type	Repeatability at 18 GHz(dB)
7 mm with 6 slot collet	59
Precision Type-N	49
PSC-N	59

Wong has shown that the impedance of a precision 7 mm coaxial air line, with uniformity of approximately $\pm 2\mu m$, varies slightly with frequency from 50.25 Ω at 0.1 GHz to 49.95 Ω at 20 GHz [18].

The repeatability of the 7 mm connectors are summarized in table 2.4 [18].

2.4.3 Sample Preparation

Samples to be used for measurements must be prepared carefully. Scratches, nicks and cracks may alter the measured dielectric properties. Minimize any unnecessary wear and tear on the sample by placing it in a secure area between measurement sessions. The sample length measurement is critical and should be performed carefully with a precision micrometer at laboratory temperatures.

The following list summarizes the preparation procedure:

- Carefully select a piece of material free of unusual inhomogeneities, cracks, etc.
- Have the sample machined to fit as tightly as possible in the sample holder. The machining process should not leave metallic residue on the sample. Note that gaps near the center conductor in coaxial line are more serious than gaps near the outer conductor. Samples which fit very tightly on the outer conductor can be inserted more easily by prior cooling.
- Measure the sample length with a high degree of precision at a temperature very close to that realized in the laboratory. The resulting strain,

Table 2.5 Metrologist tolerance specifications.

Symbol	Term
$\perp$	perpendicularity
$\odot$	concentricity
$\bigcirc$	cylindricity
$\bigcirc$	circularity
$\parallel$	parallelism
$\mathrm{—}$	flatness
$\oplus$	position
$\nearrow$	runout

$\Delta L/L$, from increased temperature can be calculated from the linear thermal expansion coefficient, α, by using the relation $\Delta L/L = \alpha \Delta T$.

- Keep the sample very clean and store in a secure area. If the sample requires cleaning, an ultrasonic cleaner will suffice.

- Keep the gap between sample and guide walls to a minimum. We have found that clearances of (2.5-7) $\times 10^{-6}$ m (0.0001 - 0.0003 in.) are acceptable.

In figures 2.5 and 2.6 examples of specifications for coaxial and waveguide samples are shown.

The parameters of interest to the machinist in this example are the cylindricity, concentricity, and perpendicularity. A list of metrology symbols is given in table (2.5). It is very important to specify precisely your tolerances to the machinist. Generally the machinist will ask that the sample holder be available for fitting purposes from time to time. Corrections for the resulting effect of the air gap on the permittivity is given by the equations in appendix C.

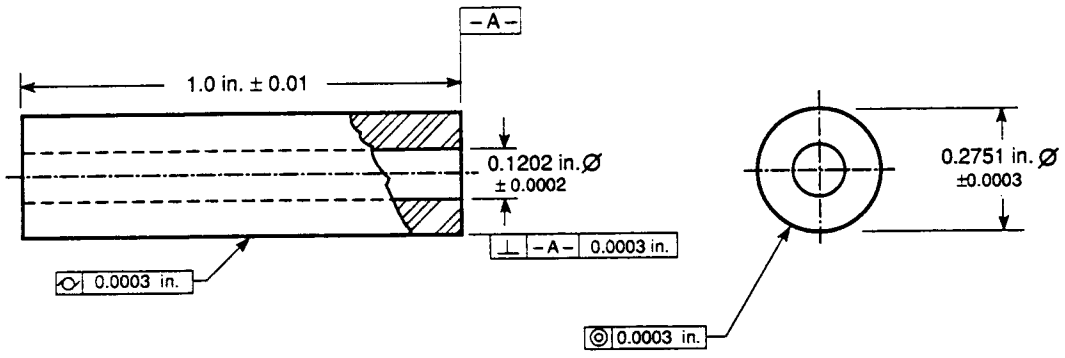

Glass Rod

MAT'L - GLASS
SCALE - 4:1

Figure 2.5 Sample specifications for a coaxial sample .

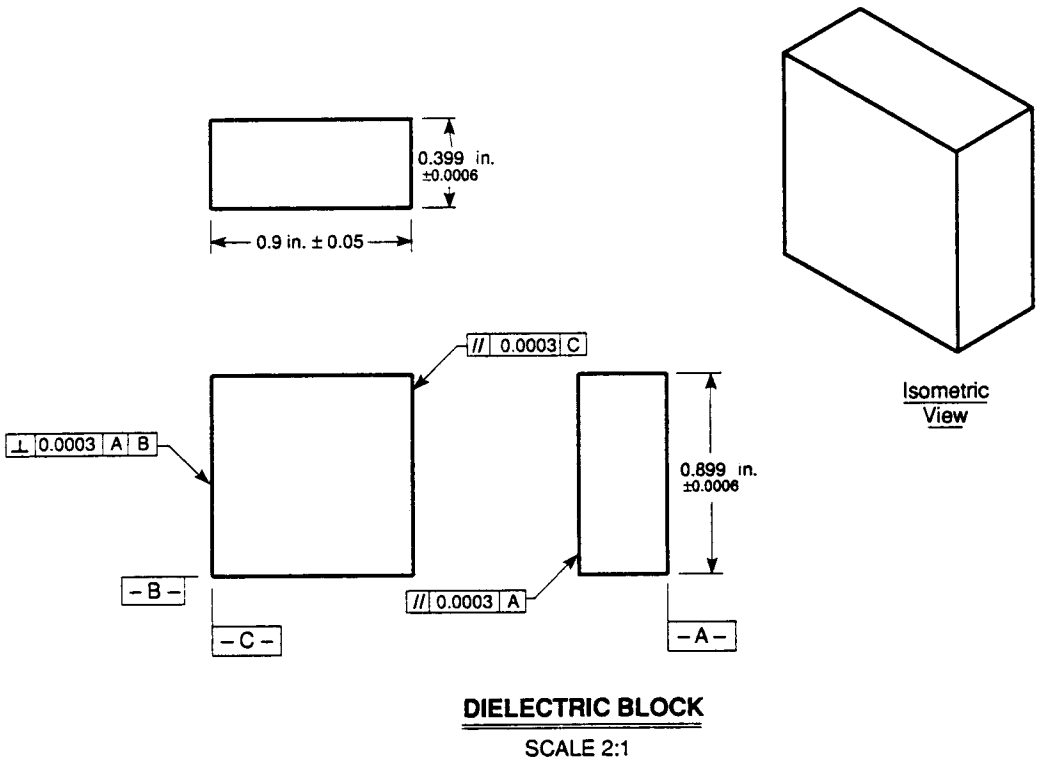

Figure 2.6 Sample specifications for a rectangular sample in inches.

2.4.4 System Diagnostics

In order to verify the accuracy of the system before each measurement it is important to have a verification test. For the TR method our standard verification procedure consists of measuring the permittivity of air in the empty sample holder and comparing the results to those of a reference set. An example reference is given in figure 2.7 and 2.8.

2.5 Measurement Results

The accuracy of TR measurements is limited by a number of factors. These factors include the uncertainties of the network analyzer, dimensional tolerances of sample holder and sample, and the accuracy of the underlying field model.

In figure 2.9 through 2.20 the permittivity of coaxial samples of air and cross-linked polystyrene and waveguide X-band samples of air, PTFE, and glass are plotted as a function of frequency. All of these data were reduced with eq (2.25). The PTFE sample, in both waveguide and coaxial line has an effectively a nonexistent air gap. It is possible to smooth the plot of the calculated permittivity in various ways. We currently use either a loss-pass filter or a maximum entropy smoothing routine. A smoothing procedure that utilizes the method of maximum entropy is given in appendix G.

2.6 Appearance of Higher Order Modes

The field model developed in this report assumes a single mode of propagation in the sample. Due to cutoff conditions, higher modes of propagation become possible in inhomogeneous samples of high dielectric constant. Air gaps also play an important role in mode conversion. If mode conversion does occur due to some type of perturbation, then the theoretical model expounded in this report will break down. The degree of breakdown of the model depends on the power coupled to the higher modes. Generally, the appearance of higher modes manifests itself as a sudden dip in $|S_{11}|$. This dip is a result of resonance of the excited higher mode. We can expect the general

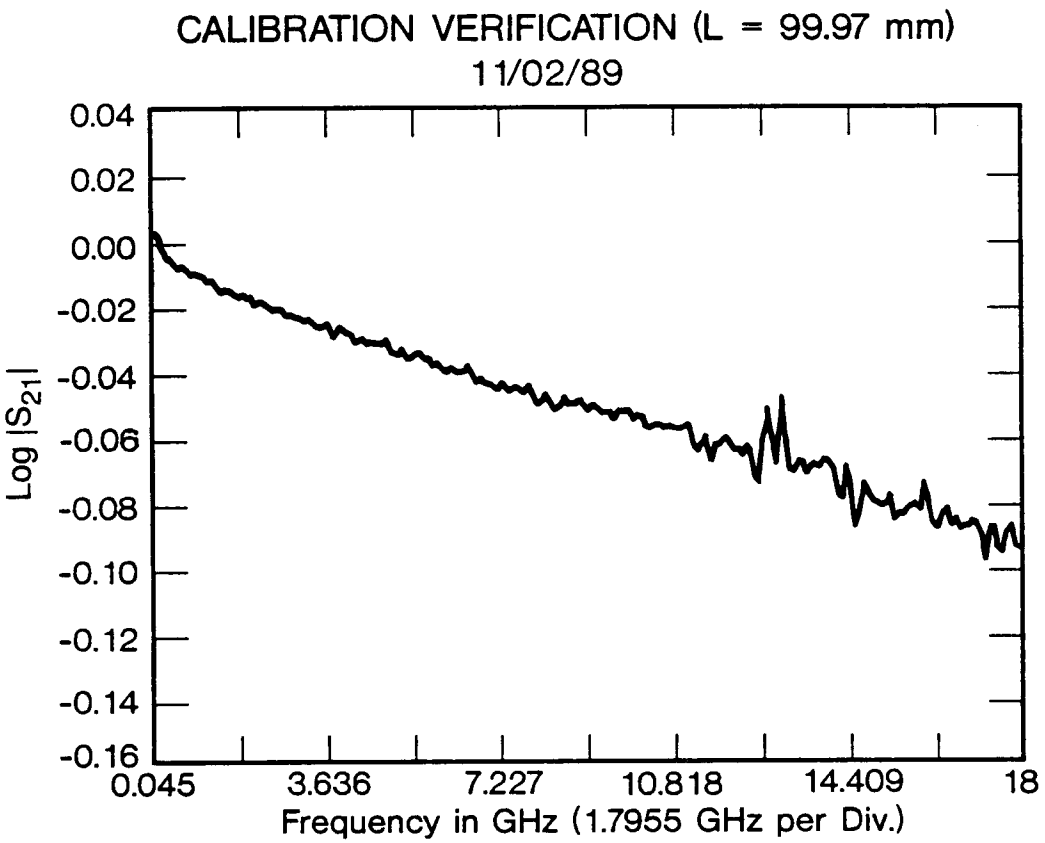

Figure 2.7 System diagnostic example for $|S_{21}|$.

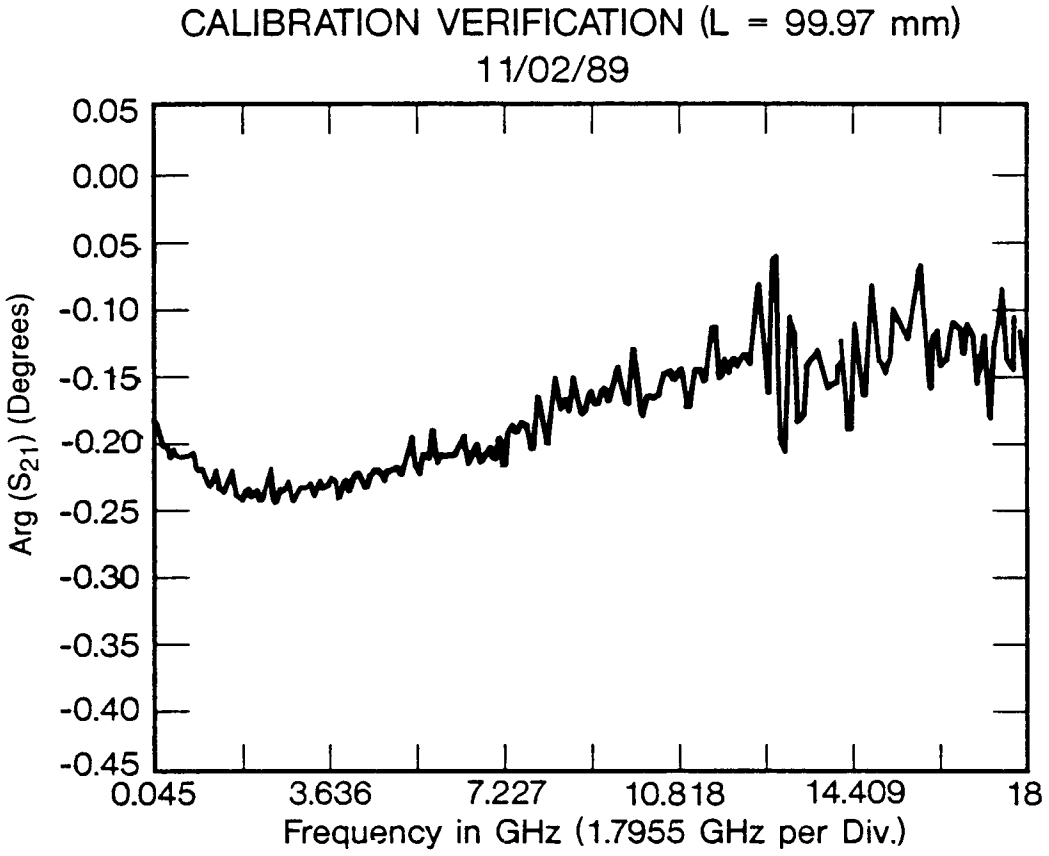

Figure 2.8 System diagnostic example for $\arg(S_{21})$.

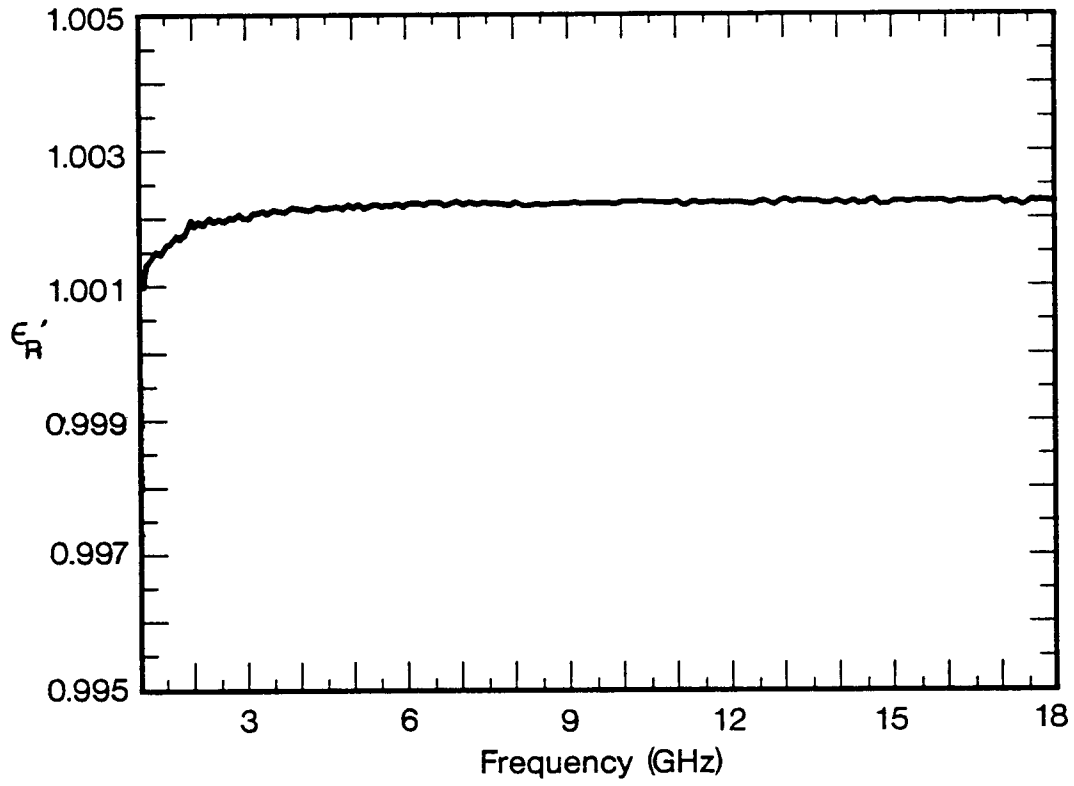

Figure 2.9 ϵ'_R of air in a coaxial line for empty air line using TR method. The worst case uncertainty at 10 GHz, $\Delta\epsilon'_R = 0.005$.

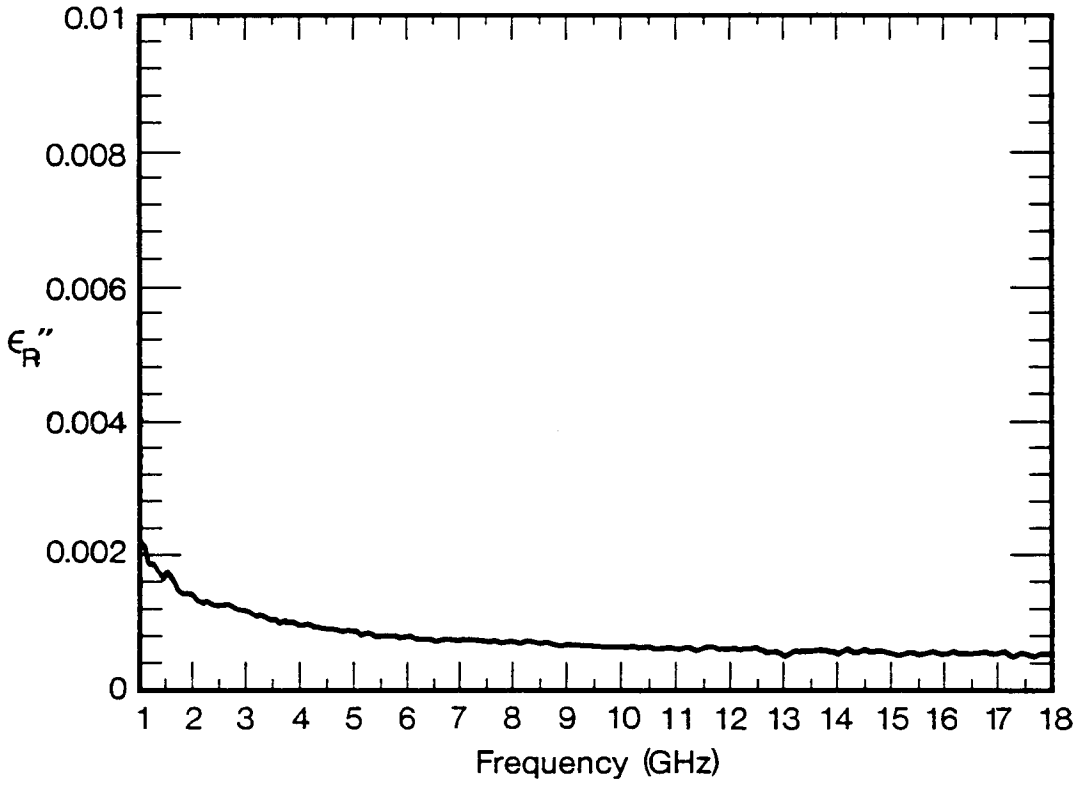

Figure 2.10 ϵ_R'' of air in a coaxial line for empty air line using TR method. The worst case uncertainty at 10 GHz, $\Delta\epsilon_R'' = 0.0012$.

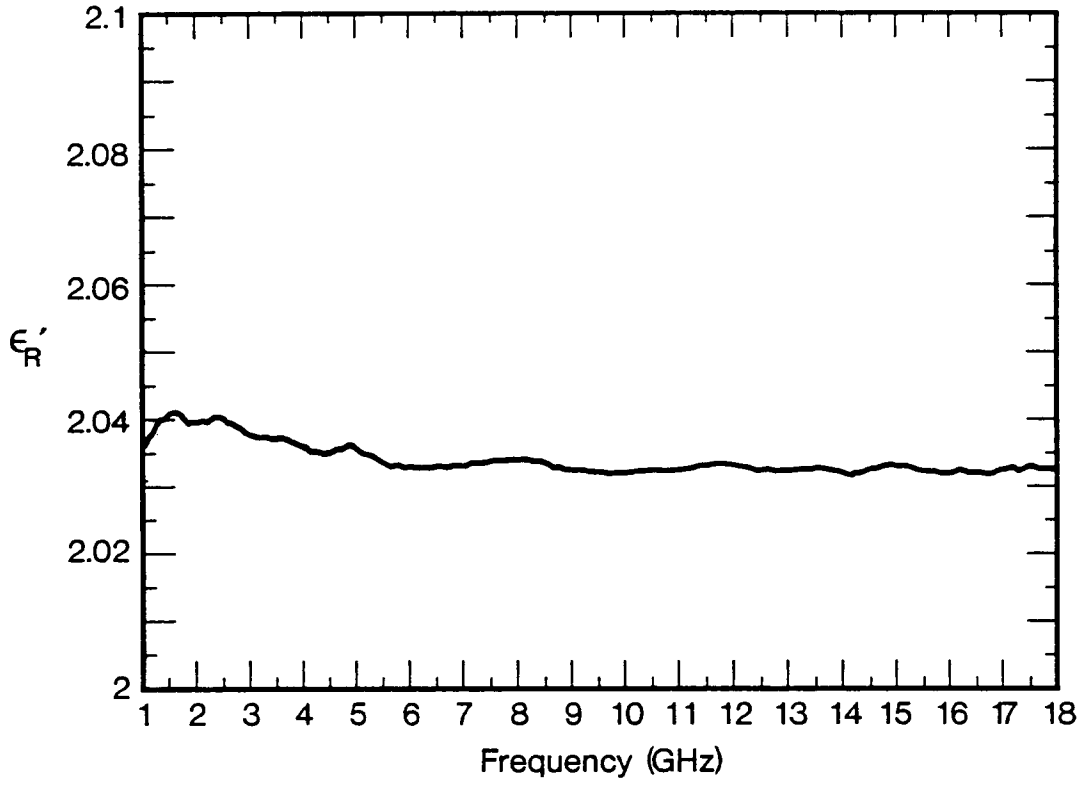

Figure 2.11 Calculated ϵ'_R for PTFE in a coaxial line as function of frequency with TR method. The worst case uncertainty at 10 GHz, $\Delta\epsilon'_R = 0.009$.

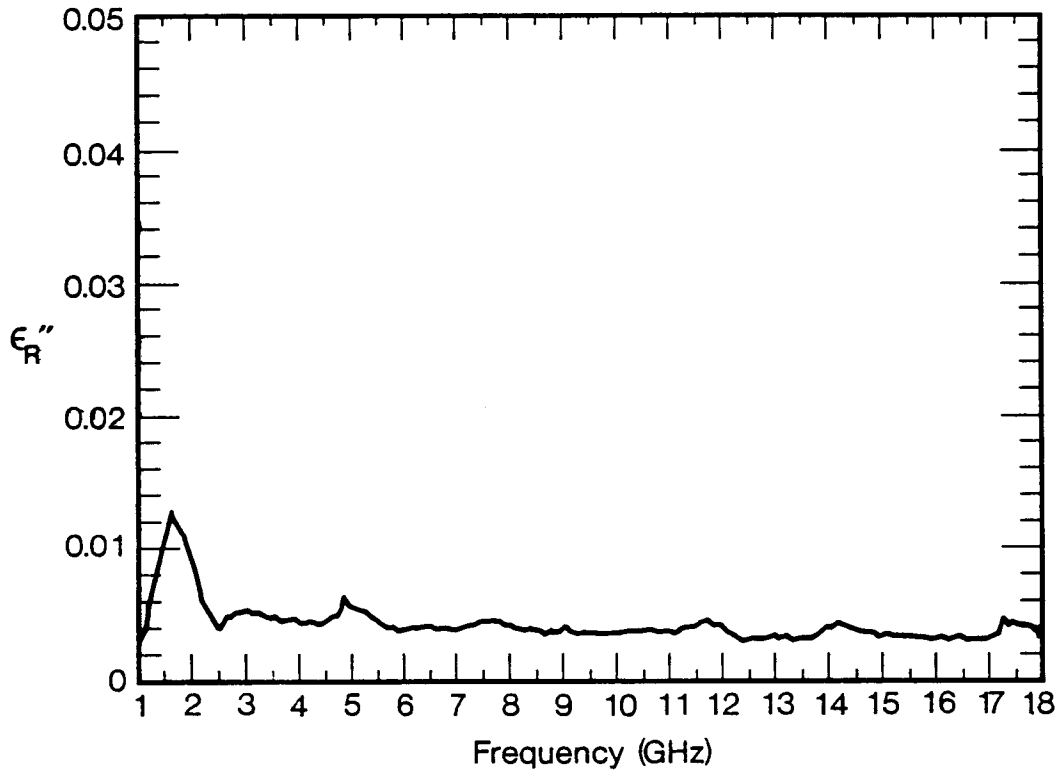

Figure 2.12 Calculated ϵ_R'' for PTFE in a coaxial line as function of frequency with TR method. The worst case uncertainty at 10 GHz, $\Delta\epsilon_R'' = 0.0017$.

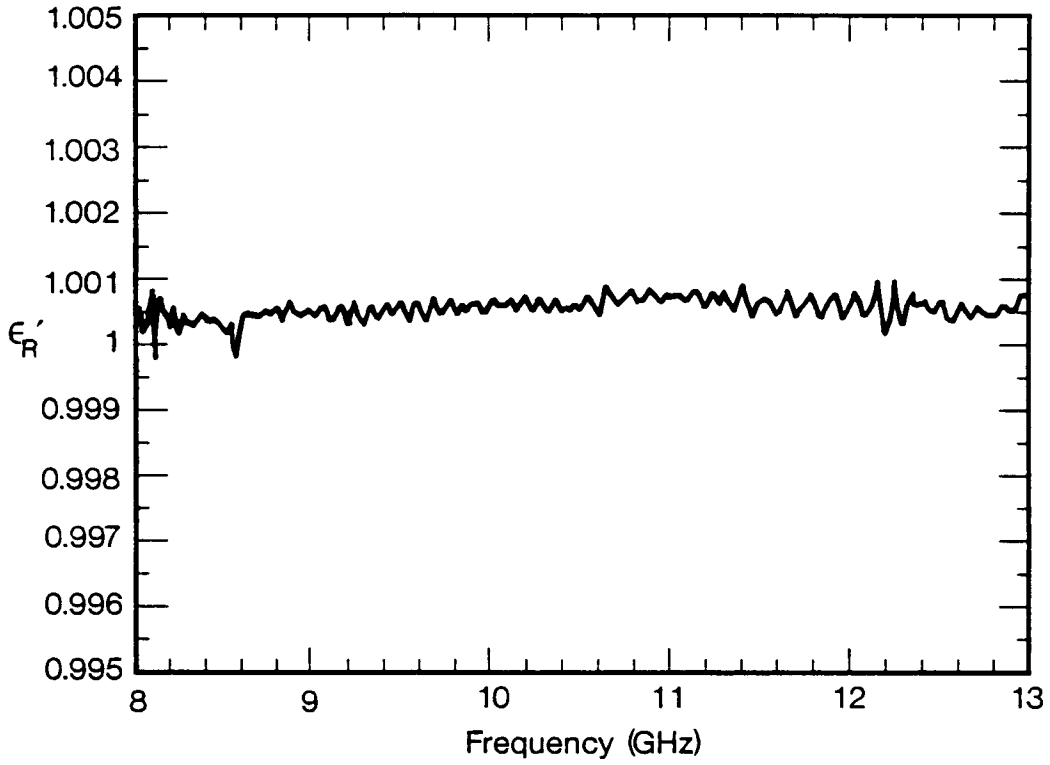

Figure 2.13 ϵ'_R of air in a X-band waveguide for empty air line using TR method. The worst case uncertainty at 10 GHz, $\Delta\epsilon'_R = 0.005$.

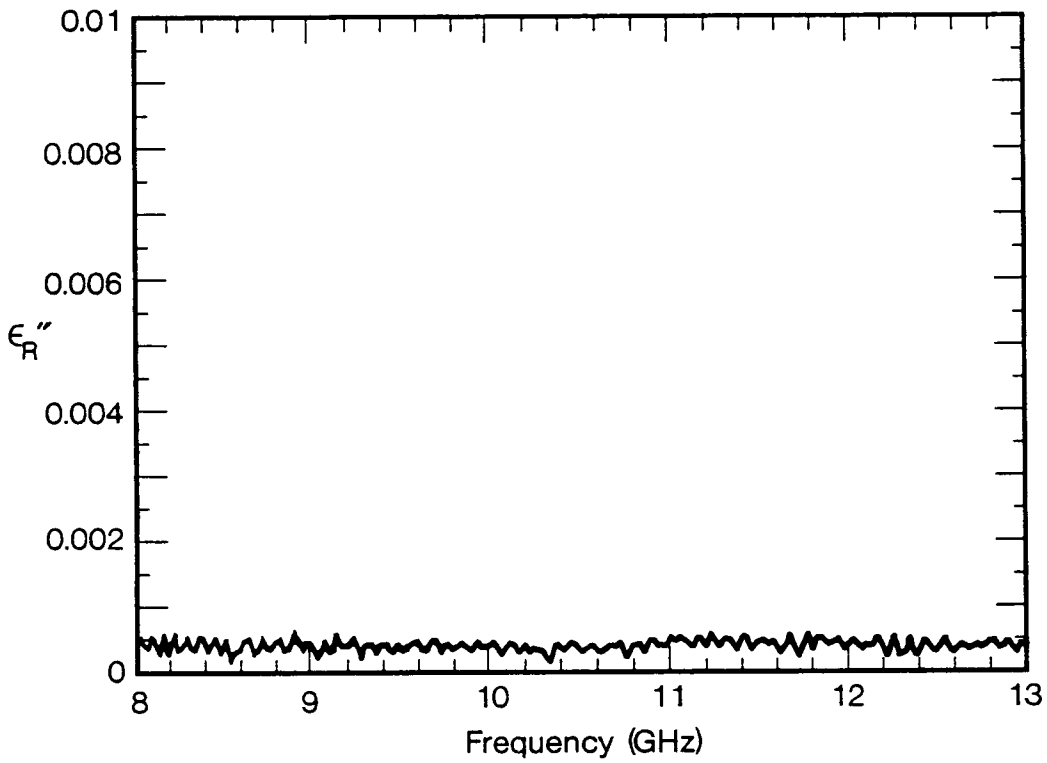

Figure 2.14 ϵ_R'' of air in a X-band waveguide for empty air line using TR method. The worst case uncertainty at 10 GHz, $\Delta\epsilon_R'' = 0.0012$.

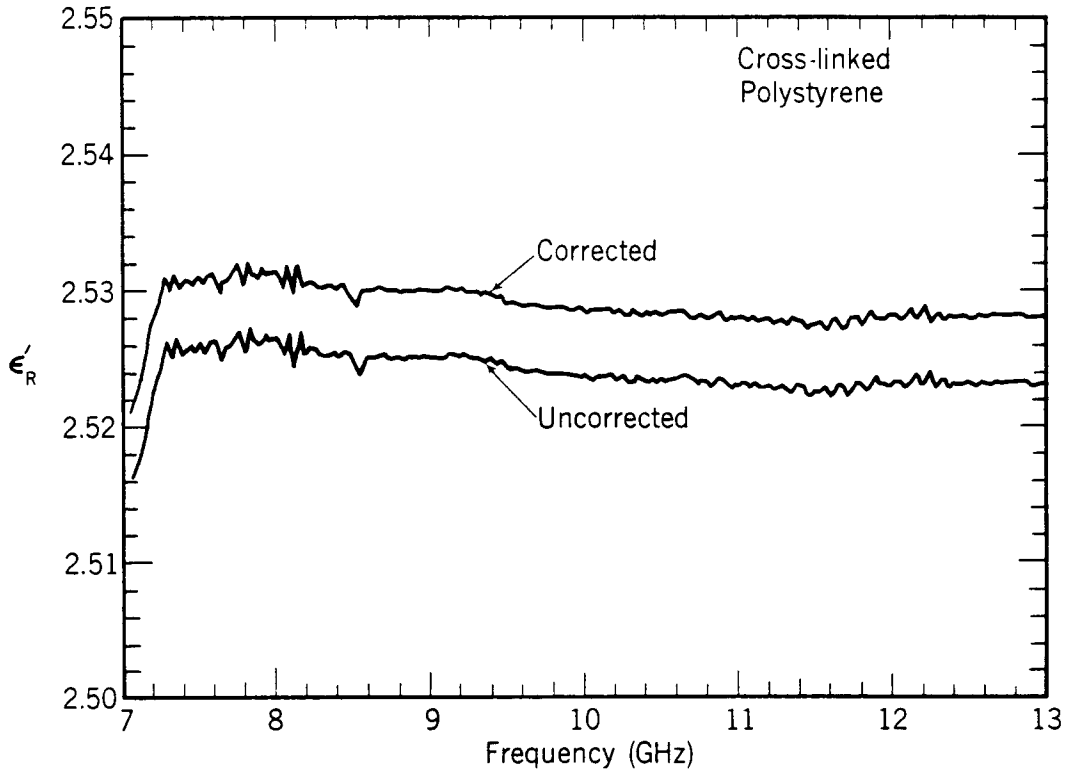

Figure 2.15 Calculated ϵ'_R with and without gap correction for cross linked polystyrene in a X-band waveguide as function of frequency with TR method. The worst case uncertainty at 10 GHz, $\Delta\epsilon'_R = 0.011$.

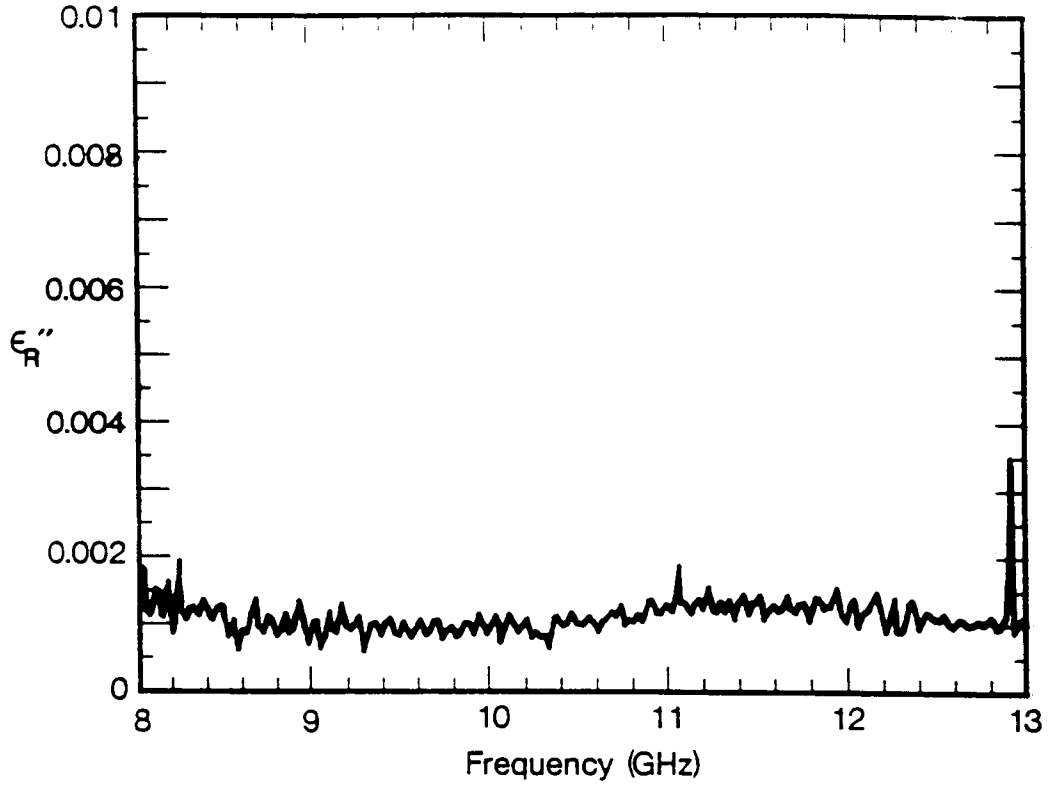

Figure 2.16 Calculated ϵ_R'' with and without gap correction for cross-linked polystyrene in a X-band waveguide as function of frequency with TR method. The worst case uncertainty at 10 GHz, $\Delta\epsilon_R'' = 0.002$.

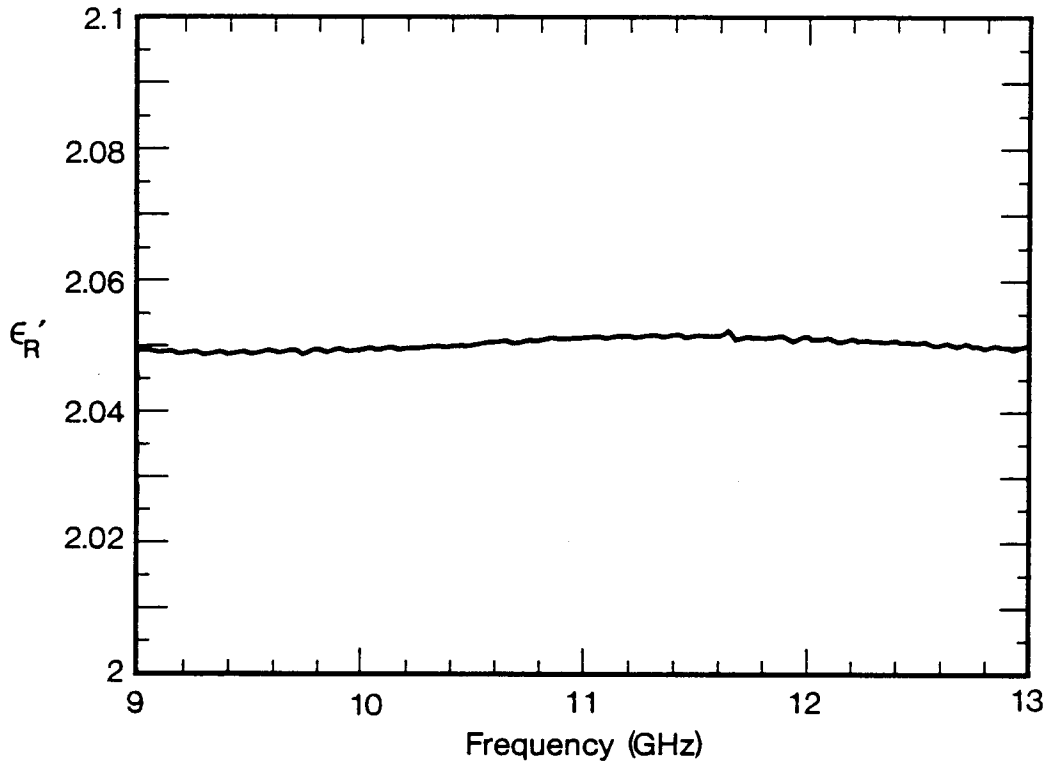

Figure 2.17 Calculated ϵ'_R for PTFE in waveguide as function of frequency with TR method. The worst case uncertainty at 10 GHz, $\Delta\epsilon'_R = 0.009$.

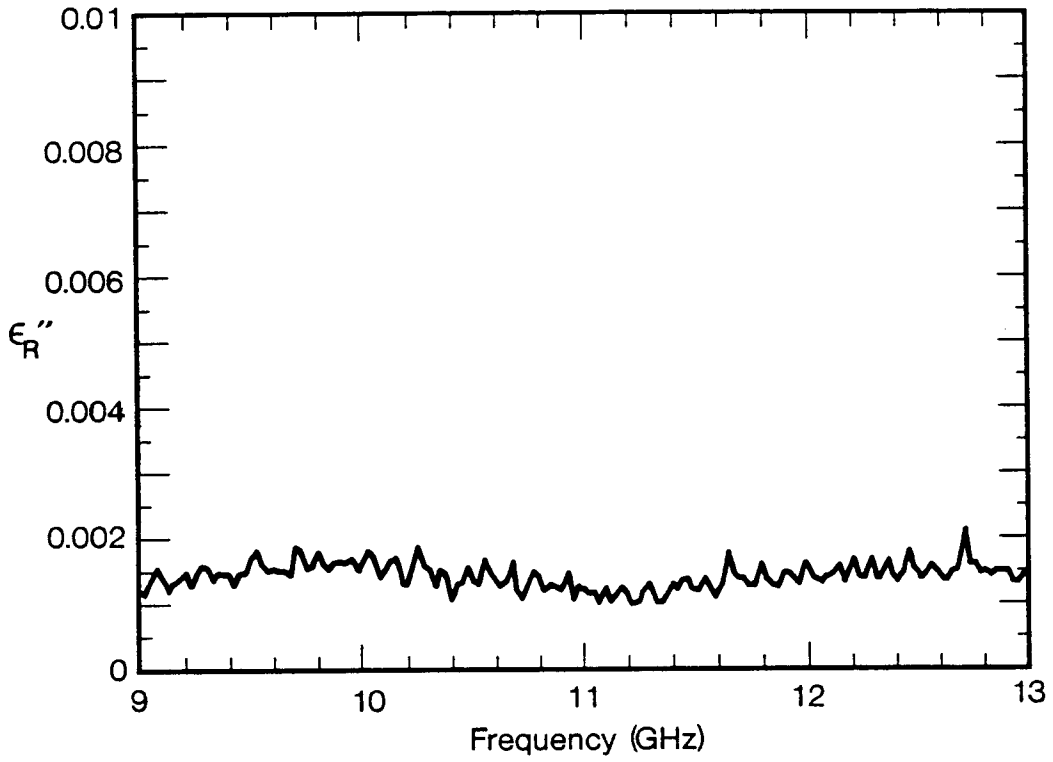

Figure 2.18 Calculated ϵ_R'' for PTFE in waveguide as function of frequency with TR method. The worst case uncertainty at 10 GHz, $\Delta\epsilon_R'' = 0.0016$.

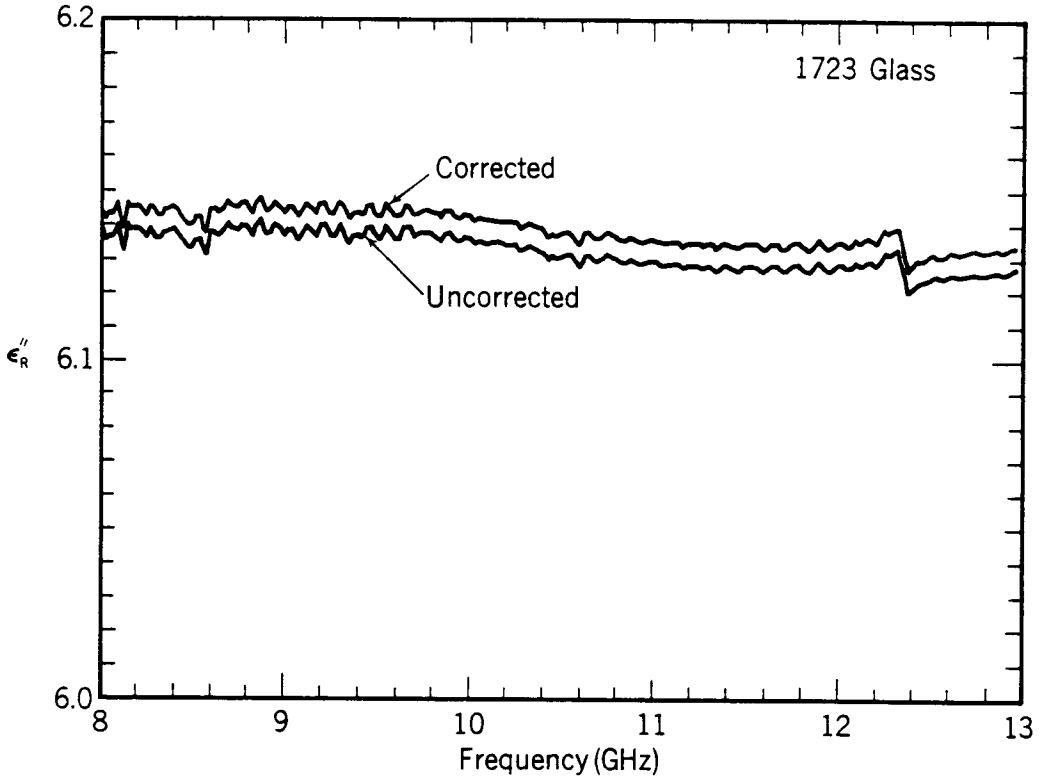

Figure 2.19 ϵ'_R with and without gap correction using TR method for 1723 glass in a X-band waveguide. The worst case uncertainty at 10 GHz, $\Delta\epsilon'_R = 0.013$.

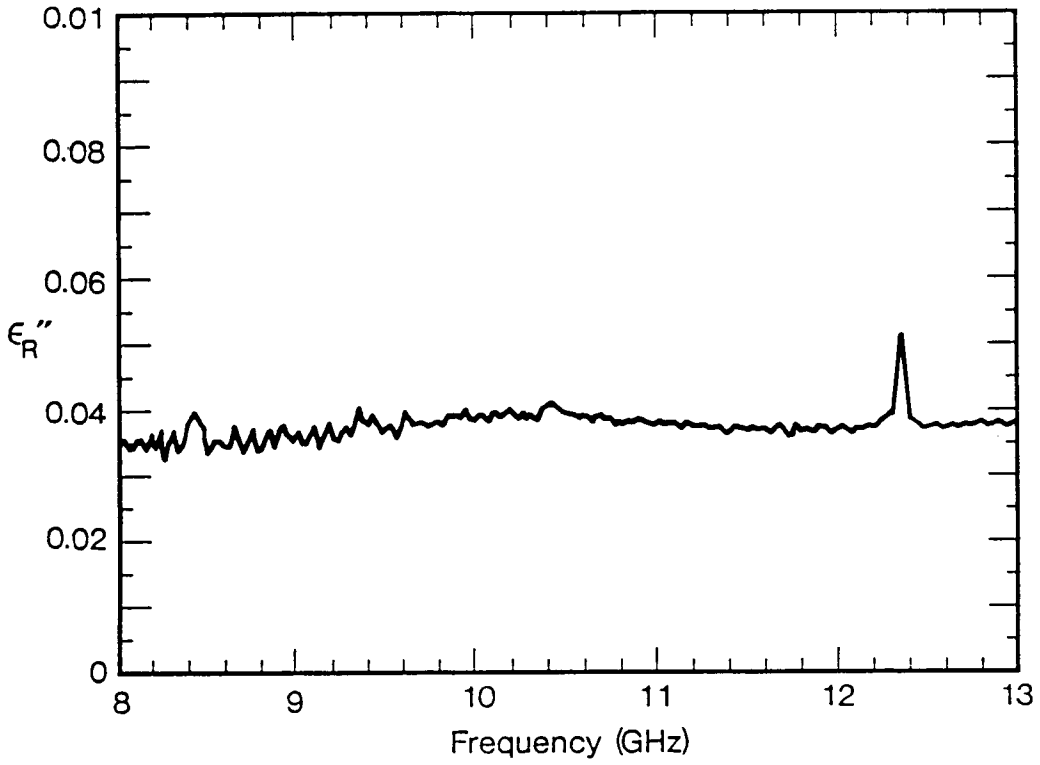

Figure 2.20 ϵ_R'' using TR method for 1723 glass in a X-band waveguide. The worst case uncertainty at 10 GHz, $\Delta\epsilon_R'' = 0.009$.

transmission/reflection models to break down (including the one developed in this report) for materials of high dielectric constant and/or inhomogeneous samples.

In order to minimize the effects of higher modes, shorter samples can be used. Higher order modes will not appear if the sample length is less than one-half guided wave length in the material.

2.7 Uncertainty Analysis

In this section the uncertainty incurred when using the equations expounded in this report will be estimated. The sources of error in TR measurement include

- Errors in measuring the magnitude and phase of the scattering parameters.
- Gaps between the sample and sample holder and sample holder dimensional variations.
- Uncertainty in sample length.
- Line losses and connector mismatch.
- Uncertainty in reference plane positions.

Correction for errors arising from gaps around the sample is obtained from equations available in the literature [12], [13], [14]. The formulas given in the literature generally undercorrect for the real part of the permittivity and overcorrect for the imaginary part of the permittivity. We assume that all measurements of permittivity have been corrected for air gaps around the sample before the following uncertainty analysis is applied. Errors from precision air-line dimensional variations have been studied by Hill [15], who showed that these uncertainties are much smaller than the systematic uncertainty introduced by the network analyzer. In order to evaluate the uncertainty introduced by the measured scattering parameters, a differential uncertainty analysis is applicable with the uncertainty due to S_{11} and S_{21} evaluated separately. We assume that the total uncertainty can be written as

$$\frac{\Delta\epsilon'_R}{\epsilon'_R} = \frac{1}{\epsilon'_R}\sqrt{\left(\frac{\partial\epsilon'_R}{\partial|S_\alpha|}\Delta|S_\alpha|\right)^2 + \left(\frac{\partial\epsilon'_R}{\partial\theta_\alpha}\Delta\theta_\alpha\right)^2 + \left(\frac{\partial\epsilon'_R}{\partial L}\Delta L\right)^2 + \left(\frac{\partial\epsilon'_R}{\partial d}\Delta d\right)^2}, \tag{2.57}$$

$$\frac{\Delta\epsilon''_R}{\epsilon''_R} = \frac{1}{\epsilon''_R}\sqrt{\left(\frac{\partial\epsilon''_R}{\partial|S_\alpha|}\Delta|S_\alpha|\right)^2 + \left(\frac{\partial\epsilon''_R}{\partial\theta_\alpha}\Delta\theta_\alpha\right)^2 + \left(\frac{\partial\epsilon''_R}{\partial L}\Delta L\right)^2 + \left(\frac{\partial\epsilon''_R}{\partial d}\Delta d\right)^2}, \tag{2.58}$$

where $\alpha = 11$ or 21, $\Delta\theta$ is the uncertainty in the phase of the scattering parameter, $\Delta|S_\alpha|$ is the uncertainty in the magnitude of the scattering parameter, Δd is the uncertainty in the air gap around the sample, and ΔL is the uncertainty in the sample length. The uncertainties used for the S-parameters depend on the specific ANA used for the measurements. The derivatives of eqs (2.12) - (2.14) can be explicitly calculated and are given below for a coaxial line:

$$\frac{\partial\epsilon^*_R}{\partial|S_{21}|} = \frac{[1-\Gamma^2z^2]\exp(j\theta)}{Q}, \tag{2.59}$$

$$\frac{\partial\epsilon^*_R}{\partial\theta_{21}} = j|S_{21}|\frac{\partial\epsilon^*_R}{\partial|S_{21}|}, \tag{2.60}$$

$$\left(\frac{\partial\epsilon^*_R}{\partial L}\right)_{S_{21}} = -C\frac{[(1-\Gamma^2)+2S_{21}\Gamma^2z]}{Q}, \tag{2.61}$$

where

$$Q = 2A\Gamma z[S_{21}z-1] + B[(1-\Gamma^2)+2S_{21}\Gamma^2z], \tag{2.62}$$

$$A = \frac{\omega^2}{2\gamma\gamma_o c_{vac}^2}\frac{1}{(1+\frac{\gamma}{\gamma_o\mu^*_R})}\left[1+\frac{1-\frac{\gamma}{\gamma_o\mu^*_R}}{1+\frac{\gamma}{\gamma_o\mu^*_R}}\right], \tag{2.63}$$

$$B = \frac{L\omega^2\mu^*_Rz}{2c_{vac}^2\gamma}, \tag{2.64}$$

$$C = -\gamma z, \tag{2.65}$$

$$\frac{\partial \epsilon_R^*}{\partial |S_{11}|} = \exp(j\theta)\frac{[1-\Gamma^2 z^2]}{P}, \tag{2.66}$$

$$\frac{\partial \epsilon_R^*}{\partial \theta_{11}} = j|S_{11}|\frac{\partial \epsilon_R^*}{\partial |S_{11}|}, \tag{2.67}$$

$$(\frac{\partial \epsilon_R^*}{\partial L})_{S_{11}} = \frac{2Cz\Gamma[1-S_{11}\Gamma]}{P}, \tag{2.68}$$

and

$$P = A[(1-z^2)+2S_{11}z^2\Gamma]+2B\Gamma z[S_{11}\Gamma-1]. \tag{2.69}$$

The measurement bounds for S-parameter data are obtained from specifications for a network analyzer. The dominant uncertainty is in the phase of S_{11} as $\mid S_{11} \mid \rightarrow 0$. The uncertainty in S_{21} is relatively constant until S_{21} $\leq$ -40 dB; it then increases abruptly. The various derivatives are plotted in figures 2.21 through 2.32.

In figures 2.33–2.38 the total uncertainty in ϵ_R^* computed from S_{21} and S_{11} is plotted as a function of normalized sample length, for low-loss and high-loss materials at 3 GHz with various values of ϵ_R^* and the guided wavelength in the material given by

$$\lambda_m = \frac{2\pi}{\sqrt{\omega^2 \frac{(\sqrt{\epsilon'^2+\epsilon''^2}+\epsilon')}{2}\mu' - (\frac{2\pi}{\lambda_c})^2}}. \tag{2.70}$$

In figures 2.33 through 2.38 the error due to the gap correction is not included. We see that the minimum uncertainty for low-loss materials occurs at multiples of one- half wavelength. The reason for this can be determined from examination of eqs (2.12), (2.14) in the limit that $S_{11} \rightarrow 0, S_{21} \rightarrow 1$ with $\Gamma \neq 0$. These equations then reduce to

$$z^2 - 1 \rightarrow 0. \tag{2.71}$$

Generally, we see a decrease in uncertainty as a function of increasing sample length. In the case of S_{21} for high-loss as shown in figures 2.35 and 2.36 we see first a general decrease in uncertainty and then an increase in uncertainty. This increase occurs because ΔS_{21} increases when the transmitted signal is less than -40 dB from the reference value. For the case of high loss

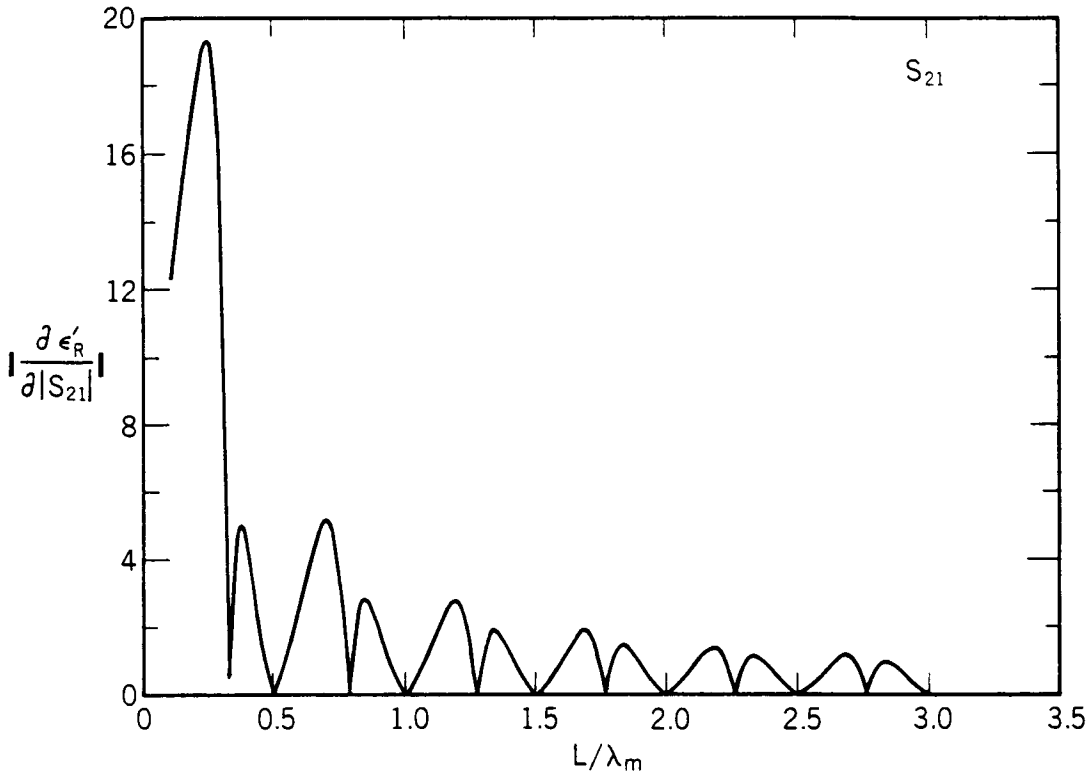

Figure 2.21 The derivative of ϵ'_R with respect to $|S_{21}|$ with $\epsilon^*_R = (10.0, 0.01)$.

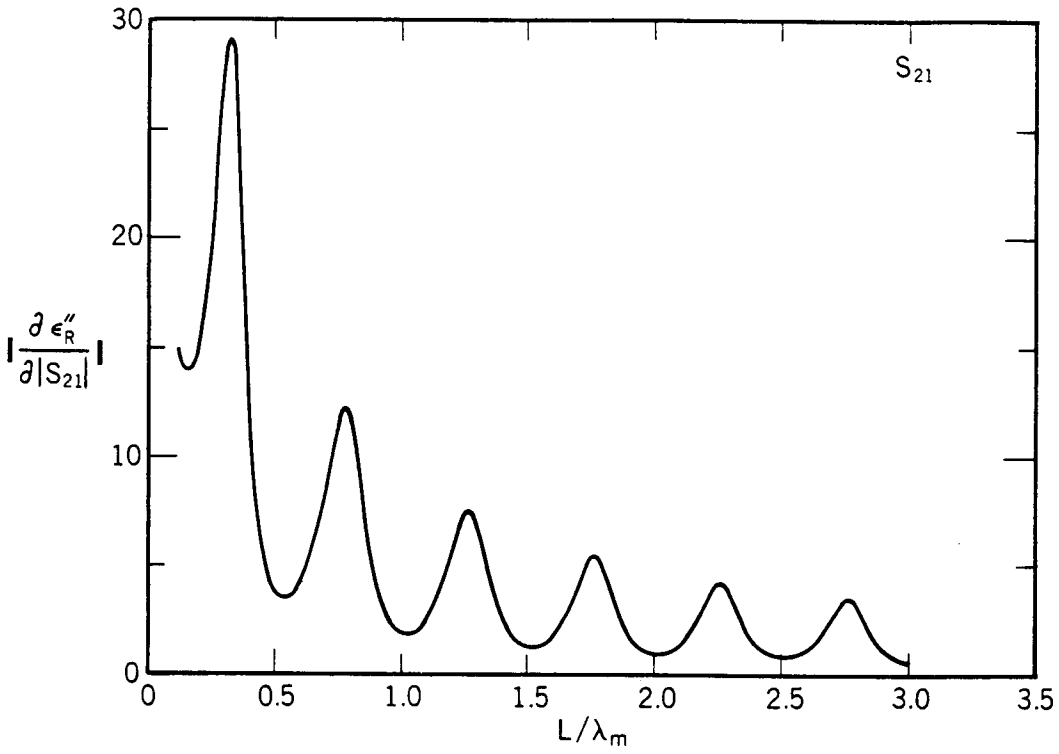

Figure 2.22 The derivative of ϵ_R'' with respect to $|S_{21}|$ with $\epsilon_R^* = (10.0, 0.01)$.

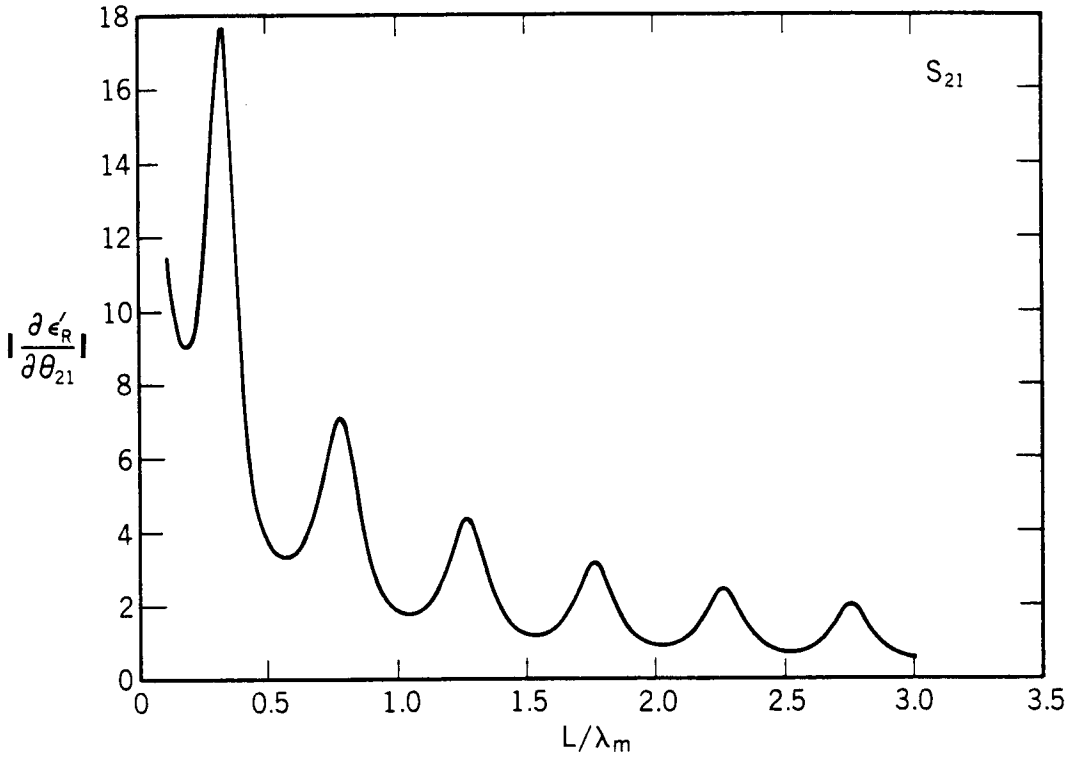

Figure 2.23 The derivative of ϵ_R' with respect to θ using S_{21} with $\epsilon_R^* = (10.0, 0.01)$.

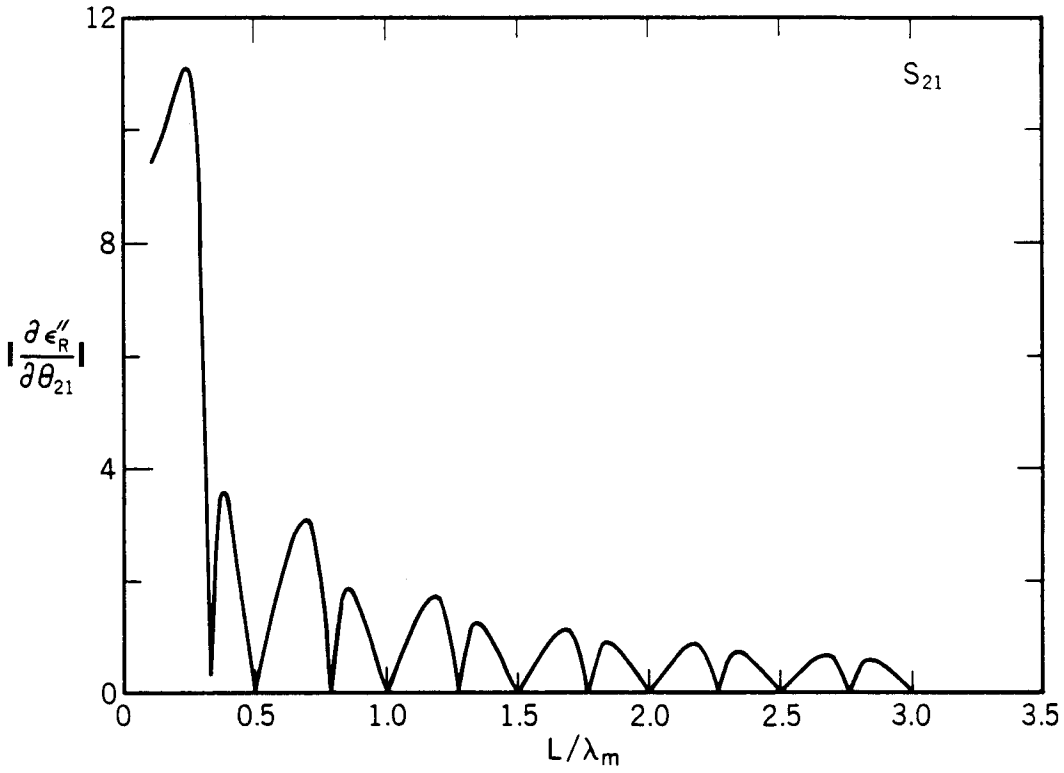

Figure 2.24 The derivative of ϵ''_R with respect to θ using S_{21} with $\epsilon^*_R = (10.0, 0.01)$.

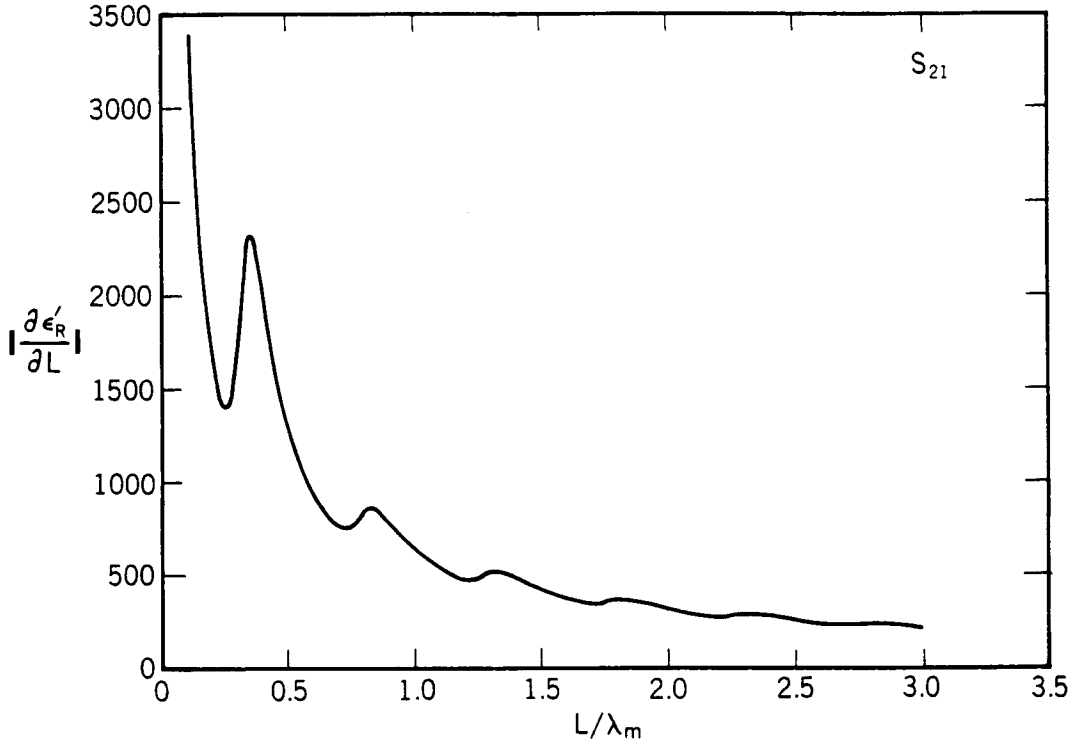

Figure 2.25 The derivative of ϵ_R' with respect to length using S_{21} with $\epsilon_R^* = (10.0, 0.01)$.

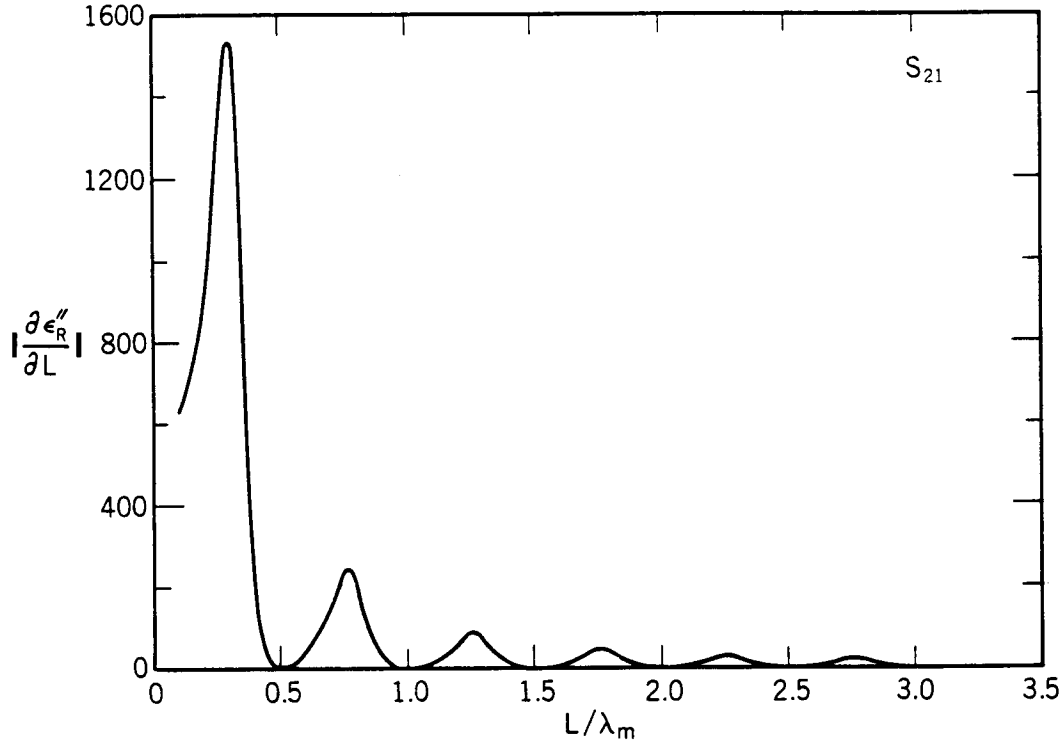

Figure 2.26 The derivative of ϵ_R'' with respect to length using S_{21} with $\epsilon_R^* = (10.0, 0.01)$.

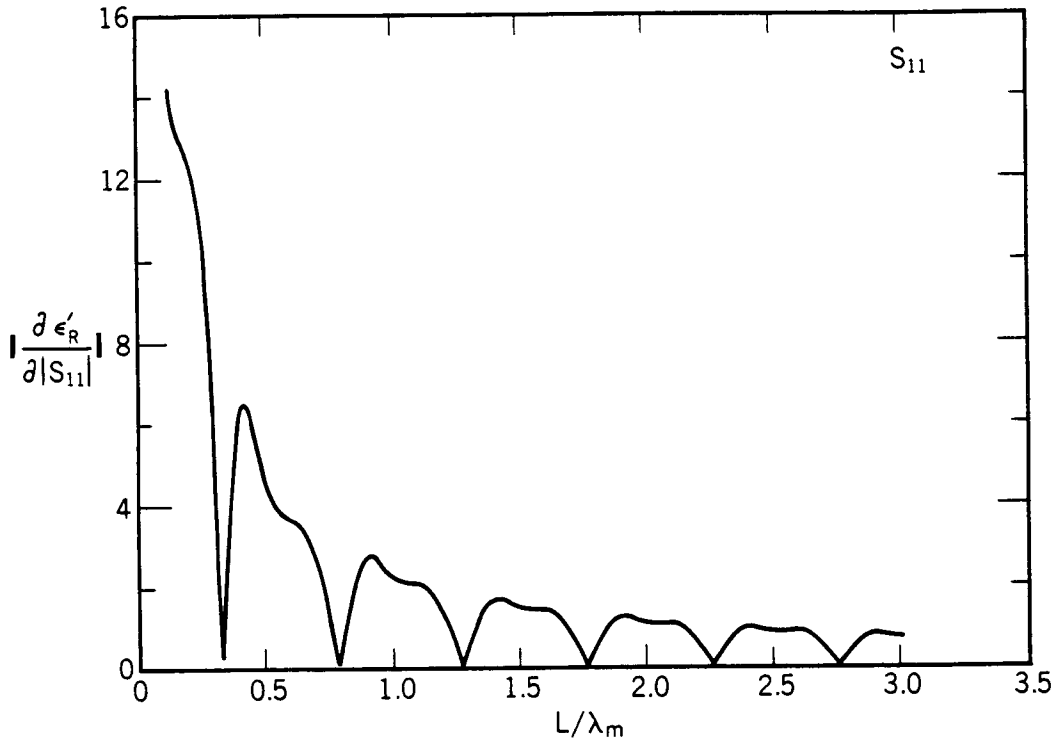

Figure 2.27 The derivative of ϵ'_R with respect to $|S_{11}|$ with $\epsilon^*_R = (5.0, 0.01)$.

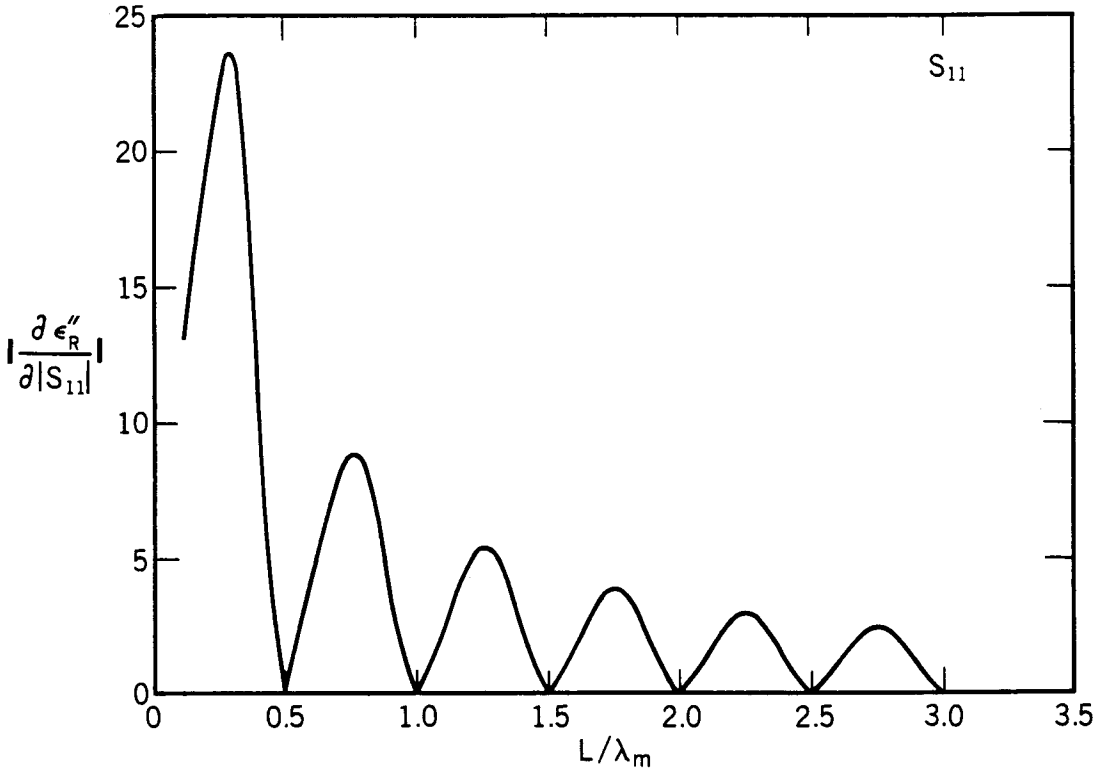

Figure 2.28 The derivative of ϵ_R'' with respect to $|S_{11}|$ with $\epsilon_R^* = (5.0, 0.01)$.

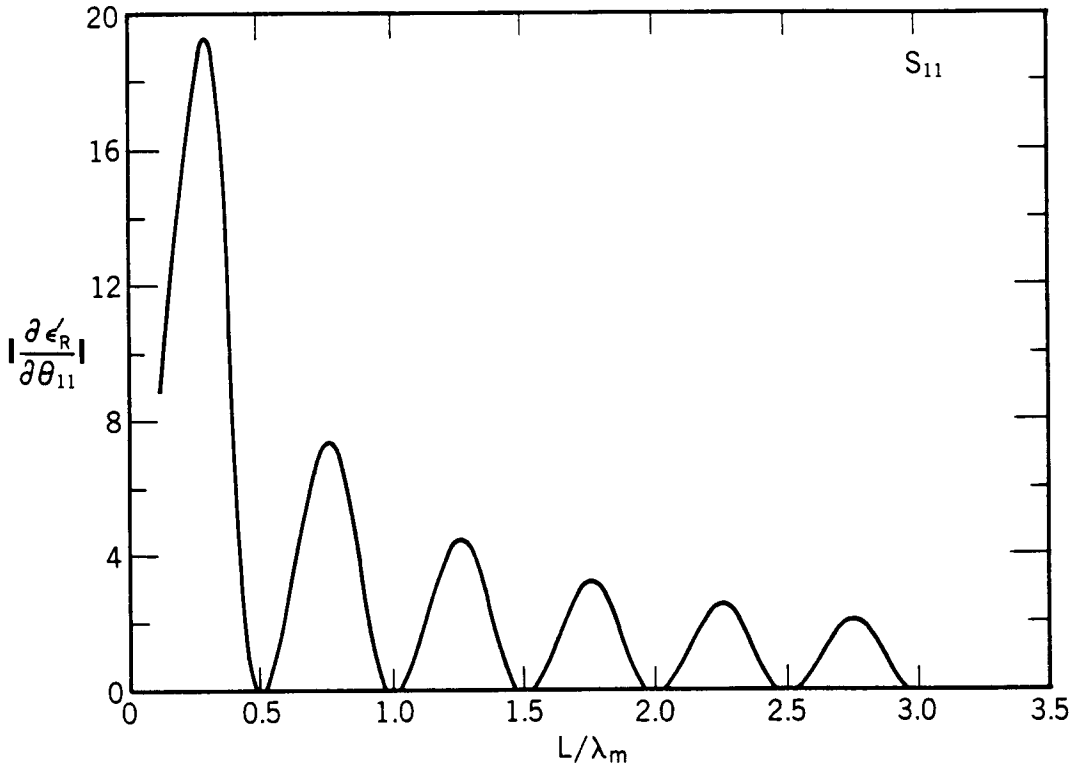

Figure 2.29 The derivative of ϵ'_R with respect to θ using S_{11} with $\epsilon^*_R = (5.0, 0.01)$.

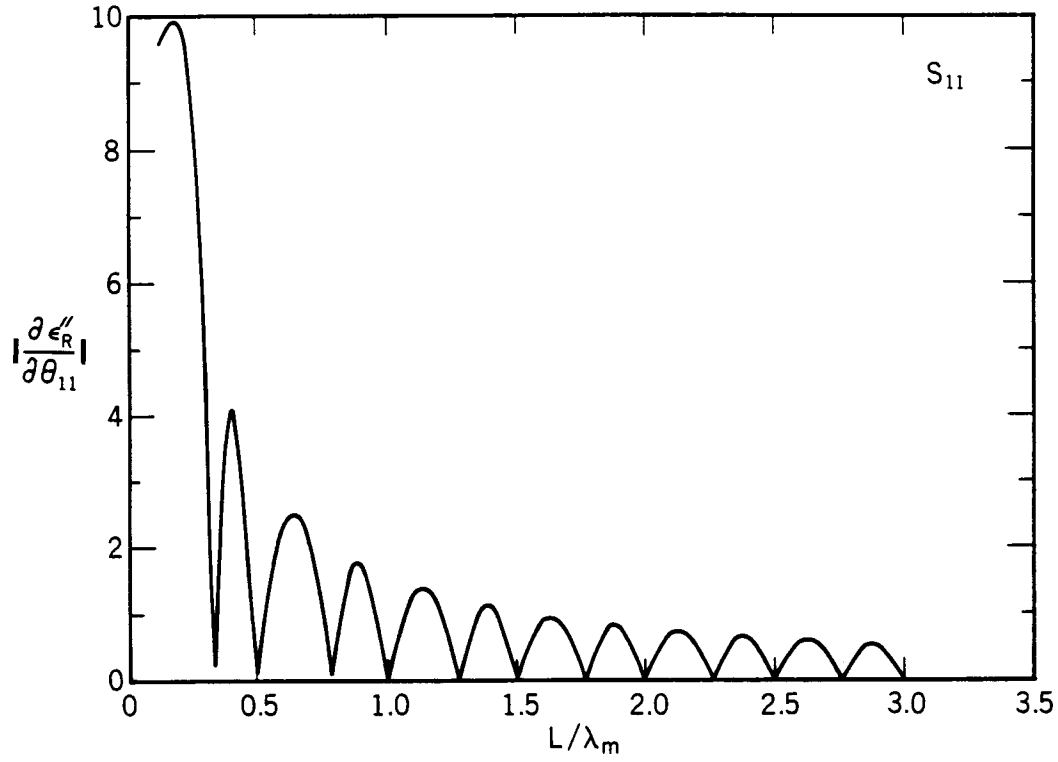

Figure 2.30 The derivative of ϵ_R'' with respect to θ using S_{11} with $\epsilon_R^* = (5.0, 0.01)$.

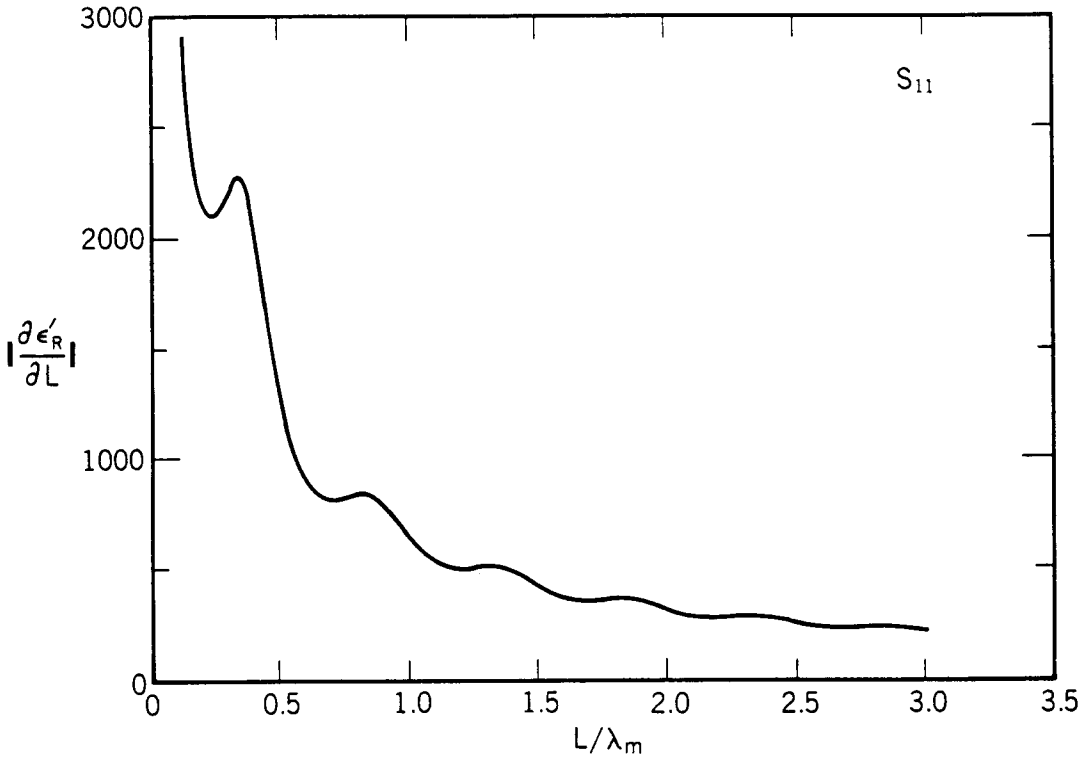

Figure 2.31 The derivative of ϵ'_R with respect to length using S_{11} with $\epsilon^*_R = (5.0, 0.01)$.

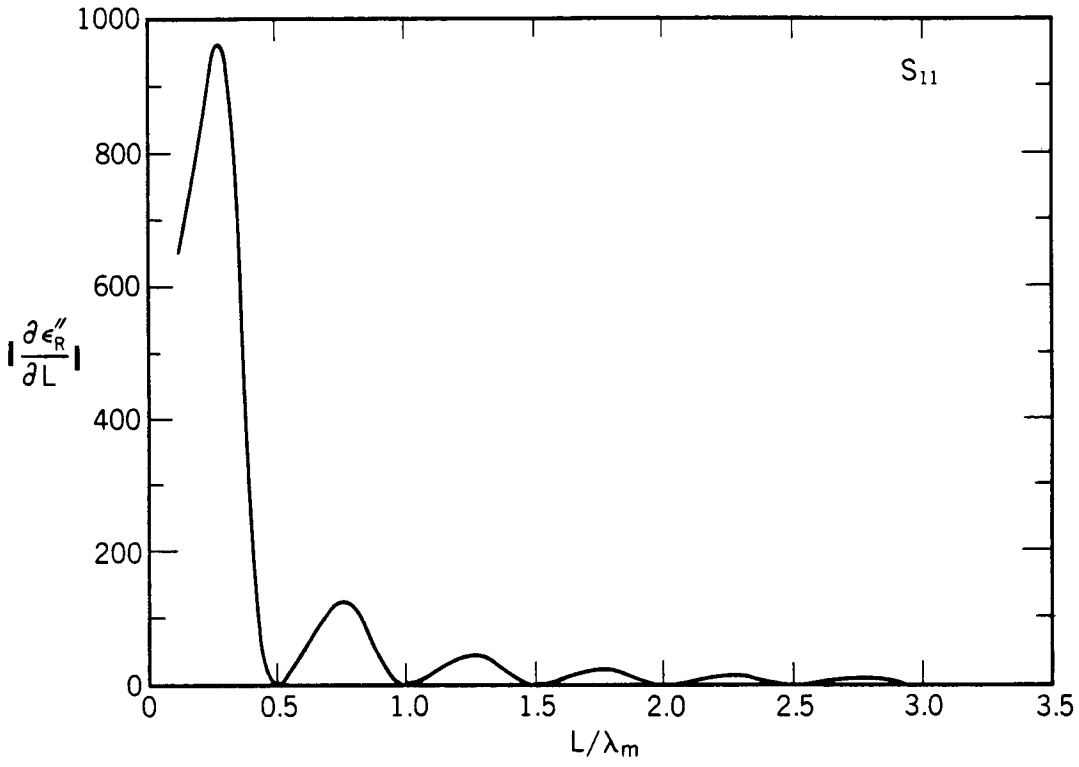

Figure 2.32 The derivative of ϵ_R'' with respect to length using S_{11} with $\epsilon_R^* = (5.0, 0.01)$.

the uncertainty in S_{11} approaches a constant value. This is so because for high-loss materials where the wavelength is much smaller than the sample length, only weak signals penetrate through the sample and thus the front face reflection dominates the S_{11} parameter.

Also, the uncertainties in the S-parameters have some frequency dependence with higher frequencies having larger uncertainties in phase. In figure 2.39 a measurement and uncertainty bounds ($\epsilon'_R \pm \Delta\epsilon'_R$) are shown; note uncertainty bounds are conservative. This is a consequence of the S-parameter uncertainties being conservatively estimated by the manufacturer.

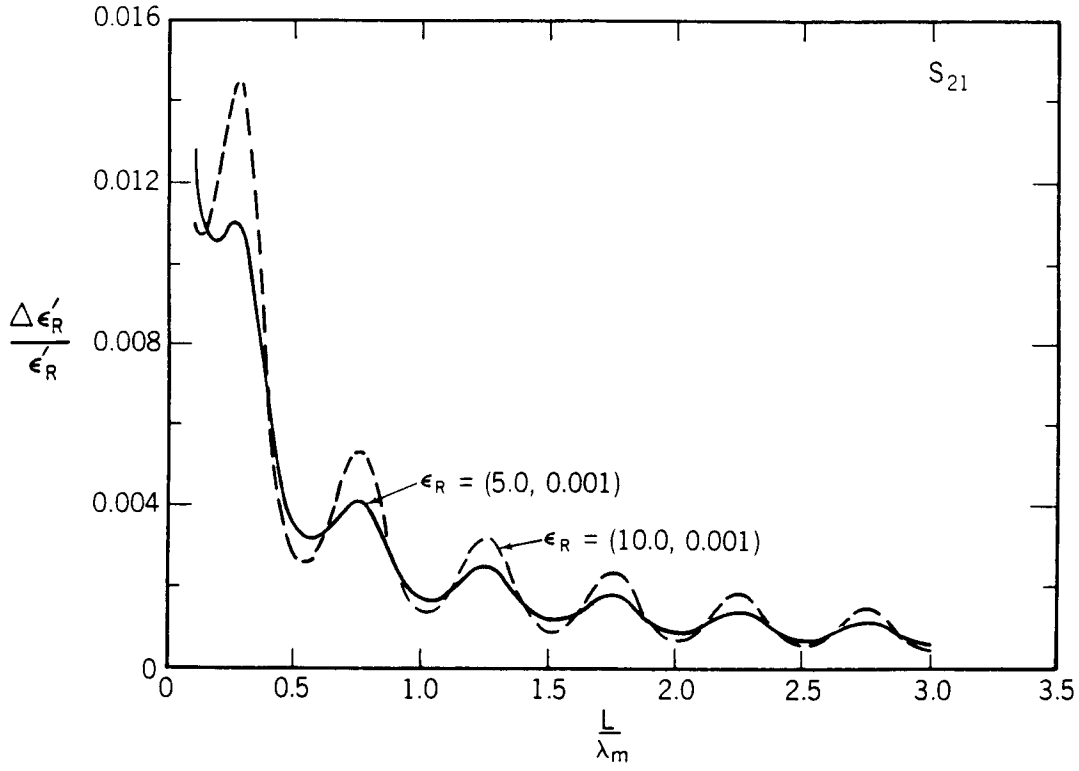

Figure 2.33 The relative uncertainty in $\epsilon'_R(\omega)$ for S_{21} for a low-loss material as a function of normalized length, with $\epsilon''_R = (5.0, 0.001)$ in solid line and (10.0,0.001) in dashed line.

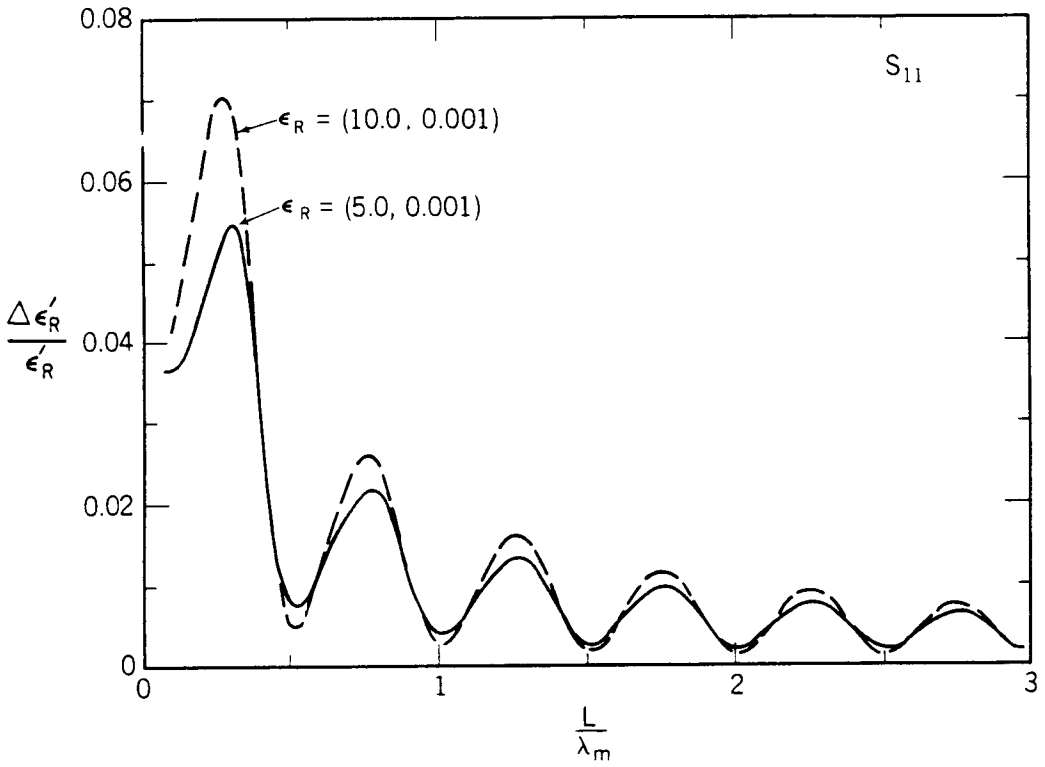

Figure 2.34 The relative uncertainty in $\epsilon'_R(\omega)$ for S_{11} for a low-loss material as a function of normalized length, with ϵ^*_R =(5.0, 0.001) in solid line and (10.0, 0.001) in dashed line.

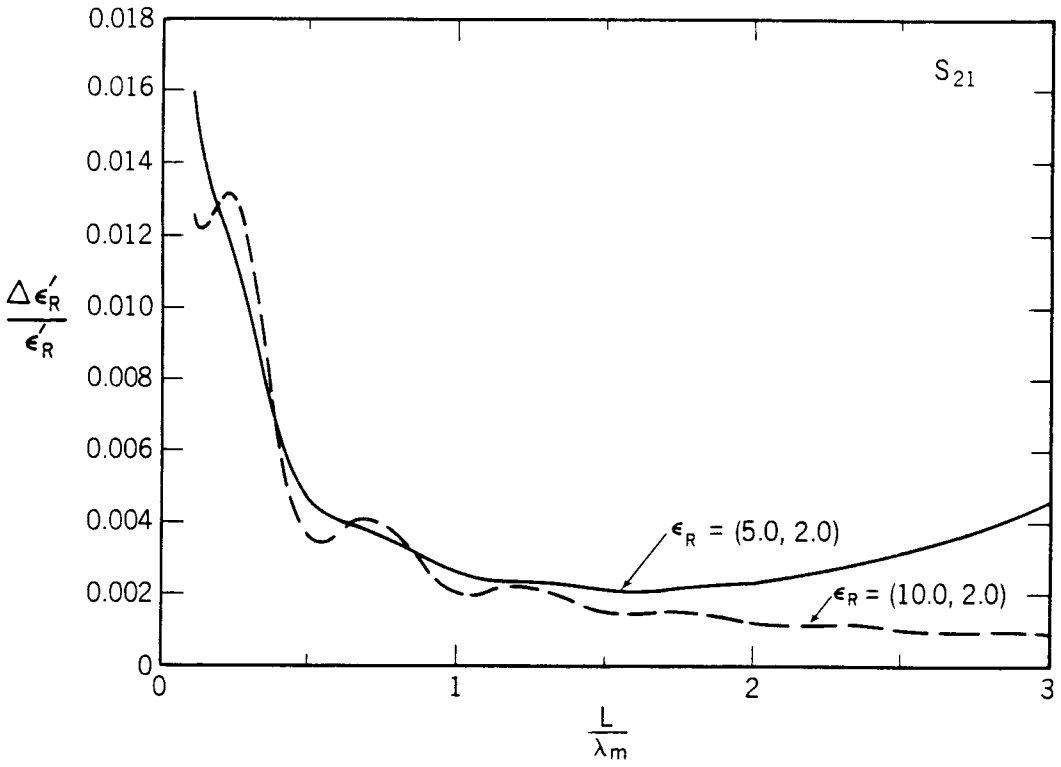

Figure 2.35 The relative uncertainty in $\epsilon'_R(\omega)$ for S_{21} for a high-loss material as a function of normalized length, with ϵ^*_R= (5.0, 2.0) in solid line and (10.0, 2.0) in dashed line.

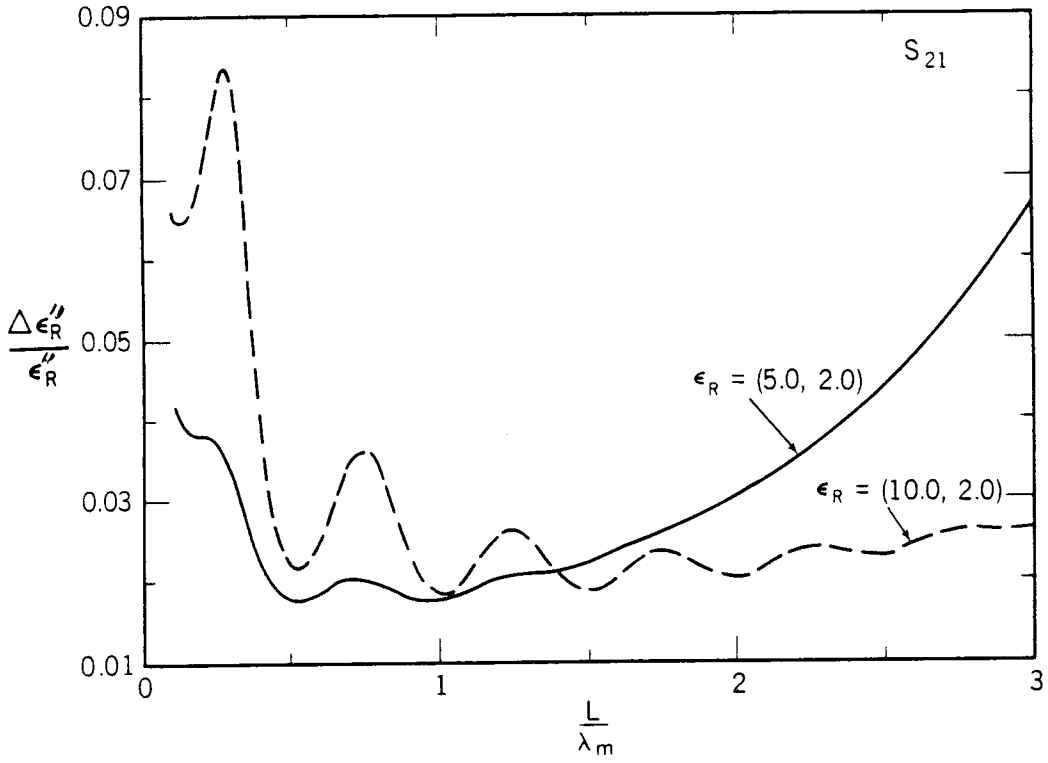

Figure 2.36 The relative uncertainty in $\epsilon''_R(\omega)$ for S_{21} for a high- loss material as a function of normalized length, for ϵ^*_R =(5.0, 2.0) in solid line and (10.0, 2.0) in dashed line.

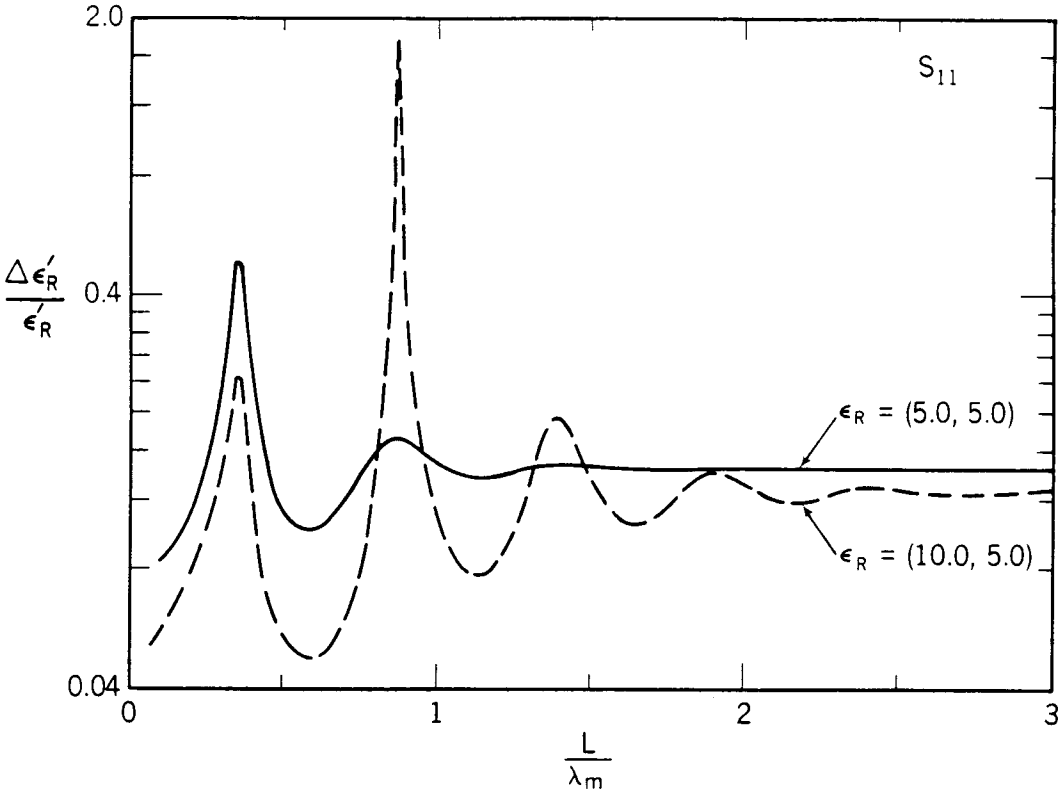

Figure 2.37 The relative uncertainty in $\epsilon_R'(\omega)$ for S_{11} as a function of frequency for a high-loss material as a function of normalized length with $\epsilon_R^* =$ (5.0, 5.0) in solid line and (10.0, 5.0) in dashed line.

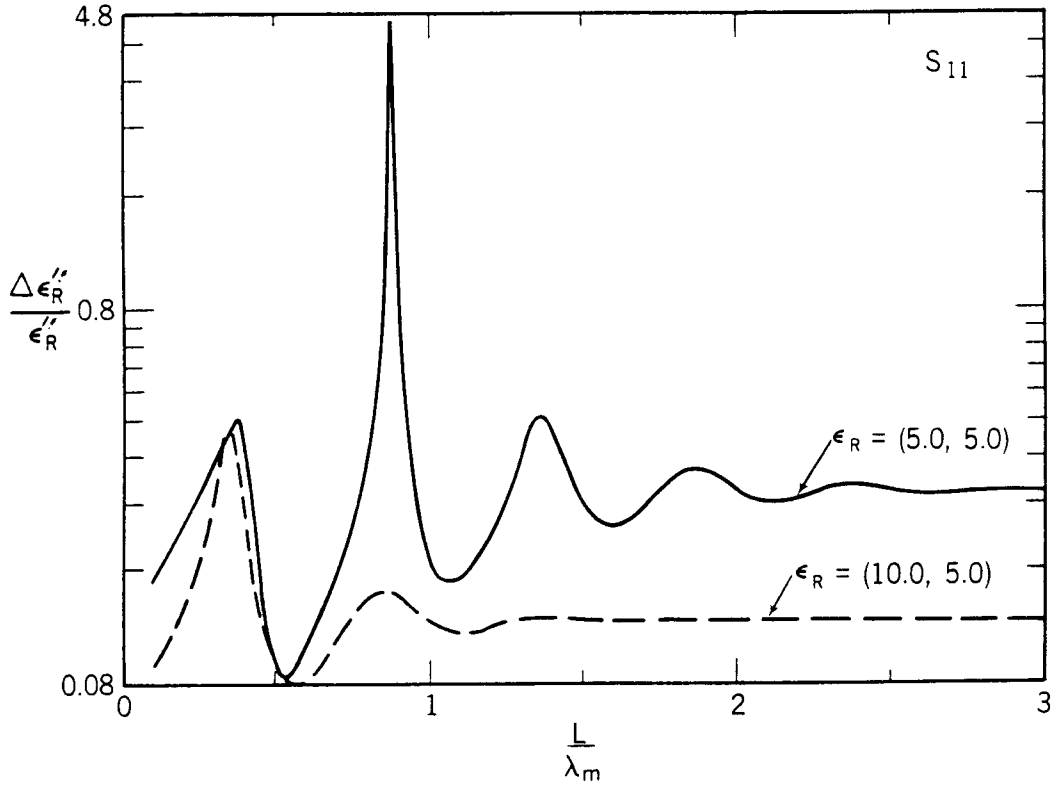

Figure 2.38 The relative uncertainty in $\epsilon_R''(\omega)$ for S_{11} for a high- loss material as a function of normalized length with $\epsilon_R^* = (5.0,5.0)$ in solid line and (10.0,5.0) in dashed line.

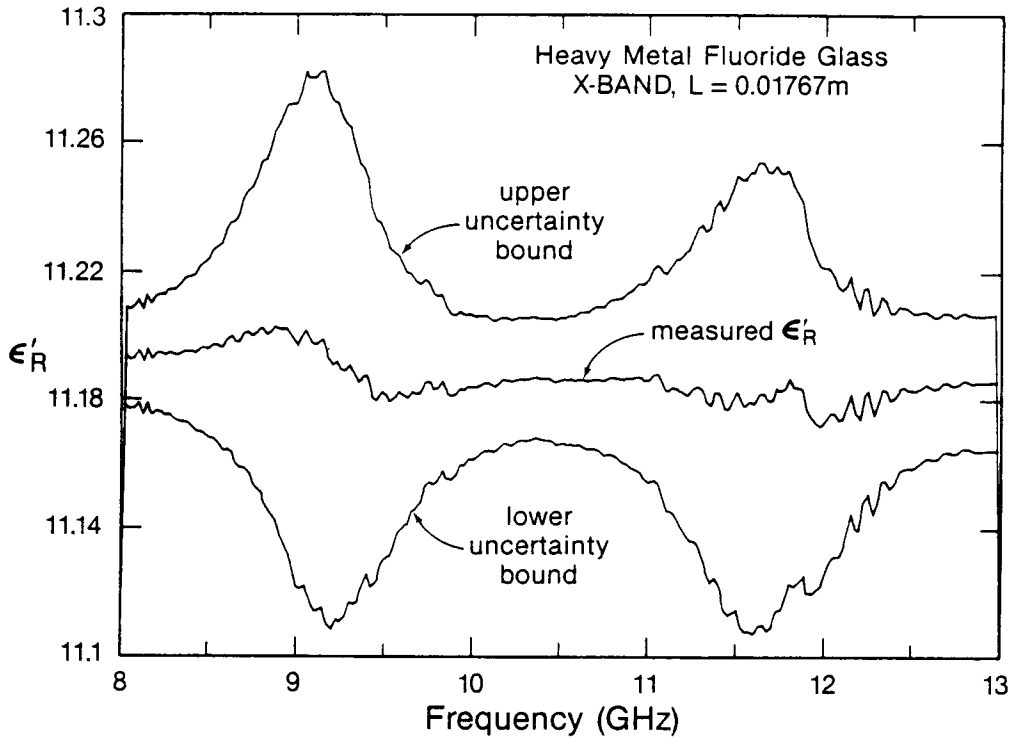

Figure 2.39 A plot of $\epsilon'_R(\omega)$ from measurements on a heavy metal fluoride glass and uncertainty bounds.

2.7.1 Uncertainty in Gap Correction

The correction for an air gap between the wall of the sample holder and sample is very important for measurements of high permittivity materials. In addition, the uncertainty in the gap correction is very important for high permittivity materials and may actually dominant the uncertainties of the measurement. In appendix C the gap correction is worked out in detail. In this section the uncertainty in the gap correction will be worked out to be used in eqs (2.57), (2.58). The uncertainty for the air gap is related to the uncertainty in the measurement of the air gap.

Waveguide Gap Uncertainty

The uncertainty due to an air gap between sample and holder can be calculated from the partial derivatives of ϵ_R^* with respect to gap thicknesses, d. The relevant derivatives for waveguide are given by

$$\frac{\partial \epsilon'_{cR}}{\partial d} = \epsilon'_{mR}\left[\frac{1}{b-(b-d)\epsilon'_{mR}}\right] - \epsilon'^2_{mR}\frac{d}{[b-(b-d)\epsilon'_{mR}]^2}\ , \tag{2.72}$$

$$\frac{\partial \tan\delta_{cR}}{\partial d} = -(\tan\delta_{mR})\epsilon'_{mR}\left[\frac{b}{(b-(b-d)\epsilon'_{mR})^2}\right]\ . \tag{2.73}$$

Coaxial Gap Correction

For coaxial line the relevant derivatives are given by

$$\frac{\partial \epsilon'_{cR}}{\partial R_2} = -\epsilon'_{mR}\frac{1}{R_2(L_3-\epsilon'_{mR}L_1)} + \epsilon'^2_{mR}\frac{L_2}{R_2(L_3-\epsilon'_{mR}L_1)^2}\ , \tag{2.74}$$

$$\frac{\partial \epsilon'_{cR}}{\partial R_3} = \epsilon'_{mR}\frac{1}{R_3(L_3-\epsilon'_{mR}L_1)} + \epsilon'^2_{mR}\frac{L_2}{R_3(L_3-\epsilon'_{mR}L_1)^2}\ , \tag{2.75}$$

$$\frac{\partial \tan\delta_{cR}}{\partial R_2} = \tan\delta_{mR}\epsilon'_{mR}\left[\frac{1}{L_2R_2} + \frac{L_1}{L_2^2R_2}\right]\ , \tag{2.76}$$

$$\frac{\partial \tan\delta_{cR}}{\partial R_3} = -\tan\delta_{mR}\epsilon'_{mR}\left[\frac{1}{L_2R_3} + \frac{L_1}{L_2^2R_3}\right]\ . \tag{2.77}$$

2.7.2 Reference Plane Position Uncertainty

Another important source of error is the uncertainty in the location of the reference planes. Generally when TR experiments are carried out, the sample is placed flush with the end of the sample holder and hence coincident with a calibration reference plane. This placement procedure leaves room for positioning errors, particularly when the sample is loose. The error introduced by incorrect positioning of the sample can be estimated in terms of the error in the reference plane transformation terms eqs (2.15), (2.16). If we have an uncertainty of ΔL in the sample position then

$$S_{11} = R_1^2|S_{11}|e^{j\theta} = |S_{11}|\exp[j\theta - 2\gamma_o(L_1 + \Delta L_1)]. \tag{2.78}$$

The error in the measured angle is given by

$$\Delta\theta \simeq 2j\gamma_o\Delta L = 4\pi\frac{\Delta L}{\lambda}. \tag{2.79}$$

Therefore small reference plane positioning errors can, in principle, introduce large uncertainties in the S_{11} phase at high frequencies. One way to minimize this is to use equations that are invariant to reference plane position.

Chapter 3

Short-Circuit Line

3.1 Theory

The short-circuit line measurement (SCL) was introduced by Roberts and von Hippel [19] over fifty years ago as an accurate broadband measurement procedure. The short-circuit line measurement is a 1-port measurement made either with a slotted line apparatus or an ANA. The short-circuit may either be fixed in the line or moveable. The advantage of a moving short-circuit [3] is that it allows many separate measurements at a given frequency and allows the sample to be placed in either a strong electric field or strong magnetic field region. Generally, a high electric field is advantageous for permittivity measurements, whereas a high magnetic field is advantageous for permeability measurements.

Ligthart [7] developed an analytical method for permittivity measurements at microwave frequencies using an averaging procedure. In Ligthardt's study, a single-mode cylindrical waveguide was filled with a homogeneous dielectric with a moving short- circuit positioned beyond the sample; however, this study focused primarily on single frequency measurements rather than on broadband measurements. Chao [20] presented results of SCL measurements using a slotted line and also an uncertainty analysis for single frequency measurements. Chao found that accuracy was reduced when the reflection coefficient was dominated by the front face contribution.

With the introduction of modern ANA systems it is possible to measure

the 1-port scattering parameters with high precision, over a broad band of frequencies. When an ANA is used the sample is positioned in either a waveguide or coaxial line and the reflection coefficient (which in this case is S_{11}) is measured. The determination of the permittivity proceeds by solving a transcendental equation which involves the sample length, sample position, and reflection coefficient. With modern computer systems, iterative procedures are easy to implement; however, they require an initial guess.

Dakin and Work [21] presented a procedure for low-loss materials and Bowie and Kelleher [22] presented a rapid graphical technique for solving the scattering equations. The short-circuit line method is well suited for high temperature measurements since these devices can be easily inserted into tube furnaces. This technique was utilized by Brydon [23] for measuring permittivity of alumina, beryllia and quartz in the temperature range of $20 - 700^{o}C$.

In the case of a slotted line, a sample is placed in the transmission line and the voltage standing wave ratio VSWR is measured. An equation that relates the VSWR to the dielectric parameters can be developed.

Uncertainties in the SCL method include network analyzer uncertainties, sample gaps, wall and short-circuit losses, and measurement of sample dimensions. There are also uncertainties in locating the sample reference planes and uncertainties in distance from sample to the short. The uncertainty in the network analyzer parameters usually are well documented by the manufacturer [4].

The goal of this second part of this technical report is to summarize the short-circuit line measuring procedure. In the following sections the ANA and slotted line measurement processes are summarized and then an uncertainty analysis for the SCL method are presented.

3.1.1 Reflection Coefficient Method

We now consider the measurement which uses the reflection coefficient (S_{11}). This method is generally used when an ANA is available. We begin with a mathematical analysis of the electric fields in the sample.

Consider a sample in a transmission line as indicated in figure 3.1. Assuming only the dominant mode in the waveguide we can write down the following expressions for the electric fields

$$E_I = \exp(-\gamma_o x) + C_1 \exp(\gamma_o x), \tag{3.1}$$

$$E_{II} = C_2 \exp(-\gamma x) + C_3 \exp(\gamma x), \tag{3.2}$$

$$E_{III} = C_4 \exp(-\gamma_o (x - L)) + C_5 \exp(\gamma_o (x - L)), \tag{3.3}$$

where

$$\gamma = j\sqrt{\frac{\omega^2 \mu_R^* \epsilon_R^*}{c_{vac}^2} - \left(\frac{2\pi}{\lambda_c}\right)^2}, \tag{3.4}$$

$$\gamma_o = j\sqrt{\left(\frac{\omega}{c_{lab}}\right)^2 - \left(\frac{2\pi}{\lambda_c}\right)^2}. \tag{3.5}$$

In eqs (3.1)-(3.3) we assumed transverse electromagnetic fields and no radial dependence. We wish to determine the coefficients in eqs (3.1)– (3.3) by imposing boundary conditions on the system of equations. The boundary conditions are:

- Tangential component of the electric field is continuous at sample interfaces.
- Tangential component of the magnetic field is continuous at sample interfaces.
- The electric field is null at the short-circuit position.

Equations for the coefficients in eqs (3.1)- (3.3) can be obtained by application of the boundary conditions at the interfaces ($x = 0$ and $x = L$):

$$1 + C_1 = C_2 + C_3, \tag{3.6}$$

$$C_2 \exp(-\gamma L) + C_3 \exp(\gamma L) = C_4 + C_5, \tag{3.7}$$

$$\frac{\gamma_o \mu}{\gamma \mu_o}[C_1 - 1] = C_3 - C_2, \tag{3.8}$$

$$\frac{\gamma \mu_o}{\gamma_o \mu}[C_2 \exp(-\gamma L) - C_3 \exp(\gamma L)] = C_4 - C_5, \tag{3.9}$$

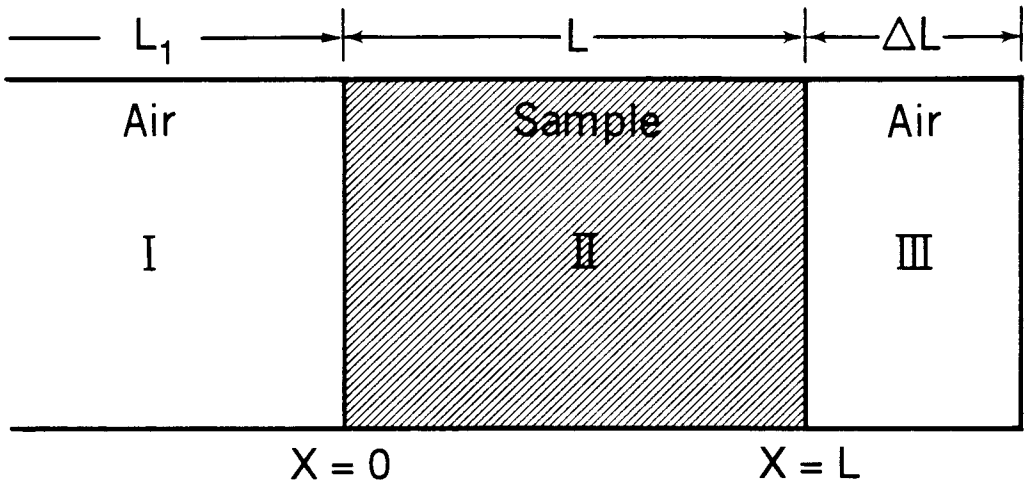

Figure 3.1 A transmission line with a short-circuit termination.

$$C_5 = -\delta C_4, \tag{3.10}$$

where

$$\delta = \exp(-2\gamma_o \Delta L), \tag{3.11}$$

and ΔL is the distance from the short-circuit to the sample. Equations (3.6)-(3.10) yield the following system of equations:

$$C_1 - C_2 - C_3 = -1, \tag{3.12}$$

$$\eta C_2 + \frac{C_3}{\eta} + (\delta - 1)C_4 = 0, \tag{3.13}$$

$$C_1 + \beta C_2 - \beta C_3 = 1, \tag{3.14}$$

$$\beta\eta C_2 - \frac{\beta}{\eta} C_3 - C_4(1 + \delta) = 0, \tag{3.15}$$

where

$$\beta = \frac{\gamma \mu_o}{\gamma_o \mu}, \tag{3.16}$$

$$\eta = \exp(-\gamma L). \tag{3.17}$$

Note that $1/\beta$ is an effective impedance. In matrix form these equations can be expressed as

$$\begin{pmatrix} 1 & -1 & -1 & 0 \\ 0 & \eta & \frac{1}{\eta} & \delta - 1 \\ 1 & \beta & -\beta & 0 \\ 0 & \beta\eta & -\frac{\beta}{\eta} & -(1+\delta) \end{pmatrix} \begin{pmatrix} C_1 \\ C_2 \\ C_3 \\ C_4 \end{pmatrix} = \begin{pmatrix} -1 \\ 0 \\ 1 \\ 0 \end{pmatrix}. \tag{3.18}$$

Solution of eqs (3.12)–(3.15) yields an equation for the permittivity in terms of the reflection coefficient, $\rho = S_{11} = C_1$, with the sample located a distance ΔL from the short:

$$S_{11} = \rho = \frac{-2\beta\delta + [(\delta + 1) + (\delta - 1)\beta^2] \tanh \gamma L}{2\beta + [(\delta + 1) - (\delta - 1)\beta^2] \tanh \gamma L}, \tag{3.19}$$

or in terms of hyperbolic functions

$$S_{11} = \frac{\tanh\gamma L + \beta\tanh\gamma_0\Delta L - \beta(1+\beta\tanh\gamma L\tanh\gamma_0\Delta L)}{\tanh\gamma L + \beta\tanh\gamma_0\Delta L + \beta(1+\beta\tanh\gamma L\tanh\gamma_0\Delta L)}. \tag{3.20}$$

In the derivation, it is assumed that the sample plane coincides with the measurement calibration plane. This is not the case in general; however, one can transform the reference plane position by a simple procedure. To accomplish this we proceed by assuming that the most general expression for the reflection coefficient is given by

$$\rho_{trans} = R_1^2\rho, \tag{3.21}$$

where ρ_{trans} is the reflection coefficient at the calibration reference plane position and

$$R_1 = \exp(-\gamma_o L_1), \tag{3.22}$$

and L_1 is the distance from the calibration plane to the sample front face. Equation (3.21) transforms the reflection coefficient from the calibration plane to the plane of sample front face. It is of interest in many applications to eliminate the distance L_1 from eq (3.19). To accomplish this it is necessary to measure S_{11} of the empty sample holder,

$$\rho_{empty} = -\exp(-2\gamma_o[L_1+\Delta L+L]) = \exp(-2\gamma_0 L_{air}), \tag{3.23}$$

and therefore,

$$\frac{\rho_{trans}}{\rho_{empty}} = -\exp(2\gamma_0[\Delta L+L])\rho. \tag{3.24}$$

If both the permeability and the permittivity are required then measurement data for two different short-circuit positions are required.

Equations for Two Short-Circuit Positions

It is possible to obtain an explicit solution to eq (3.19) when measurements at two different short-circuit positions are taken. The explicit solution is obtained by solving eq (3.19) at a given short-circuit position for $\tanh\gamma L$ and then substituting this expression into eq (3.19) at another short-circuit

position. For two different short-circuit positions at the same frequency we obtain

$$\rho_1 = \frac{2\beta\delta_1 - [(\delta_1+1)+(\delta_1-1)\beta^2]\tanh\gamma L}{-2\beta + [(\delta_1-1)\beta^2 - (\delta_1+1)]\tanh\gamma L}, \tag{3.25}$$

$$\rho_2 = \frac{2\beta\delta_2 - [(\delta_2+1)+(\delta_2-1)\beta^2]\tanh\gamma L}{-2\beta + [(\delta_2-1)\beta^2 - (\delta_2+1)]\tanh\gamma L}, \tag{3.26}$$

where δ_1, δ_2 denote the phases calculated from eq (3.11) for $\Delta L_1, \Delta L_2$. These equations yield:

$$\tanh\gamma L = \frac{2\beta(\delta_1+\rho_1)}{\beta^2(\rho_1+1)(\delta_1-1)+(1-\rho_1)(\delta_1+1)}, \tag{3.27}$$

$$\beta^2 = \frac{\delta_1(\delta_2(\rho_1-\rho_2)+\rho_1\rho_2+1-2\rho_2)-(\delta_2(\rho_1(\rho_2-2)+1)+\rho_2-\rho_1)}{\delta_1(\delta_2(\rho_1-\rho_2)+\rho_1\rho_2+1+2\rho_2)-(\delta_2(\rho_1(\rho_2+2)+1)+\rho_2-\rho_1)}. \tag{3.28}$$

Thus, when two measurements are made at different short-circuit positions then we can obtain ϵ_R^* explicitly; note that this solution does not contain sample length explicitly. Once β is known then eq (3.27) can be used to find permeability for magnetic materials.

3.1.2 Slotted Line Technique

In the past, another measurement procedure was commonly used for short-circuit line measurements. This measurement was based on the slotted line, which can measure the position of the VSWR relative to the sample. Consider a sample in a short- circuited transmission line as depicted in figure 3.2. We can write for the input impedance

$$Z_{in} = Z_b \tanh\gamma_2 L, \tag{3.29}$$

$$Z_{in} = Z_a \frac{\gamma_1}{\gamma_2}\tanh\gamma_2 L, \tag{3.30}$$

where Z_b is the impedance of the dielectric filled section of the line, Z_a is the characteristic impedance of the empty transmission line, and

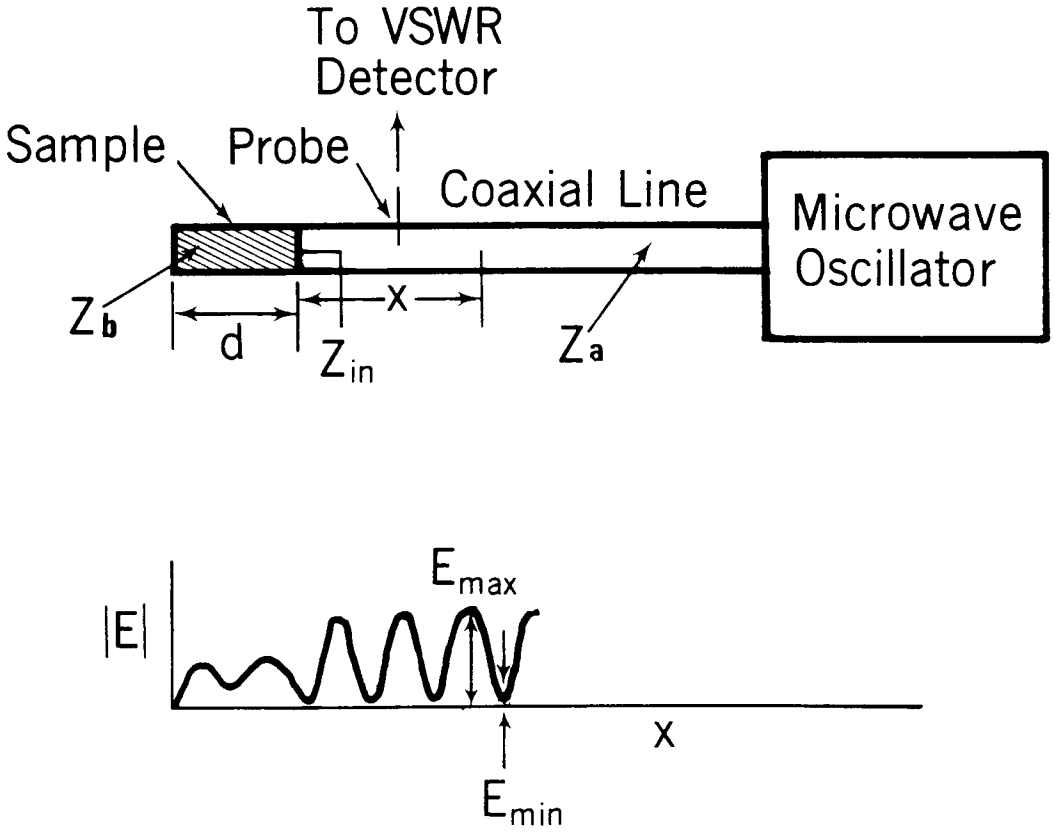

Figure 3.2 A transmission line containing sample with a slotted line measuring device for VSWR.

$$\gamma_1^2 = [(\frac{2\pi}{\lambda_c})^2 - \frac{\omega^2}{c_{lab}^2}], \tag{3.31}$$

$$\gamma_2^2 = [(\frac{2\pi}{\lambda_c})^2 - \frac{\omega^2 \epsilon_R^* \mu_R^*}{c_{vac}^2}]. \tag{3.32}$$

The impedance can be transformed along the line to a point x_o from the sample where the voltage is a maximum value. This impedance is equal to the VSWR (S) times the impedance of the line, or

$$Z = Z_{o1} \frac{[Z_{in} + Z_a \tanh \gamma_1 x_o]}{[Z_a + Z_{in} \tanh \gamma_1 x_o]} = S Z_a, \tag{3.33}$$

where

$$Z_{in} = Z_a \frac{[S - \tanh \gamma_1 x_o]}{[1 - S \tanh \gamma_1 x_o]}. \tag{3.34}$$

Therefore, we can obtain a transcendental equation

$$\frac{\tanh \gamma_2 L}{\gamma_2 L} = (\frac{1}{\gamma_1 L}) \frac{S - \tanh \gamma_1 x_o}{1 - S \tanh \gamma_1 x_o}, \tag{3.35}$$

for the permittivity. This equation can be solved by general iterative methods, for example, a Newton-Raphson procedure. Iterative solutions require an initial guess of the dielectric parameters. If this initial guess is in the neighborhood of the correct solution, the iteration will rapidly converge, in a quartic manner, to the correct root. There are an infinite number of roots of this equation so care must be taken in selecting the proper root. Generally, however, some knowledge of the correct solution is known *a priori* and can be used in the root selection process.

3.2 Corrections to Data

Once a set of measurements has been made, it is necessary to correct the data for known errors. Known error sources include air gaps around samples, short-circuit and waveguide wall imperfections, together with waveguide and short- circuit losses. The wall losses can be taken into account by attenuation measurements in the guide.

Gap correction formulas (see appendix C) which are relatively easy to implement [12], [13], [14], can be found in the literature. Imperfect waveguide or coaxial line walls can also be modeled. Hill [15] has studied this problem and his results are summarized in appendix B. Waveguide losses can be corrected for by measuring the scattering parameters of the empty waveguide and calculating the appropriate attenuation constant of the guide. Also the calculated permittivity data can be smoothed. A smoothing routine using the method of maximum entropy is given in appendix G.

3.3 Instrumentation

The following apparatus is needed for broadband SCL measurements:

- Automated network analyzer or slotted line
- Data acquisition system
- Precision waveguide or coaxial line
- Data analysis system

When using an ANA it is important to know its frequency limitations. Network analyzer systems have various error sources. These errors include

- matching at connectors
- imperfect calibration standards
- non-linearity of mixers, gain and phase drifts in IF amplifiers, noise introduced by the analogue to digital converter
- imperfect tracking in dual channel systems

Generally the manufacturer furnishes the performance specifications for its system.

3.3.1 Sample Holder Specifications

The sample holder should consist of high precision waveguide or coaxial line. When 7 mm coaxial beadless air line is used, APC-7 connectors are generally preferred. Since the cutoff frequency is related to the dimensions of the guide it is important to measure the guide dimensions precisely and from these measurements to calculate the cutoff frequency. Slight discrepancies in the cutoff wavelength or sample holder length manifest themselves in the calculated permittivity.

3.3.2 Sample Preparation

The samples to be used for SCL measurements should be prepared carefully since scratches, nicks and cracks will alter the dielectric properties. The sample should be machined with care to minimize any gaps between sample holder and sample. Also the front and rear sample end faces must be machined to be very perpendicular to the rest of the sample in order to minimize mode conversion. It is also very important to minimize any unnecessary wear and tear on the sample by placing it in a secure area between measurements. The sample length measurement is critical and should be performed carefully with a precision micrometer. The following list summarizes the preparation procedure:

- Carefully select a piece of material free of unusual inhomogeneities, cracks, etc.
- Have the sample machined to fit as tightly as possible in the sample holder (generally gaps should be $< 5 \times 10^{-5}$ m (0.0004 in)).
- Measure the sample length precisely at a temperature very close to that realized in the laboratory.
- Keep the sample very clean and store in a secure area.
- Carefully store the sample holder as surface scratches or conductor bends can erode the line characteristics.

3.3.3 System Diagnostics

In order to verify the accuracy of the measurement system before each measurement, it is important to have a verification test. For the SCL method a standard comparison may consist of measuring the S-parameters of air in an empty sample holder and comparing the results to a designated standard measurement.

3.3.4 Measurement Procedure

The measurement depends on whether an ANA system or a slotted line apparatus is used. For slotted lines it is necessary to measure the VSWR and the location this VSWR maximum along the line. Then eq (3.35) can be used to calculate the complex dielectric constants. When an ANA is used the scattering parameter S_{11} is measured, over a broad band of frequencies, with the sample at a given position in the sample holder. The distance from the sample to the short- circuit must be known accurately. If both permeability and the permittivity are required, the sample must be moved in the line and the S-parameters measured in the second location.

In general it is better to make permittivity measurements when the sample is predominantly in a strong electric field region, whereas it is advantageous to perform permeability measurements when the sample is in a region of strong magnetic field. When taking broadband measurements on an ANA it is possible to calculate when the sample is immersed in the various fields strengths and then one can select the measurements to be used for permittivity and permeability calculations [13].

3.4 Measurement Results

Measurements were made on an ANA for various samples. Using eq (3.19) the permittivity was calculated and is shown in figures 3.3–3.8 for various materials. The associated uncertainties are given in figures 3.15 – 3.16. In the case of PTFE there was no measurable gap.

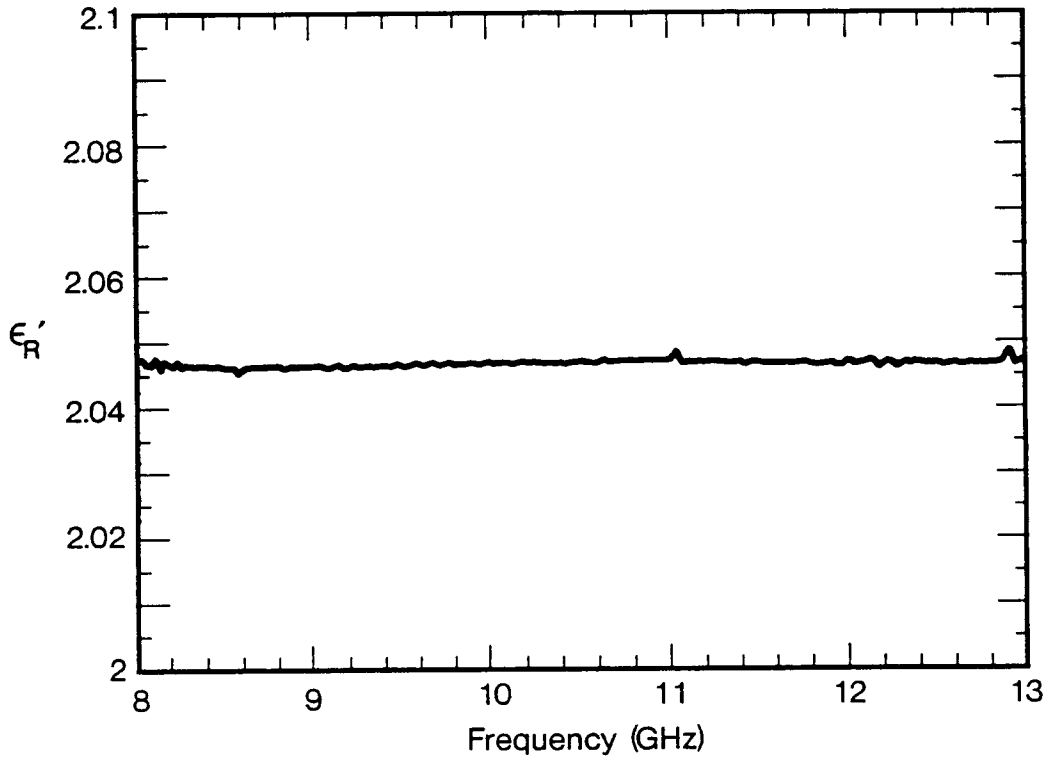

Figure 3.3 ϵ'_R using SCL in X-band waveguide for PTFE. The worst case uncertainty, $\Delta\epsilon'_R = 0.011$, at 10 GHz.

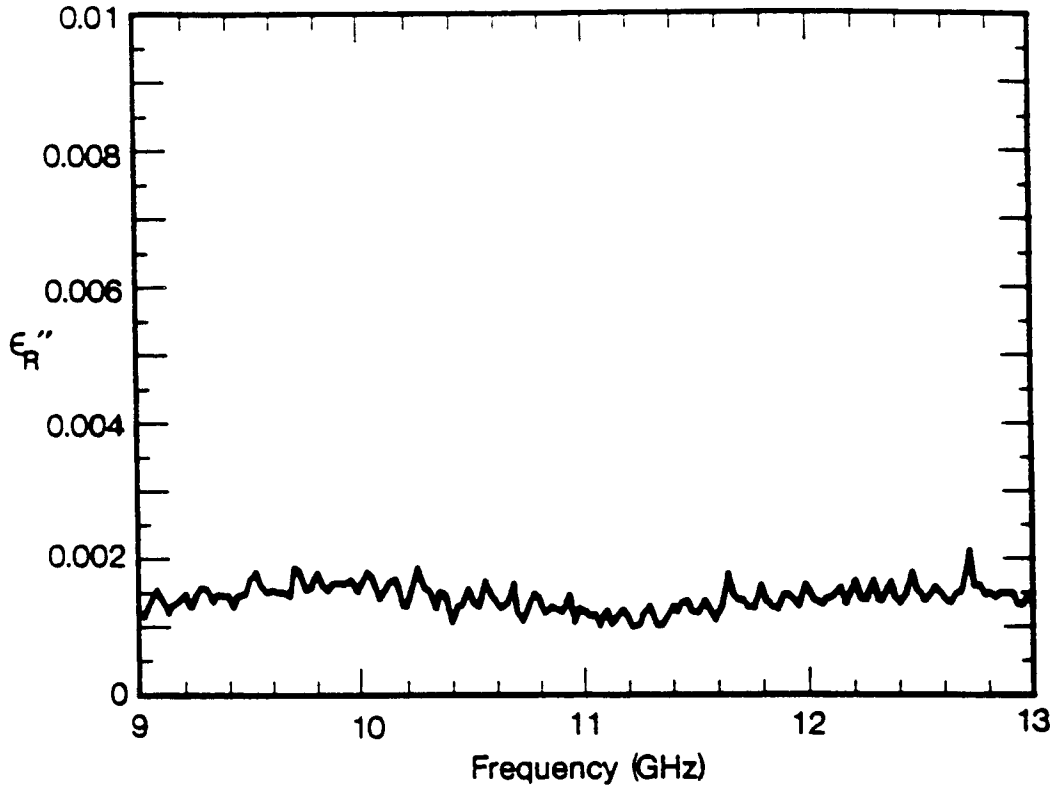

Figure 3.4 ϵ_R'' using SCL in X-band waveguide for PTFE. The worst case uncertainty, $\Delta\epsilon_R'' = 0.004$, at 10 GHz.

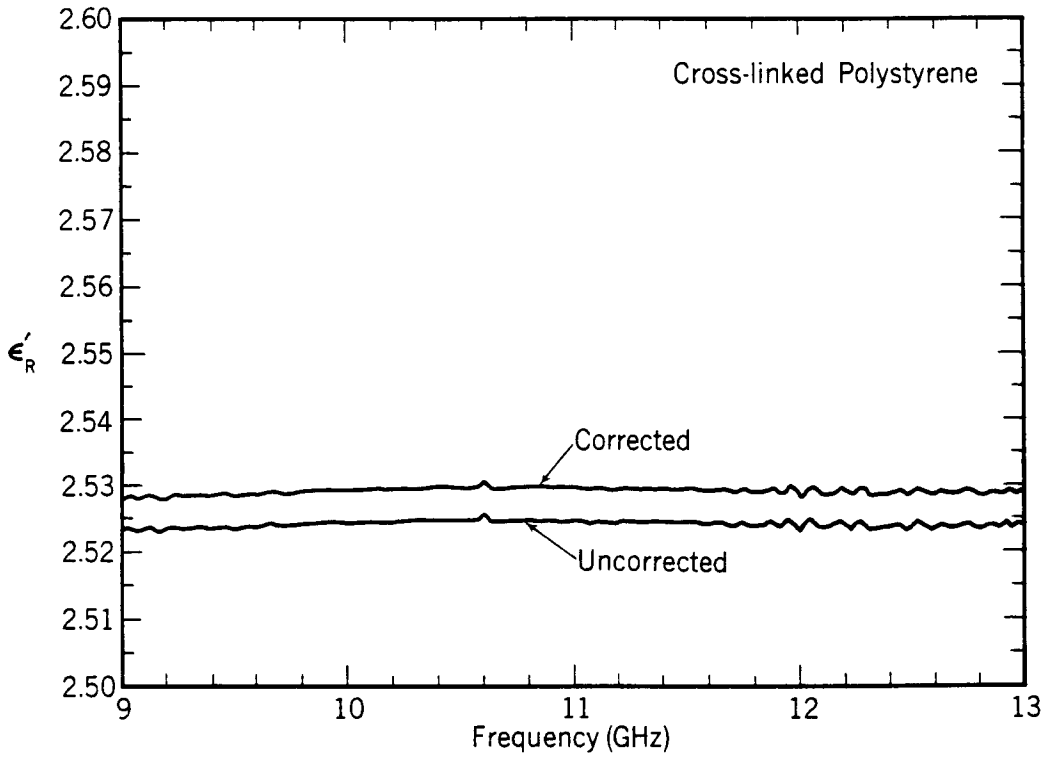

Figure 3.5 ϵ'_R with and without gap correction using SCL in X-band waveguide for cross-linked polystyrene. The worst case uncertainty, $\Delta\epsilon'_R = 0.009$, at 10 GHz.

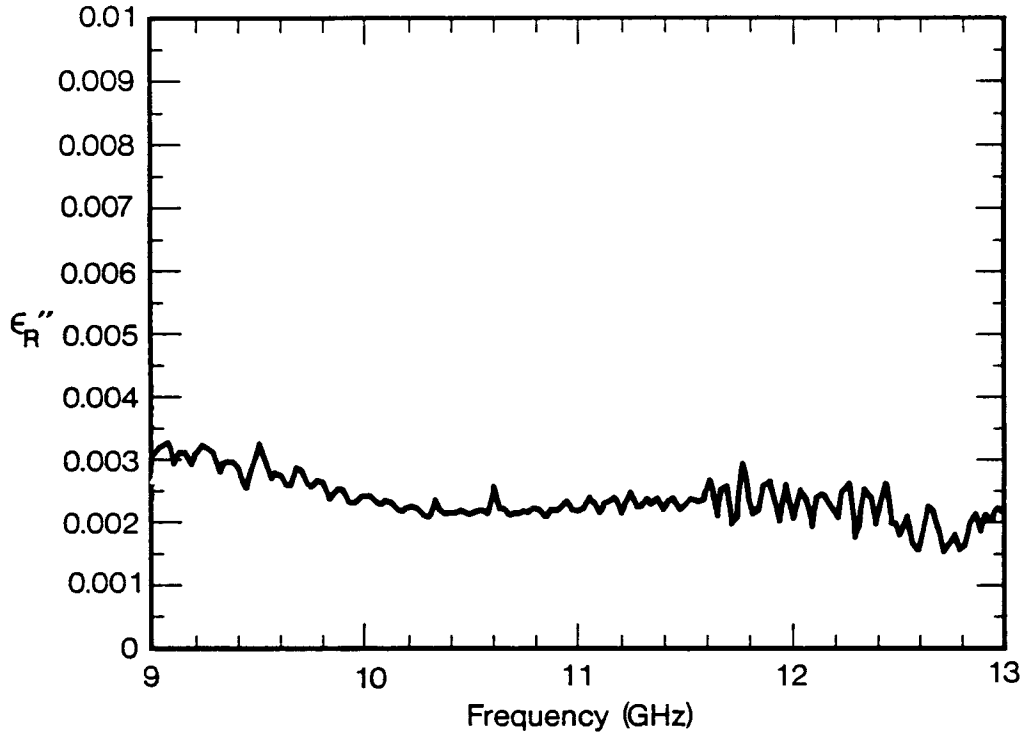

Figure 3.6 ϵ_R'' using SCL in X-band waveguide for cross-linked polystyrene. The worst case uncertainty, $\Delta\epsilon_R'' = 0.003$, at 10 GHz.

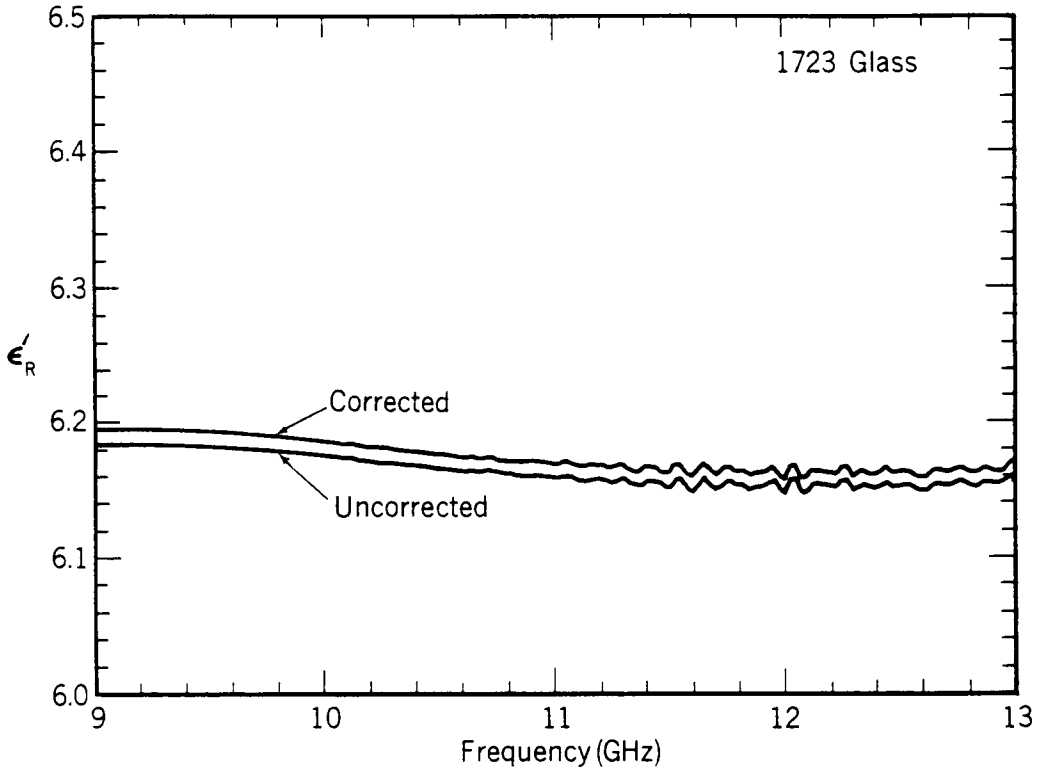

Figure 3.7 ϵ'_R with and without gap correction using SCL for 1723 glass. The worst case uncertainty, $\Delta\epsilon'_R = 0.021$, at 10 GHz.

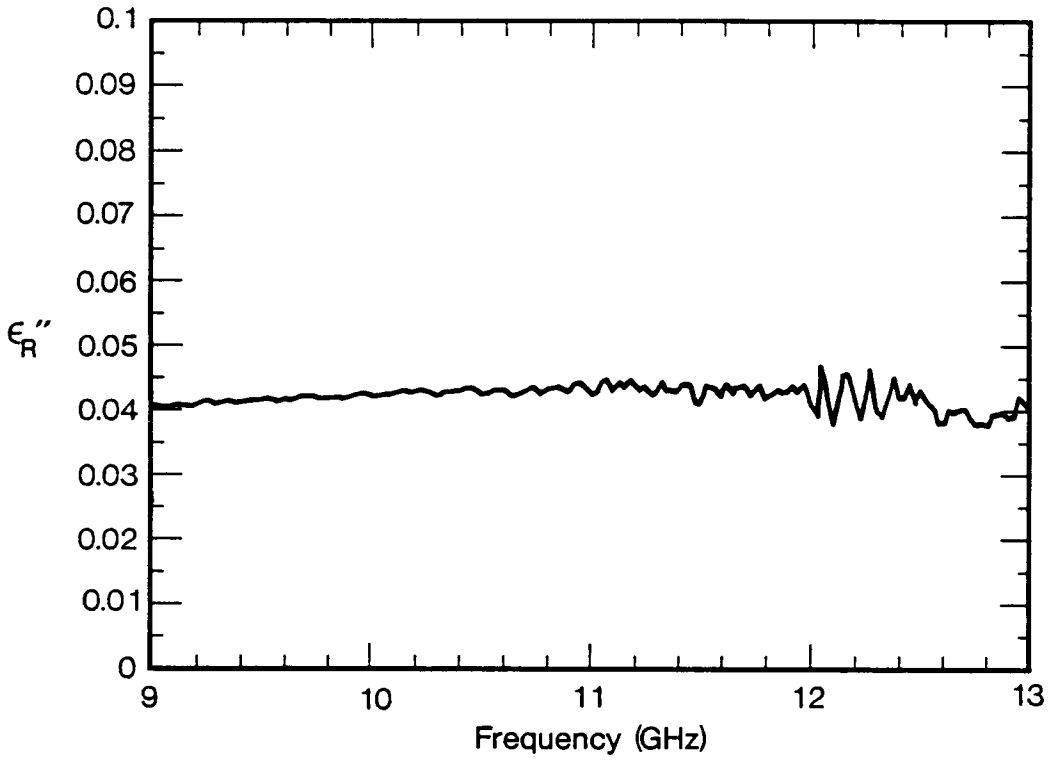

Figure 3.8 ϵ_R'' with and without gap correction using SCL for 1723 glass. The worst case uncertainty, $\Delta\epsilon_R'' = 0.009$, at 10 GHz.

3.5 Uncertainty Analysis

The independent sources of uncertainty for a short- circuit line measurement are basically the same as those for the T/R method except for the additional uncertainty introduced by an imperfect short-circuit.

The calculation of the theoretical uncertainty in the permittivity due to the uncertainties in the magnitude and phase of the scattering parameters requires the calculation of the various partial derivatives with respect to the various independent variables. For the analysis we will assume that the sample fits tightly to a perfect short-circuit, so the reflection coefficient is given by

$$\rho = \frac{\gamma_o \tanh \gamma L - \gamma}{\gamma_o \tanh \gamma L + \gamma}. \tag{3.36}$$

In an attempt to evaluate the uncertainty introduced by the measured scattering parameters a differential uncertainty analysis is applicable. We assume that the total uncertainty can be written as

$$\frac{\Delta \epsilon'_R}{\epsilon'_R} = \frac{1}{\epsilon'_R}\sqrt{\left(\frac{\partial \epsilon'_R}{\partial |S_\alpha|}\Delta |S_\alpha|\right)^2 + \left(\frac{\partial \epsilon'_R}{\partial \theta_\alpha}\Delta \theta_\alpha\right)^2 + \left(\frac{\partial \epsilon'_R}{\partial L}\Delta L\right)^2 + \left(\frac{\partial \epsilon'_R}{\partial d}\Delta d\right)^2}, \tag{3.37}$$

$$\frac{\Delta \epsilon''_R}{\epsilon''_R} = \frac{1}{\epsilon''_R}\sqrt{\left(\frac{\partial \epsilon''_R}{\partial |S_\alpha|}\Delta |S_\alpha|\right)^2 + \left(\frac{\partial \epsilon''_R}{\partial \theta_\alpha}\Delta \theta_\alpha\right)^2 + \left(\frac{\partial \epsilon''_R}{\partial L}\Delta L\right)^2 + \left(\frac{\partial \epsilon''_R}{\partial d}\Delta d\right)^2}, \tag{3.38}$$

where $\alpha = 11$, $\Delta\theta_\alpha$ is the uncertainty in the phase of the scattering parameter and $\Delta|S_\alpha|$ is the uncertainty in the magnitude of the S-parameter. This uncertainty estimate assumes that the independent sources of uncertainty are small enough for a linear approximation to be valid.

If we define a variable f by

$$f = \frac{\gamma_o \tanh \gamma L - \gamma}{\gamma_o \tanh \gamma L + \gamma} - \rho, \tag{3.39}$$

we can calculate

$$\frac{\partial f}{\partial L} = \frac{\gamma_o \gamma \mathrm{sech}^2 \gamma L}{\gamma_o \tanh \gamma L + \gamma}[1 - \frac{\gamma_o \tanh \gamma L - \gamma}{\gamma_o \tanh \gamma L + \gamma}], \tag{3.40}$$

$$\frac{\partial f}{\partial \gamma} = \frac{1}{\gamma_o \tanh \gamma L + \gamma}[(\gamma_o L \mathrm{sech}^2 \gamma L - 1) - \frac{\gamma_o \tanh \gamma L - \gamma}{\gamma_o \tanh \gamma L + \gamma}[\gamma_o L \mathrm{sech}^2 \gamma L + 1]], \tag{3.41}$$

$$\frac{\partial \gamma}{\partial \epsilon_R^*} = -\frac{\mu_o \epsilon_o \omega^2}{2\gamma}. \tag{3.42}$$

Since we can write

$$\rho = |\rho| \exp j\theta, \tag{3.43}$$

we obtain

$$\frac{\partial \epsilon_R^*}{\partial |\rho|} = \frac{\exp j\theta}{\frac{\partial f}{\partial \gamma}\frac{\partial \gamma}{\partial \epsilon_R^*}}, \tag{3.44}$$

$$\frac{\partial \epsilon_R^*}{\partial \theta} = \frac{j|\rho| \exp j\theta}{[\frac{\partial f}{\partial \gamma}\frac{\partial \gamma}{\partial \epsilon_R^*}]}, \tag{3.45}$$

$$\frac{\partial \epsilon_R^*}{\partial L} = -\frac{\frac{\partial f}{\partial L}}{[\frac{\partial f}{\partial \gamma}\frac{\partial \gamma}{\partial \epsilon_R^*}]}. \tag{3.46}$$

The partial derivatives are given in figures 3.9 – 3.14 and the calculated uncertainty is shown in figs 3.15 – 3.16.

For high-loss materials it is possible for the reflection coefficient to go to 0, and this results in a high uncertainty. The possibility of zero reflection coefficient can be understood by letting eq (3.36) go to zero and then finding an ϵ_R^* which is consistent with this condition. Consider the case when $S_{11} \approx 0$; then for coaxial line:

$$\tanh \gamma L \approx \frac{\gamma}{\gamma_0} \approx \sqrt{\epsilon_R^*}. \tag{3.47}$$

This yields the following relations between real and imaginary components:

$$\frac{\sinh 2\alpha L}{\cosh 2\alpha L + \cos 2\beta L} = \frac{1}{\sqrt{2}}\sqrt{(\epsilon_R'^2 + \epsilon_R''^2) + \epsilon_R' \sqrt{\epsilon_R'^2 + \epsilon_R''^2}}, \tag{3.48}$$

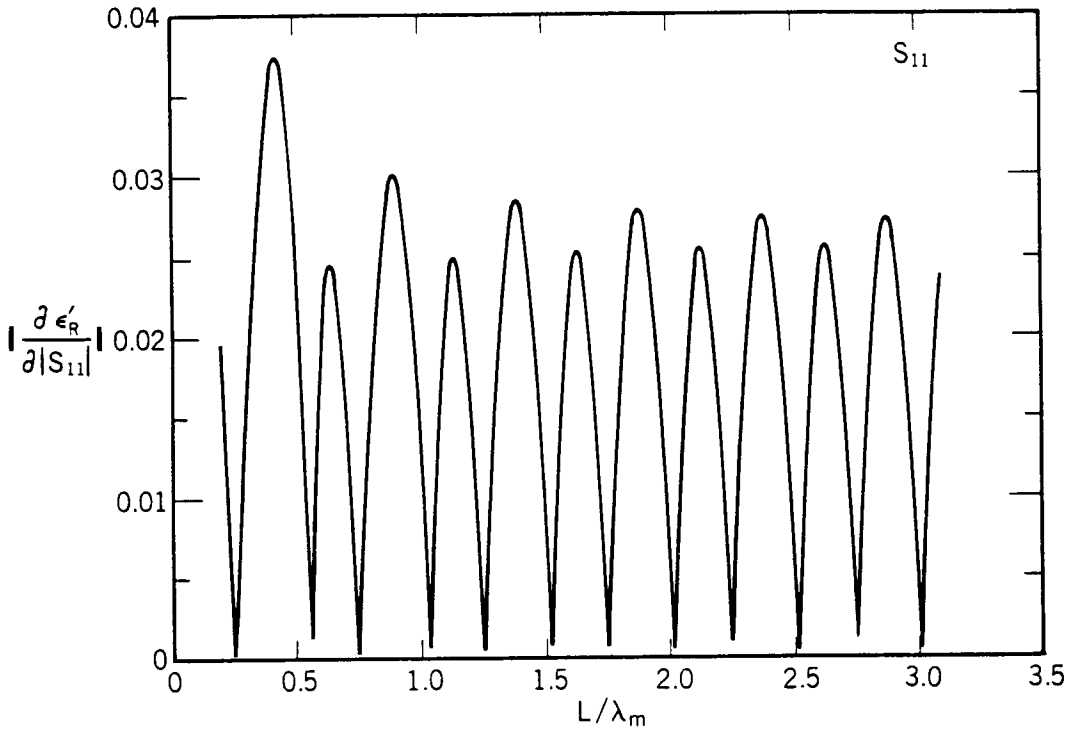

Figure 3.9 The derivative of ϵ'_R with respect to $|S_{11}|$ with $\epsilon^*_R = (30.0, 0.01)$.

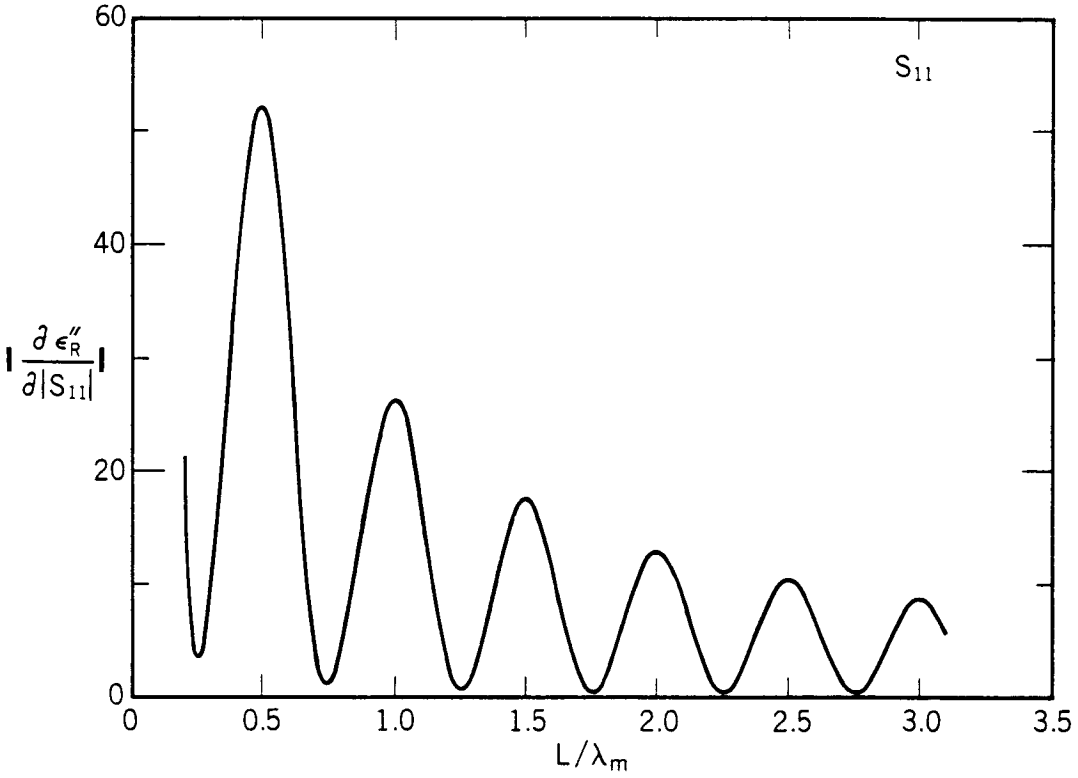

Figure 3.10 The derivative of ϵ_R'' with respect to $|S_{11}|$ with $\epsilon_R^* = (30.0, 0.01)$.

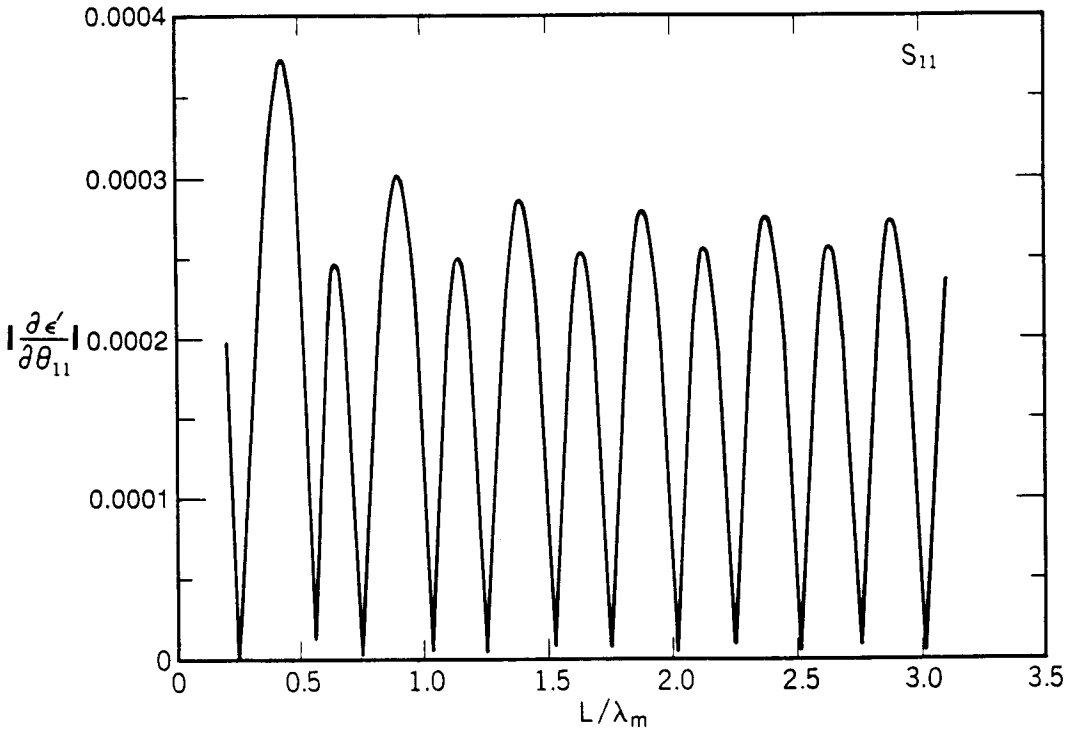

Figure 3.11 The derivative of ϵ'_R with respect to θ with $\epsilon^*_R = (30.0, 0.01)$.

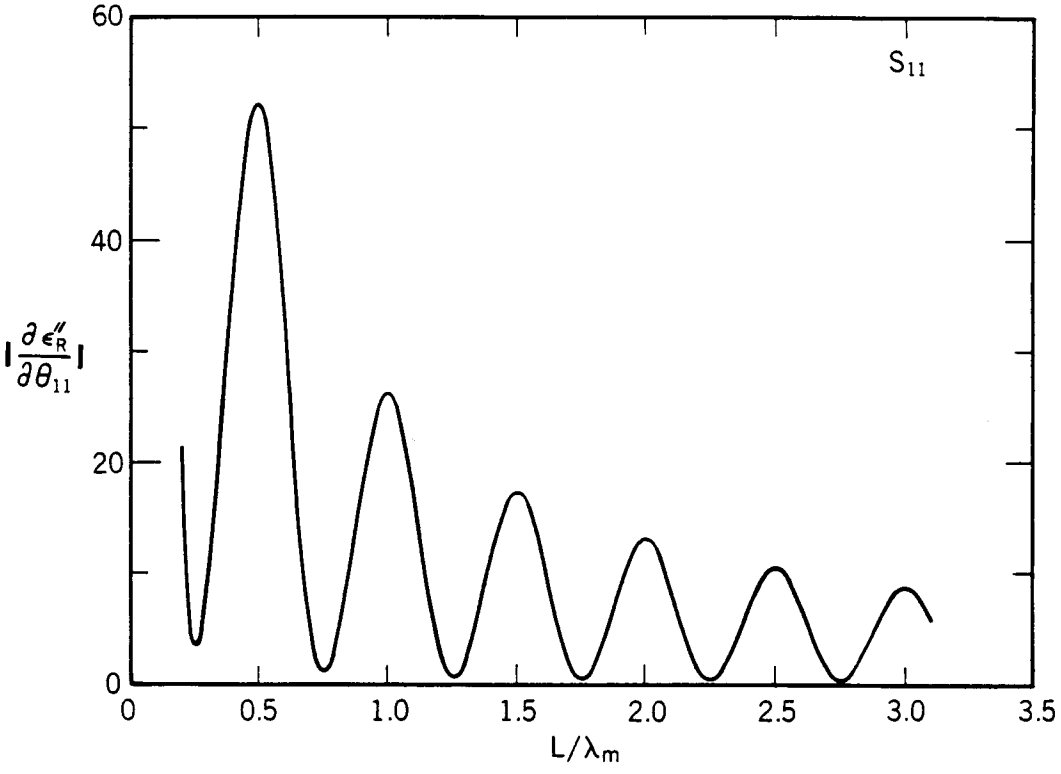

Figure 3.12 The derivative of ϵ_R'' with respect to θ with $\epsilon_R^* = (30.0, 0.01)$.

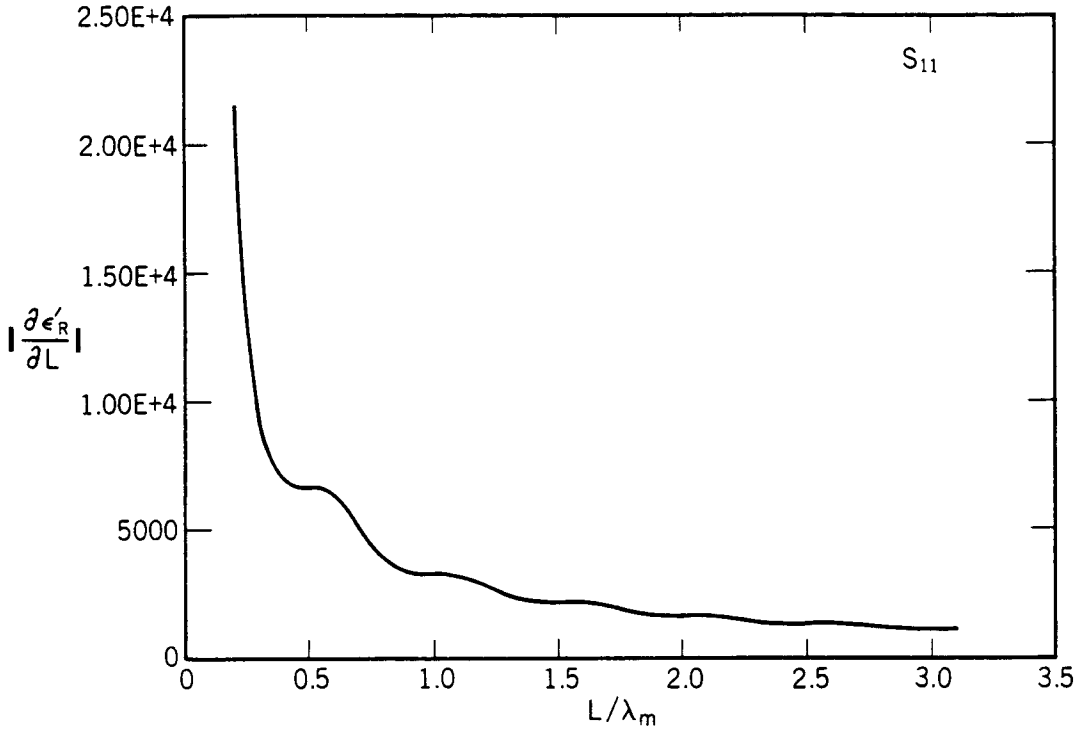

Figure 3.13 The derivative of ϵ'_R with respect to length with $\epsilon^*_R = (30.0, 0.01)$.

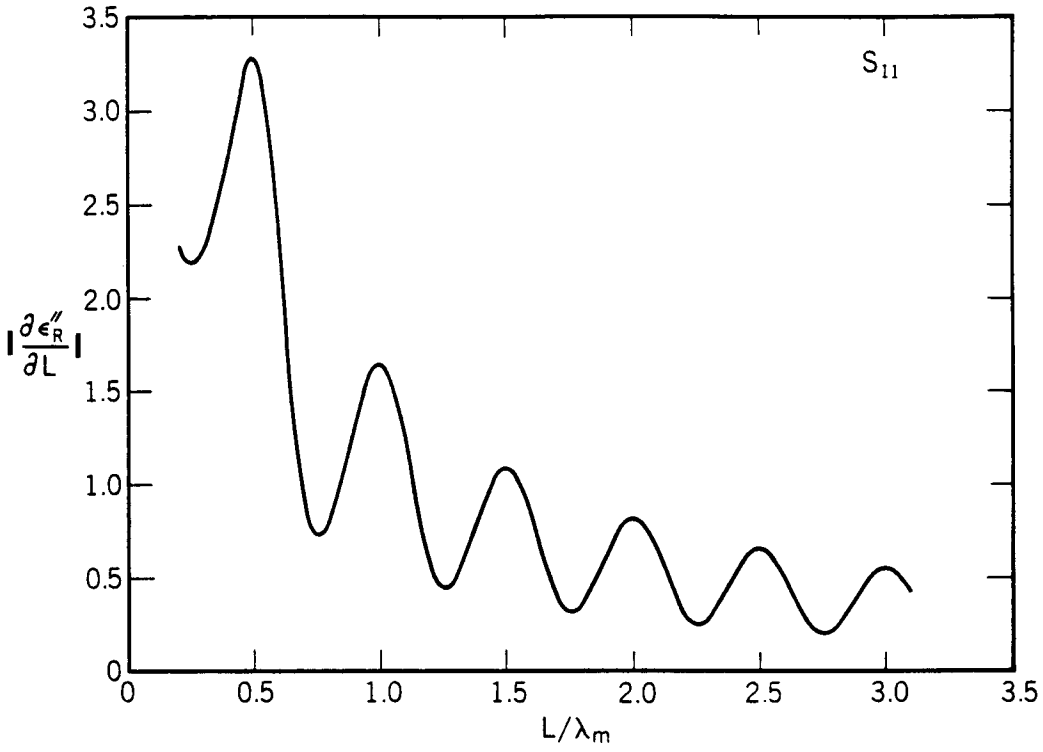

Figure 3.14 The derivative of ϵ_R'' with respect to length with $\epsilon_R^* = (30.0, 0.01)$.

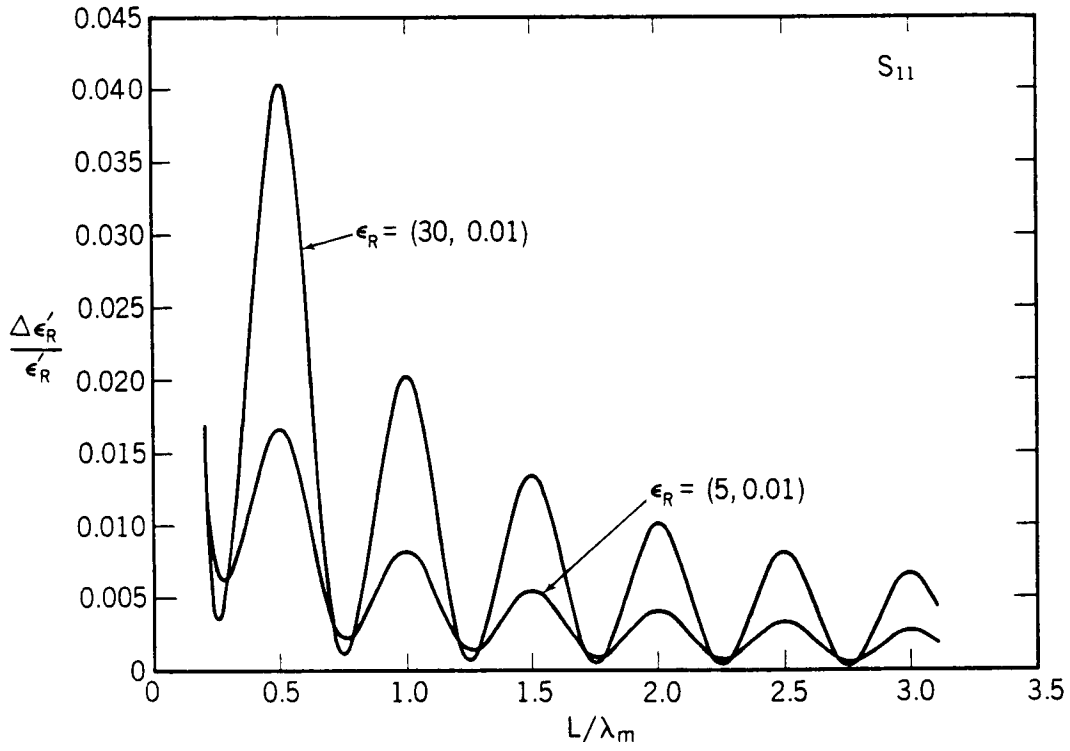

Figure 3.15 The relative uncertainty in ϵ'_R for S_{11} using SCL for a low-loss material, with ϵ^*_R =(5.0,0.01) and (30.0,0.01).

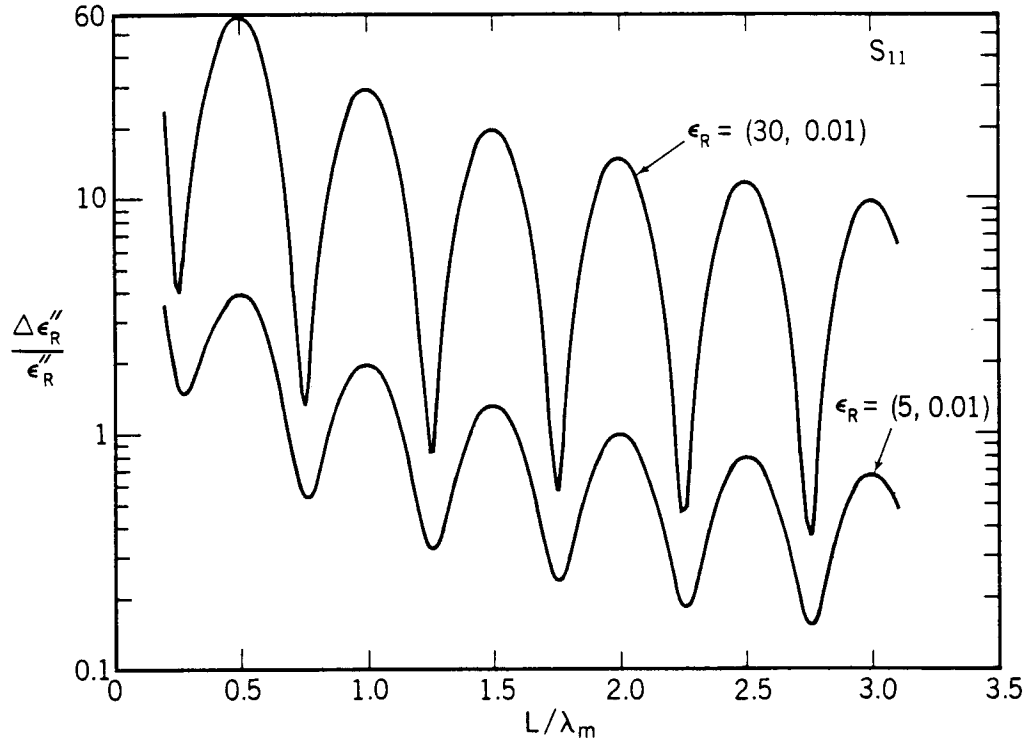

Figure 3.16 The relative uncertainty in ϵ''_R for S_{11} for a low-loss material, with ϵ^*_R = (5.0,0.01) and (30.0,0.01).

$$\frac{\sin 2\beta L}{\cosh 2\alpha L + \cos 2\beta L} = \frac{1}{\sqrt{2}}\sqrt{(\epsilon_R'^2 + \epsilon_R''^2) - \epsilon_R''\sqrt{\epsilon_R'^2 + \epsilon_R''^2}}, \tag{3.49}$$

where we have used

$$\gamma = \alpha + j\beta, \tag{3.50}$$

and

$$\alpha = \omega\sqrt{\frac{\epsilon\mu}{2}}\sqrt{\sqrt{1 + (\frac{\epsilon''}{\epsilon'})^2} - 1}, \tag{3.51}$$

$$\beta = \omega\sqrt{\frac{\epsilon\mu}{2}}\sqrt{\sqrt{1 + (\frac{\epsilon''}{\epsilon'})^2} + 1}, \tag{3.52}$$

In the case of very low loss, since $\alpha \to 0$, there is not an allowable value of ϵ_R^* that satisfies these equations, whereas for cases of appreciable loss, a solution is possible.

Chapter 4

Discussion and Conclusions

We have examined TR and SCL measurement procedures in detail. In this chapter I will summarize the important results obtained in the analysis.

As we have seen, although the Nicolson-Ross-Weir approach is easy to implement numerically, it fails for broadband measurement of low-loss samples of arbitrary length. The solution presented in this report uses a Newton-Raphson iteration procedure on linear combinations of the scattering parameters. This procedure yields solutions that are stable at integral multiples of one-half wavelength in the sample and at the same time does not unduly increase the complexity of the numerical solution. For materials where the transmitted signal is greater than -40 dB from the reference signal, S_{21} data by themselves are sufficient to calculate permittivity. For materials of large attenuation, S_{11} by itself will produce optimal results. In general, we have found eq (2.25) to be robust for high-loss and low-loss materials. For magnetic problems it is necessary to use both S_{11} and S_{21} data. The problem of reference plane position has been addressed, and approaches for the minimization of the error have been presented. Equations that are independent of reference plane position and sample length have been presented. Equations that are independent of reference plane position should be very useful in elevated temperature applications. Generally, sample length can be measured with great accuracy at laboratory temperature, and for these problems it is preferable to use a measured length. However, in temperature dependent applications it may be better to use equations independent of both sample length and reference plane position.

An uncertainty estimate for the solution expounded in this report has been presented. The uncertainty analysis presented here differs in some respects from that presented in the literature previously. This difference is due primarily to the fact that the uncertainties in this paper are derived from S_{11} and S_{21} in isolation. The trend indicates that for low-loss materials the uncertainty decreases as a function of increasing sample length. For high-loss materials the uncertainty in S_{21} decreases until the signal reaches -40 to -50 dB, and thereafter the uncertainty increases and thus $\Delta\epsilon_R^*$ increases.

The theory for short-circuit line measurements was presented and an uncertainty analysis for the procedure was presented. The uncertainty is a function of the sample length, dielectric constant and S-parameters. For fixed frequency measurements, samples of length $n\lambda/4$, n=1, 3, 5, . . ., yield minimum uncertainty, a result of the fact that at these frequencies the electric field is a relative maximum over the sample length. In general, for low-loss materials, samples lengths that are large in relation to wavelength give more accurate results; thus for broadband measurements it is preferable to use long samples for low-loss materials. However, for the case of lossy materials very long samples result in only front face reflection information. Thus, for relatively lossy materials, sample lengths on the order of one attenuation length are optimum.

Chapter 5

Acknowledgments and References

5.1 Acknowledgments

I would like to thank Eleanor Livingston for her excellent comments and suggestions, Michael Janezic for help with measurements and software and John Grosvenor for help with measurements; also Richard Geyer, William Kissick and Howard Bussey for various discussions and as sources of encouragement. Finally, I would like to thank Ray King, Steve Buckner, and David Blackham for reading the manuscript and providing excellent suggestions.

5.2 References

[1] Nicolson, A. M. and Ross, G. "Measurement of the intrinsic properties of materials by time domain techniques," *IEEE Trans. Instrum. Meas.*, vol.IM-19, pp.377–382, November 1970.

[2] Weir, W. B. "Automatic measurement of complex dielectric constant and permeability at microwave frequencies," *Proc. IEEE*, vol.62, pp.33–36, January 1974.

[3] Deschamps, G. A. "Determination of reflection coefficients and insertion loss of a wave-guide junction," *J. Appl. Phys.*, vol.2, pp.1046–1050, August 1953.

[4] "Measuring dielectric constant with the HP 8510 network analyzer," Product note no. 8510-3, Hewlett Packard.

[5] Freeman, M. S., Nottenburg, R. N. and DuBow, J. B. "An automated frequency domain technique for dielectric spectroscopy of materials," *J. Phys. E: Sci. Instrum.*, vol.12, pp.899–903, 1979.

[6] Stuchly, S. and Matuszewski, M. "A combined total reflection transmission method in application to dielectric spectroscopy," *IEEE Trans. Instrum. Meas.*, vol.IM-27, pp.285–288, September 1978.

[7] Ligthardt, L. P. "A fast computational technique for accurate permittivity determination using transmission line methods," *IEEE Trans. Microwave Theory Tech.*, vol.MTT-31, pp.249–254, March 1983.

[8] Altschuler, H. M. *Dielectric Constant*, ch.9, p.502. Vol.3, Polytechnic Press: NY, 1963.

[9] Harris, F. J. "On the use of windows for harmonic analysis with discrete fourier transform," *Proc. IEEE*, vol.66, pp.51–83, 1978.

[10] Scott, W. and Smith, G. S. "Dielectric spectroscopy using monopole antennas of general electrical length," *IEEE Trans. Antennas Propagat.*, vol.AP-35, pp.962–967, 1987.

[11] Kerns, D. M. and Beatty, R. *Basic Theory of Waveguide Junctions and Introductory Microwave Network Analysis.* NY: Pergamon Press, 1967.

[12] Westphal, W. P. "Techniques of measuring the permittivity and permeability of liquids and solids in the frequency range 3 c/s to 50 kmc/s," Laboratory for Insulation Research Technical Report, MIT, 1950.

[13] Bussey, H. E. "Measurement of rf properties of materials a survey," *Proc. IEEE*, vol.55, pp.1046–1053, June 1967.

[14] Bussey, H. E. and Gray, J. E. "Measurement and standardization of dielectric samples," *IRE Trans. Inst.*, vol.I-11, no.3, pp.162–165, 1962.

[15] Hill, D. A. "Reflection coefficient of a waveguide with slightly uneven walls," *IEEE Trans. Microwave Theory Tech.*, vol.37, pp.244–252, January 1989.

[16] Ramo, S., Whinnery, J. R. and Duzer, T. V. *Fields and Waves in Communication Electronics.* New York: John Wiley and Sons, 1984.

[17] Bailey, A. E. *Microwave Measurement.* London: Peter Peregrinus, 1985.

[18] Wong, K. H. "Using precision coaxial air dielectric transmission lines as calibration and verification standards," *Microwave Journal*, pp.83–90, December 1988.

[19] Roberts, S. and von Hippel, A. "A new method for measuring dielectric constant and loss in the range of centimeter waves," *J. Appl. Phys.*, vol.7, pp.610–616, July 1946.

[20] Chao, S. "An uncertainty analysis for the measurement of microwave conductivity and dielectric constant by the short–circuited line method," *IEEE Trans. Instru. and Meas.*, vol.IM-35, pp.36–41, March 1986.

[21] Dakin, T. W. and Works, C. N. "Microwave dielectric measurements," *J. Appl. Phys.*, vol.18, pp.789–796, September 1947.

[22] Bowie, D. M. and Kelleher, K. S. "Rapid measurement of dielectric constant and loss tangent," *IRE Trans. Microwave Theory Tech.*, vol.MTT-4, pp.137–140, 1956.

[23] Brydon, G. M. and Hepplestone, D. J. "Microwave measurements of permittivity and $\tan\delta$ over the temperature range $20 - 700^{o}c$," *Proc. Inst. Elec. Eng.*, vol.112, pp.421–425, 1965.

[24] Kurokawa, K. "Power waves and the scattering matrix" *IEEE Trans. Microwave Theory Tech.*, vol.MTT-13, pp.194–202, March 1965.

[25] Reiter, G. "Generalized telegraphist's equation for waveguides of varying cross section," *Proc. Inst. Elec. Eng.*, vol.106, Pt. B, Suppl. 13, pp.54–57, 1959.

[26] Champlin, K. S. and Glover, G. H. "Influence of waveguide contact on measured complex permittivity of semiconductors," *J. Appl. Phys.*, vol.37, pp.2355–2360, May 1966.

[27] Schwinger, J. and Saxon, D. S. *Discontinuities in Waveguides.* New York: Gordon and Breach Science Publishers, 1968.

[28] Champlin, K. S. and Glover, G. H. "Gap effect in measurement of large permittivities," *IEEE Trans. Microwave Theory Tech.*, pp.397–398, August 1966.

[29] King, R. W. P. and Smith, G. *Antennas in Matter.* Cambridge, Mass.: MIT Press, 1981.

[30] Morse, P. M. and Feshbach, H. *Methods of Theoretical Physics.* New York: McGraw-Hill Book Company, 1953.

[31] Roberts, D. *Electromagnetic wave propagation in dissipative dielectrics such as oil shales.* Master's thesis, University of Wyoming, 1983.

[32] Tai, C. *Dyadic Green's Functions in Electromagnetic Theory.* Intext Educational Publishers, 1971.

[33] Jackson, J. D. *Classical Electrodynamics.* New York: John Wiley and Sons, 1975.

[34] Ben-Menahem, A. and Singh, S. J. *Seismic Waves and Sources.* New York: Springer-Verlag, 1981.

[35] Baker-Jarvis, J., Racine, M. and Alameddine, J. "Solving differential equations by a maximum entropy-minimum norm method with applications to Fokker-Planck equations," *J. Math. Phys.*, vol.30, no.7, pp.1459–1463, 1989.

Chapter 6

Appendices

6.1 Appendix A: The Scattering Matrix

6.1.1 Theory

In this appendix the basic features of the two-port scattering equations will be reviewed. We consider incident (a_i) and reflected (b_i) power waves defined by [24]

$$a_i = \frac{V_i + Z_i I_i}{2\sqrt{|ReZ_i|}}, \tag{6.1}$$

$$b_i = \frac{V_i - Z_i^* I_i}{2\sqrt{|ReZ_i|}}, \tag{6.2}$$

where Z_i, V_i, I_i are the impedance, voltage and current associated with a power wave. The voltage and current are given by

$$V_i = \frac{p_i}{\sqrt{|ReZ_i|}}[Z_i^* a_i + Z_i b_i], \tag{6.3}$$

$$I_i = \frac{p_i}{\sqrt{|ReZ_i|}}[a_i - b_i], \tag{6.4}$$

where

$$p_i = \begin{cases} 1 & \text{if Re } Z_i \geq 0 \\ -1 & \text{otherwise} \end{cases} . \tag{6.5}$$

The impedance matrix $\mathbf{Z}$ is

$$\mathbf{Z} = \begin{pmatrix} Z_{11} & Z_{12} \\ Z_{21} & Z_{22} \end{pmatrix}. \tag{6.6}$$

The voltage vector and impedance matrix are related to the current vector by Ohm's law:

$$\vec{V} = \mathbf{Z}\vec{I}. \tag{6.7}$$

The voltage and current in a waveguide can be represented by voltage and current waves:

$$V(z) = A \exp -\gamma z + B \exp \gamma z, \tag{6.8}$$

$$I(z) = \frac{A \exp -\gamma z - B \exp \gamma z}{Z_o}. \tag{6.9}$$

The two-port scattering equations relate the incident voltage wave to the reflected wave. The two-port scattering equations can be written as

$$b_1 = S_{11}a_1 + S_{12}a_2, \tag{6.10}$$

$$b_2 = S_{21}a_1 + S_{22}a_2, \tag{6.11}$$

or in vector notation

$$\vec{b} = \mathbf{S}\vec{a}, \tag{6.12}$$

where

$$\mathbf{S} = \begin{pmatrix} S_{11} & S_{12} \\ S_{21} & S_{22} \end{pmatrix}. \tag{6.13}$$

A general n-port junction possesses the following properties [24]:

- reciprocity

- losslessness
- symmetry

If off-diagonal elements are equal $S_{21} = S_{12}$ we then say the n-port is reciprocal; if $S_{11} = S_{22}$, we say the n-port is symmetrical. A junction is lossless if the impedance is pure reactance. The impedance matrix that satisfies a reciprocal network is symmetric:

$$\mathbf{Z} = \mathbf{Z^t}. \tag{6.14}$$

The scattering matrix under a similarity transform behaves as

$$\mathbf{S}^t = \mathbf{P}^t\mathbf{S}\mathbf{P}, \tag{6.15}$$

where

$$\mathbf{P} = \begin{pmatrix} p_1 & 0 \\ 0 & p_2 \end{pmatrix}; \tag{6.16}$$

therefore

$$S_{mn} = p_n p_m S_{nm}, \tag{6.17}$$

and

$$|S_{ij}|^2 = |S_{ji}|^2. \tag{6.18}$$

6.1.2 Lossless Network

The net power fed into a network is given by

$$W = \sum_i p_i[|a_i|^2 - |b_i|^2], \tag{6.19}$$

thus for lossless circuits we have:

$$W = \sum_i p_i[|a_i|^2 - |b_i|^2] = 0, \tag{6.20}$$

or in matrix form

$$\mathbf{A}^{+}(\mathbf{P} - \mathbf{S}^{+}\mathbf{P}\mathbf{S})\mathbf{A} = \mathbf{P}, \tag{6.21}$$

where (+) denotes adjoint. This equation is equivalent to

$$\mathbf{P} = \mathbf{S}^{+}\mathbf{P}\mathbf{S}, \tag{6.22}$$

which yields three independent conditions:

$$p_1|S_{11}|^2 + p_2|S_{21}|^2 = p_1, \tag{6.23}$$

$$p_1|S_{12}|^2 + p_2|S_{22}|^2 = p_2, \tag{6.24}$$

$$p_1 S_{11}S_{12}^{*} + p_2 S_{21}S_{22}^{*} = 0. \tag{6.25}$$

Therefore

$$|S_{11}|^2|S_{12}|^2 = |S_{21}|^2|S_{22}|^2, \tag{6.26}$$

$$|S_{11}|^2 = |S_{22}|^2, \tag{6.27}$$

$$|S_{12}|^2 = |S_{21}|^2. \tag{6.28}$$

6.1.3 Lossy Networks

When the material is lossy we obtain

$$\mathbf{A}^{t}(\mathbf{P} - \mathbf{S}^{t}\mathbf{P}\mathbf{S})\mathbf{A} \geq 0. \tag{6.29}$$

Therefore $(\mathbf{P} - \mathbf{S}^{t}\mathbf{P}\mathbf{S})$ must be positive definite or semi-positive definite. This relation is basically a statement of increasing entropy.

6.2 Appendix B: Imperfect Waveguide Walls

No waveguide or coaxial line is perfectly uniform and the non-uniformity of the walls will affect the measured S-parameters. The goal of this section is to study these effects and estimate the significance of this effect.

Hill [15] recently presented a thorough theoretical analysis of waveguides with slightly uneven walls. What follows is an overview and summary of Hill's [15] results. The perturbations in the waveguide wall excites spurious modes in the structure. The existence of spurious modes in the transmission line will influence the measurement results. Of course spurious modes are also generated by inhomogeneities in samples and discontinuities at connectors. The amplitude and phase of the spurious modes can be studied by use of the telegrapher's equation developed by Reiter [25]:

$$\frac{dA_i^+}{dz} = -j\beta_i A_i^+ - \frac{1}{2}\frac{d(\ln Z_i)}{dz}A_i^- + \sum_{p=1}^{\infty}[S_{ip}^+ A_p^+ + S_{ip}^- A_p^-], \tag{6.30}$$

$$\frac{dA_i^-}{dz} = j\beta_i A_i^- - \frac{1}{2}\frac{d(\ln Z_i)}{dz}A_i^+ + \sum_{p=1}^{\infty}[S_{ip}^- A_p^+ + S_{ip}^+ A_p^-], \tag{6.31}$$

where $A_i^{\pm}$ are the amplitudes of the forward and backward traveling modes, Z_i are the impedance of the ith mode, S_{ip} are the coupling coefficients, and β_i are the wave numbers and time dependence is $\exp(j\omega t)$. The boundary conditions for a waveguide, of length L, fed by a single mode are:

$$A_m^+(0) = A_o,\ A_m^-(L) = 0, \tag{6.32}$$

$$A_i^+(0) = 0,\ A_i^-(L) = 0 \text{ for } i \neq m. \tag{6.33}$$

Hill assumes the inner and outer radii for a coaxial line, ρ_i and ρ_o are a function of z. The variation from a base radii, ρ_{i0}, ρ_{o0} is given by $\Delta_i(z)$, and therefore

$$\rho_i(z) = \rho_{i0} + \Delta_i(z), \tag{6.34}$$

$$\rho_o(z) = \rho_{o0} + \Delta_o(z), \tag{6.35}$$

where $\Delta_i/\rho_{i0} \ll 1, \Delta_o/\rho_{o0} \ll 1$. Hill has shown that the S-parameters due to uneven walls can be approximated by the equation

$$S_{11} = \int_o^L [C_i \frac{d\Delta_i}{dz} + C_o \frac{d\Delta_o}{dz}] \exp(-2jkz) dz, \tag{6.36}$$

where $k = 2\pi/\lambda$ and

$$C_i = -[2\rho_{io} \ln(\rho_{o0}/\rho_{io}]^{-1}, \tag{6.37}$$

$$C_o = -[2\rho_{o0} \ln(\rho_{o0}/\rho_{io}]^{-1}. \tag{6.38}$$

This can be written as

$$S_{11} = S_{11i} + S_{11o}, \tag{6.39}$$

where

$$S_{11i} = 2jkC_i \int_0^L \Delta_i(z) \exp(-2jkz) dz, \tag{6.40}$$

$$S_{11o} = 2jkC_o \int_0^L \Delta_o(z) \exp(-2jkz) dz. \tag{6.41}$$

Hill has calculated upper bounds on $|S_{11}|$

$$|S_{11i}| \leq 2kL|C_i|\Delta_{i\ max}, \tag{6.42}$$

$$|S_{11o}| \leq 2kL|C_o|\Delta_{o\ max}. \tag{6.43}$$

Hill has shown that for a precision coaxial air line the change in $|S_{11}|$ due to uneven walls is $< 1 \times 10^{-3}$. Therefore for precision air line in good condition the wall unevenness will contribute to a lesser degree to the uncertainty than the uncertainty of the ANA parameters, since $\Delta|S_{11}| \approx 1 \times 10^{-3}$ for network uncertainties alone.

6.3 Appendix C: The Gap Correction

6.3.1 Frequency Independent Approaches

Various researchers have approached the gap problem by representing the sample with air gap as a layered capacitor [12], [13], [26]. This approach assumes that the gaps between transmission line and sample are effectively modeled by a set of capacitors in series. Champlin [26] approached the problem using as a starting point the perturbation formula developed by Schwinger [27]. By substituting into the perturbation formula approximations to the field distribution in the various regions they obtain an estimate for the effective permittivity. Their answer turns out to be fully equivalent to the capacitor model of Westphal [12]. Champlin showed that Bussey's theory [13] is the first two terms in an expansion of Westphal [12] and Champlin's models.

The capacitor model is frequency independent and thus is strictly valid only at lower frequencies and d.c. We would expect the capacitor model to break down at higher frequencies because the wavelength decreases with increasing frequency to a point where multiple scattering dominants. In order to account for multiple scattering it is necessary to develop a theory that is frequency dependent.

Coaxial Capacitor model

Consider a capacitor consisting of layers of dielectric and layers of air in a coaxial line. The various dimensions are shown in figure 6.1.

We treat the system as capacitors in series, so that

$$\frac{1}{C_m} = \frac{1}{C_1} + \frac{1}{C_2} + \frac{1}{C_3}. \tag{6.44}$$

We know that for a coaxial line the electric field distribution is given by

$$E_r = \frac{V}{\ln(\frac{b}{a})r}, \tag{6.45}$$

and the voltage between the conductors is given by

$$V = -\int_a^b E(r)dr. \tag{6.46}$$

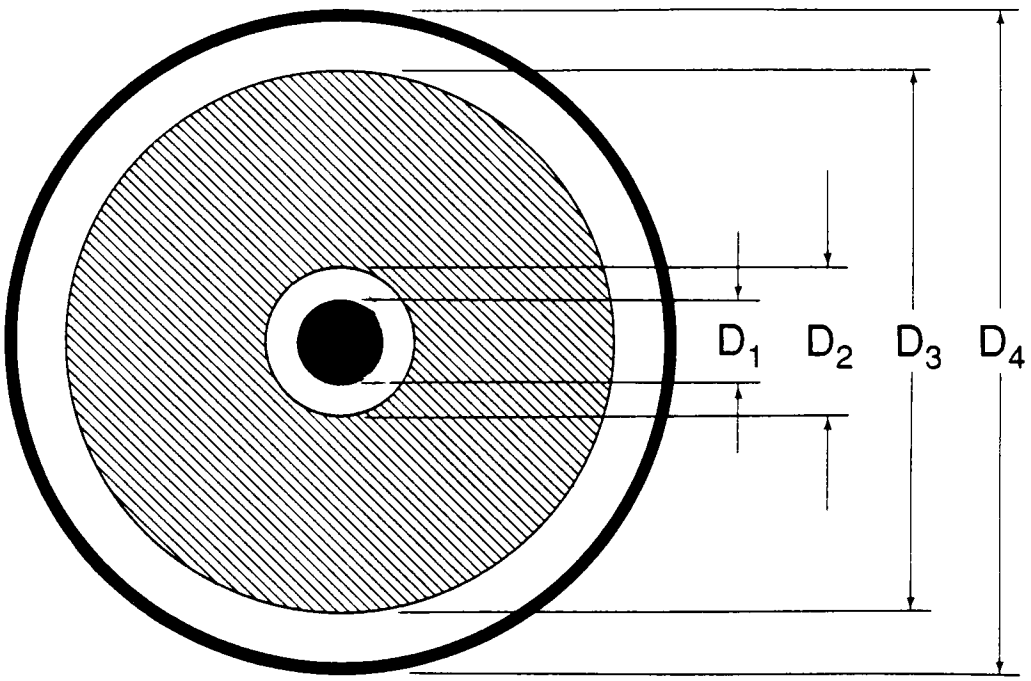

Figure 6.1 A coaxial sample in holder with air gaps near conductors.

The capacitance of a coaxial line of length L is given by

$$C = \frac{2\pi\epsilon L}{\ln \frac{R_2}{R_1}}; \tag{6.47}$$

thus, for a system of three capacitors in series we have

$$\frac{\ln \frac{R_4}{R_1}}{\epsilon'_m} = \frac{\ln \frac{R_2}{R_1}}{\epsilon'_1} + \frac{\ln \frac{R_3}{R_2}}{\epsilon'_c} + \frac{\ln \frac{R_4}{R_3}}{\epsilon'_1} , \tag{6.48}$$

where ϵ'_c, ϵ'_m are the corrected and measured values of the real part of the permittivity and ϵ'_1, is the real part of the permittivity of the air gap, respectively. Therefore

$$\epsilon'_c = \frac{\epsilon'_1 \epsilon'_m \ln \frac{R_3}{R_2}}{\epsilon'_1 \ln \frac{R_4}{R_1} - \epsilon'_m [\ln \frac{R_2}{R_1} + \ln \frac{R_4}{R_3}]} . \tag{6.49}$$

We can then write

$$\epsilon'_c = \epsilon'_m \frac{L_2}{L_3 - \epsilon'_m L_1} , \tag{6.50}$$

$$\tan \delta_c = \tan \delta_m [1 + \epsilon'_c \frac{L_1}{L_2}] , \tag{6.51}$$

where

$$L_1 = \ln \frac{R_2}{R_1} + \ln \frac{R_4}{R_3} , \tag{6.52}$$

$$L_2 = \ln \frac{R_3}{R_2} , \tag{6.53}$$

$$L_3 = \ln \frac{R_4}{R_1} . \tag{6.54}$$

Equation (6.50) breaks down when $\epsilon'_m \geq \frac{L_3}{L_1}$. An example is plotted in figure 6.2 for a 7 mm coaxial line.

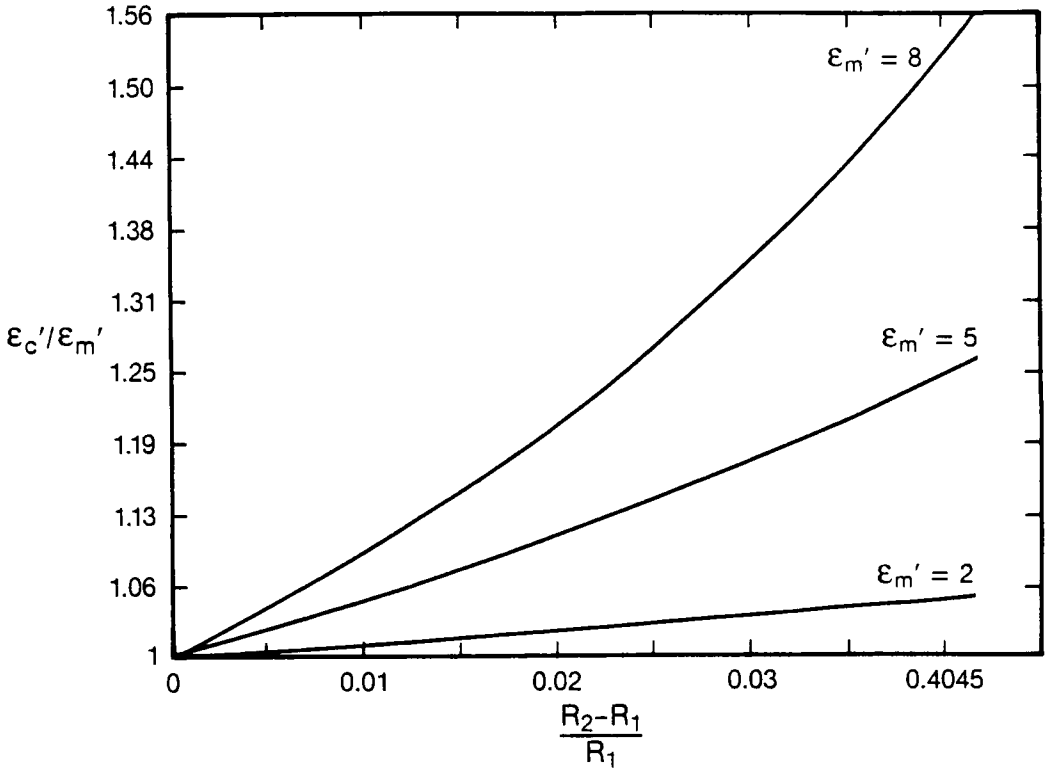

Figure 6.2 The gap correction calculated for various values of ϵ'_R, where R_2, R_1 are the radii of the inner conductor and sample respectively.

Rectangular Waveguide Model

For the case of a rectangular guide eqs (6.50) and (6.51) are modified slightly

$$\epsilon_c' = \epsilon_m' \frac{d}{b-(b-d)\epsilon_m'}, \tag{6.55}$$

$$\tan\delta_c = \tan\delta_m \frac{b}{b-(b-d)\epsilon_m'}, \tag{6.56}$$

where b and d refer to the waveguide and sample dimensions and (c) and (m) refer to corrected value and measured value respectively.

Frequency Independent Model of Bussey

Bussey and Gray used a perturbation theory developed by Bethe and Schwinger [27] for cavities. We will summarize the theory in this section.

The difference in the propagation constant for a waveguide with and without an airgap is given by

$$\gamma_{gap}^2 - \gamma_{no\ gap}^2 = \Delta\gamma^2 = (\epsilon_R' - 1)(\frac{\omega}{c})^2 \frac{\int_{gap} \vec{E}_1 \cdot \vec{E}_2 dS}{\int_S |\vec{E}_1|^2 dS}, \tag{6.57}$$

where E_1 is the electric field of the dielectric filled line with no air gap, E_2 is the electric field with an air gap present, S is the cross sectional area. The following boundary conditions must be satisfied at the dielectric interface,

$$E_{2,n} = \epsilon_R' E_{1,n}, \tag{6.58}$$

$$E_{2,t} = E_{1,t}, \tag{6.59}$$

where $(_n)$ denotes normal component,

$$\gamma_{gap}^2 - \gamma_{no\ gap}^2 = \Delta\gamma^2 = (\epsilon_R' - 1)(\frac{\omega}{c})^2 \frac{\int_{gap}[\epsilon_R'|E_{1,n}|^2 + |E_{1,t}|^2]dS}{\int_S |E_1|^2 dS}; \tag{6.60}$$

thus we have

$$\Delta\epsilon_R' = (\epsilon_R' - 1)\frac{\int_{gap}[\epsilon_R'|E_{1,n}|^2 + |E_{1,t}|^2]dS}{\int_S |E_1|^2 dS}. \tag{6.61}$$

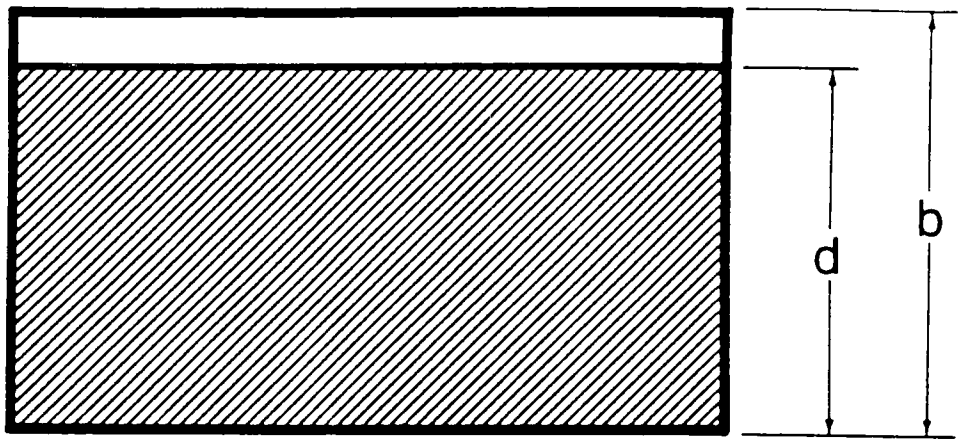

Figure 6.3 A rectangular sample in holder with gaps near conductors.

Bussey and Gray showed that for small air gaps, this equation reduces to

$$\frac{\Delta\epsilon'_R}{\epsilon'_R} = (\epsilon'_R - 1)\frac{(b-d)}{b}. \tag{6.62}$$

We see that eq (6.62) is equivalent to the first two terms in a series expansion of the capacitor eqs (6.55).

Perturbation Model of Champlin

Champlin [26], [28] has used a perturbation approach to the air gap problem. Using a perturbation formula of Schwinger [27] for a single mode in an inhomogeneously filled waveguide:

$$\gamma_2 - \gamma_1 = -j\omega \frac{\int\int \Delta\epsilon'_R \vec{E}_1 \cdot \vec{E}_2 dS}{\int\int [\vec{E}_1 \times \vec{H}_2 - \vec{E}_2 \times \vec{H}_1] \cdot \vec{k} dS}, \tag{6.63}$$

where

$$\Delta\epsilon'_R = 0 \text{ in region(1)}, \tag{6.64}$$

and

$$\Delta\epsilon'_R = \epsilon'_{2R} - \epsilon'_{1R} \text{ in region (2)}. \tag{6.65}$$

The following boundary conditions apply

$$E_2 = E_1 \text{ in region(1)}, \tag{6.66}$$

$$E_2 = \frac{\epsilon_1}{\epsilon_2} E_1 \text{ in region(2)}, \tag{6.67}$$

and

$$H_{2t} = -\frac{\gamma_2}{\gamma_1} H_{1t} \text{ in region(1)}, \tag{6.68}$$

$$H_{2t} = -\frac{\gamma_2 \epsilon_1}{\gamma_1 \epsilon_2} H_{1t} \text{ in region(2)}, \tag{6.69}$$

$$[\epsilon_{R_{eff}} - 1] = \frac{\gamma_o^2 - \gamma_2^2}{\omega^2 \mu_o \epsilon_o}. \tag{6.70}$$

Substituting eqs (6.64)–(6.69) into eq (6.63) and integrating yields an expression for an effective permittivity which is equivalent to Westphal's formula in eq (6.55) for rectangular waveguide. Bussey's result in eq (6.62) is an approximation of Champlin's and Westphal's results.

6.3.2 Frequency Dependent Capacitor Model

The capacitor model was independent of frequency. At high frequencies the capacitor models given in previous sections break down due to multiple scattering effects at the material interfaces. It is possible to include frequency in a medium frequency capacitor model by considering the admittance of a material filled capacitor. The model which was originally developed to model Maxwell-Wagner effects should work for layered materials in waveguides. We consider capacitors of cross-sectional area A and admittance Y in series such that [29]:

$$\frac{1}{Y} = \frac{1}{Y_1} + \frac{1}{Y_2}. \tag{6.71}$$

The admittance of a capacitor is given by

$$Y = [\sigma + j\omega\epsilon'_R\epsilon_o]\frac{A}{d}, \tag{6.72}$$

where d is the thickness of the sample and therefore for two samples in series

$$\frac{1}{[\sigma + j\omega\epsilon'_R\epsilon_o]\frac{A}{d}} = \frac{1}{[\sigma_1 + j\omega\epsilon'_{R1}\epsilon_o]\frac{A}{d_1}} + \frac{1}{[\sigma_2 + j\omega\epsilon'_{R2}\epsilon_o]\frac{A}{d_2}}. \tag{6.73}$$

The effective d.c. conductivity can be obtained from the zero frequency limit:

$$\sigma = \frac{\sigma_1\sigma_2}{\sigma_1\frac{d_2}{d} + \sigma_2\frac{d_1}{d}}. \tag{6.74}$$

We can also solve eq (6.73) for ϵ'_R:

$$\epsilon'_R = \epsilon'_{R\infty} + \frac{\epsilon'_{Rs} - \epsilon'_{R\infty}}{1 + \omega^2\tau^2} - j\frac{j\omega\tau[\epsilon'_{Rs} - \epsilon'_{R\infty}]}{1 + \omega^2\tau^2}, \tag{6.75}$$

where

$$\epsilon'_{R\infty} = \frac{\epsilon'_{R1}\epsilon'_{R2}}{\epsilon'_{R1}\frac{d_2}{d} + \epsilon'_{R2}\frac{d_1}{d}}, \tag{6.76}$$

$$\epsilon'_{Rs} = \frac{\epsilon'_{R1}\sigma_2^2(\frac{d_1}{d}) + \epsilon'_{R2}\sigma_1^2(\frac{d_2}{d})}{[\sigma_1(\frac{d_2}{d}) + \sigma_2(\frac{d_1}{d})]^2}, \tag{6.77}$$

$$\tau = \frac{[\epsilon'_{R1}d_2 + \epsilon'_{R2}d_1]\epsilon_o}{\sigma_1 d_2 + \sigma_2 d_1}. \tag{6.78}$$

Equation (6.75) reduces in the high frequency limit to the previous capacitor model and in the low frequency limit to an expression containing the d.c. conductivity. The effective relaxation time τ depends both on the conductivity and permittivity. In this model the layered structure acts as a material with a single relaxation time. Many materials have a distribution of relaxation times.

6.4 Appendix D: Fields in a Transmission Line

6.4.1 Theory

In this appendix we wish to review the field equations for a general, arbitrarily shaped waveguides. We will first review the theory behind propagation of TE, TM and TEM waves in waveguide, then generalize the theory by means of dyadic Green functions. The solution will be presented in terms of the vector potential in the so called nameless gauge where the scalar potential is zero [30], [31], [32]. In this gauge only the vector potential needs to be calculated and the electric and magnetic fields can be obtained from it. The treatment in this appendix is kept sufficiently general to allow application to various geometries.

The Fourier-transformed Maxwell equations are

$$\nabla \times \vec{E} = -j\omega\vec{B}, \tag{6.79}$$

$$\nabla \times \vec{H} = \vec{J} + j\omega\vec{D}, \tag{6.80}$$

$$\nabla \cdot \vec{D} = \rho, \tag{6.81}$$

$$\nabla \cdot \vec{B} = 0. \tag{6.82}$$

The boundary conditions at material interfaces are

$$\vec{n} \times (\vec{E}_2 - \vec{E}_1) = 0, \tag{6.83}$$

$$\vec{n} \times (\vec{H}_2 - \vec{H}_1) = \vec{J}_s, \tag{6.84}$$

$$\vec{n} \cdot (\vec{D}_2 - \vec{D}_1) = \Omega, \tag{6.85}$$

$$\vec{n} \cdot (\vec{B}_2 - \vec{B}_1) = 0, \tag{6.86}$$

where J_s is the surface current density and Ω is the surface charge density. In eqs (6.83)–(6.86) we have used a Fourier transform (F) defined as follows

$$F(\omega) = \int_{-\infty}^{\infty} f(t) \exp(j\omega t) dt. \tag{6.87}$$

The Fourier-transformed fields in terms of the vector potential $\vec{A}$ and scalar potential ϕ are

$$\vec{E} = -j\omega\vec{A} - \nabla\phi, \tag{6.88}$$

$$\vec{B} = \nabla \times \vec{A}, \tag{6.89}$$

$$\vec{H} = \bar{\bar{\mu}}^{-1} \cdot \nabla \times \vec{A}, \tag{6.90}$$

$$\vec{D} = \bar{\bar{\epsilon}} \cdot \vec{E}. \tag{6.91}$$

The displacement field is related to the electric field by

$$\vec{\mathcal{D}}(\vec{r}, t) = \vec{\mathcal{E}}(\vec{r}, t) + \int_{-\infty}^{t} \bar{\bar{X}}\,(t - \tau) \cdot \vec{\mathcal{E}}(\vec{r}, \tau) d\tau, \tag{6.92}$$

and

$$\bar{\bar{X}}\,(t < 0) = 0, \tag{6.93}$$

and hence the Fourier transform yields the dielectric constant

$$\bar{\bar{\epsilon}}\,(\vec{r}, \omega) = \bar{\bar{I}} + \int_{-\infty}^{\infty} \bar{\bar{X}}\,(z) \exp(-j\omega z) dz. \tag{6.94}$$

6.4.2 TE, TM and TEM Modes

We assume in the analysis the following:

- There exists in the guide a preferred direction in the guide which we call $\vec{z}$.
- The cross sectional area of the guide is perpendicular to $\vec{z}$ and constant throughout the length of the guide.

In this section we assume no sources of electric and magnetic fields ($\vec{J} = 0$) in the guide, so the fields satisfy

$$\nabla^2 \vec{E} + k^2 \vec{E} = 0, \tag{6.95}$$

$$\nabla^2 \vec{H} + k^2 \vec{H} = 0. \tag{6.96}$$

It is possible to spectrally decompose the combined fields in a waveguide into TE, TM and TEM modes. If we assume a preferred direction $\vec{z}$, we can write

$$\vec{\mathcal{E}}(\vec{r}, t) = \int_{-\infty}^{\infty} d\omega \sum_n \vec{E}_n(\vec{r}, \omega) \exp(\pm\gamma_n z) \exp(-j\omega t), \tag{6.97}$$

$$\vec{\mathcal{H}}(\vec{r}, t) = \int_{-\infty}^{\infty} d\omega \sum_n \vec{H}_n(\vec{r}, \omega) \exp(\pm\gamma_n z) \exp(-j\omega t), \tag{6.98}$$

where $\vec{r}$ is a transverse vector and E_n, H_n are the amplitudes of the modes. The fields separate into a transverse (T) component which is independent of z and a longitudinal component which is z dependent. Since the TE, TM and TEM modes form a complete set of functions, we can expand the transverse Fourier transformed fields as

$$\begin{aligned}
&\vec{E}_T(\vec{r}, \omega) = \\
&\quad \sum_{n=1}^{\infty} \{E^+_{nTE} \exp(\gamma_n z) + E^-_{nTE} \exp(-\gamma_n z)\} \vec{E}_{T(TE)} \\
&\quad + \sum_{n=1}^{\infty} \{E^+_{nTM} \exp(\gamma'_n z) + E^-_{nTM} \exp(-\gamma'_n z)\} \vec{E}_{T(TM)} \\
&\quad + \sum_{n=1}^{N-1} \{E^+_{nTEM} \exp(\gamma''_n z) + E^-_{nTEM} \exp(-\gamma''_n z)\} \vec{E}_{T(TEM)}
\end{aligned} \tag{6.99}$$

$$\begin{aligned}
&\vec{H}_T(\vec{r}, \omega) = \\
&\quad \sum_{n=1}^{\infty} \frac{1}{Z_{TE}} \{E^+_{nTE} \exp(\gamma_n z) - E^-_{nTE} \exp(-\gamma_n z)\} (\vec{z} \times \vec{E}_{T(TE)}) +
\end{aligned}$$

$$\sum_{n=1}^{\infty} \frac{1}{Z_{TM}} \{E_{nTM}^{+} \exp(\gamma_n' z) - E_{nTM}^{-} \exp(-\gamma_n' z)\} (\vec{z} \times \vec{E}_{T(TM)}) +$$
$$\sum_{n=1}^{N-1} \sqrt{\frac{\epsilon}{\mu}} \{E_{nTEM}^{+} \exp(\gamma_n'' z) -$$
$$E_{nTEM}^{-} \exp(-\gamma_n'' z)\} (\vec{z} \times \vec{E}_{T(TEM)}), \tag{6.100}$$

where

$$Z_{TM} = \frac{\gamma}{j\omega\epsilon}, \tag{6.101}$$

$$Z_{TE} = \frac{j\omega\mu}{\gamma}. \tag{6.102}$$

Also N is the number of disjoint conductors.

Although the sums for the TE and the TM waves in eq (6.100) go to ∞, in many practical problems some of the coefficients in the sums are 0 due to cutoff conditions. Two or more modes may have the same eigenvalue; the eigenvectors in these cases are called degenerate. Generally, it is useful to separate the gradient into longitudinal and transverse components

$$\nabla = \nabla_T + \vec{z} \frac{\partial}{\partial z}, \tag{6.103}$$

where $\vec{z} \cdot \nabla_T = 0$. The electromagnetic field can also be separated into transverse and longitudinal components,

$$\vec{E} = \vec{E}_T + E_z \vec{z}, \tag{6.104}$$

$$\vec{H} = \vec{H}_T + H_z \vec{z}. \tag{6.105}$$

Maxwell's equations in terms of longitudinal and transverse parts are [33]

$$\vec{E}_z = \vec{z} E_z, \tag{6.106}$$

$$\vec{E}_T = (\vec{z} \times \vec{E}) \times \vec{z}, \tag{6.107}$$

$$\frac{\partial \vec{E}_z}{\partial z} - j\omega \vec{z} \times \vec{B}_T = \nabla_T E_z, \tag{6.108}$$

$$\frac{\partial \vec{B}_T}{\partial z} + j\omega\epsilon\mu\vec{z} \times \vec{E}_T = \nabla_T B_z, \tag{6.109}$$

$$\vec{z} \cdot (\nabla \times \vec{E}_T) = -j\omega B_z, \tag{6.110}$$

$$\vec{z} \cdot (\nabla \times \vec{B}_T) = j\omega\epsilon\mu E_z, \tag{6.111}$$

$$\nabla_T \cdot \vec{E}_T = -\frac{\partial \vec{E}_z}{\partial z}, \tag{6.112}$$

$$\nabla_T \cdot \vec{B}_T = -\frac{\partial \vec{B}_z}{\partial z}. \tag{6.113}$$

The component E_z is the generator of the TM mode. The z component of the electric field for TM modes satisfies the following boundary value problem:

$$\{\nabla_T^2 + k_c^2\} E_{z(TM)} = 0, \tag{6.114}$$

where k_c^2 are real, positive eigenvalues we determine the cutoff frequency. The boundary conditions are

$$E_{(z(TM))}|_{on\ conductor} = 0, \tag{6.115}$$

$$H_{z(TM)} = 0. \tag{6.116}$$

The other field components are formed by use of eqs (6.108) and (6.109):

$$\vec{E}_{T(TM)} = \pm\frac{\gamma}{k_c^2}\nabla_T E_z, \tag{6.117}$$

$$\vec{H}_{T(TM)} = \frac{1}{Z_{TM}}(\vec{z} \times \vec{E}_{T(TM)}), \tag{6.118}$$

$$\gamma = j\sqrt{k^2 - k_c^2}. \tag{6.119}$$

If the mode H_z exists, it is the generator of the TE mode. The TE modes satisfy the boundary value problem,

$$\{\nabla_T^2 + k_c^2\} H_{z(TE)} = 0, \tag{6.120}$$

where k_c^2 are real, positive eigenvalues. The boundary conditions are

$$\vec{n} \cdot (\nabla H_{(z(TE))})|_{on\ conductor} = 0, \tag{6.121}$$

$$E_{z(TE)} = 0. \tag{6.122}$$

The other field components are then formed from eqs (6.108) and (6.109)

$$\vec{H}_{T(TE)} = -\frac{\gamma}{k_c^2}\nabla_T H_z, \tag{6.123}$$

$$\vec{E}_{T(TE)} = -Z_{TE}(\vec{z} \times \vec{H}_{T(TE)}). \tag{6.124}$$

There is also the possibility of TEM modes; TEM modes occur if a structure has more than one conductor ($N > 1$). For N conductors there are $(N-1)$ TEM modes. The TEM modes are the solution of an electrostatic problem with the eigenvalue $k_c^2 = 0$. Since both the electric and magnetic fields are transverse in this case, the TEM modes can be constructed from the conditions that

$$\nabla_T \times \vec{E}_{TEM} = 0, \tag{6.125}$$

$$\nabla_T \cdot \vec{E}_{TEM} = 0, \tag{6.126}$$

and therefore we must have for the potential ς,

$$\varsigma|_{\text{on conductor}} = \text{constant}, \tag{6.127}$$

$$\vec{E}_{T(TEM)} = \nabla_T \varsigma, \tag{6.128}$$

$$\vec{H}_{T(TEM)} = \sqrt{\frac{\mu}{\epsilon}}(\vec{z} \times \vec{E}_{T(TEM)}). \tag{6.129}$$

A TEM mode requires a minimum of two conductors in order to be supported.

6.4.3 Green's Dyadic Function

We now generalize our review to waves in an arbitrarily shaped fixture. In this section we relax the restriction on the assumption that the waveguide has constant cross sectional area.

The wave equation for the vector potential in the nameless gauge is

$$(\nabla^2 + k^2)\vec{A} + \mu[\vec{J} + \frac{1}{k^2}\nabla\nabla \cdot \vec{J}] = 0, \tag{6.130}$$

where we have used the relations,

$$\nabla \cdot \vec{A} = -\frac{\mu}{k^2} \nabla \cdot \vec{J}, \tag{6.131}$$

$$k^2 = \omega^2 \epsilon \mu. \tag{6.132}$$

The boundary condition on the conductors is the vanishing of the tangential electric field

$$\vec{n} \times \vec{A}|_{on\ conductors} = 0. \tag{6.133}$$

We also require the asymptotic boundary condition for outgoing waves : ($\vec{A}$ $\approx$ damped outgoing wave for large r).

The Green's dyadic function satisfies

$$(\nabla^{2'} + k^2)\mathbf{G}(r', r) = -\delta(r' - r)\mathbf{I}, \tag{6.134}$$

where $\mathbf{I}$ is the unit dyadic. We assume that Green's function satisfies the boundary conditions,

$$\vec{n'} \times \mathbf{G}|_{S'} = 0, \tag{6.135}$$

$$\nabla' \cdot \mathbf{G}|_{S'} = 0, \tag{6.136}$$

where $\mathbf{G}$ is reciprocal, $\mathbf{G}(\vec{r}, \vec{r'}) = \mathbf{G^T}(\vec{r'}, \vec{r})$, and $\mathbf{G}$ is a damped outgoing wave for large r. The vector potential can then be written as

$$\begin{aligned}
&\vec{A}(r, \omega) = \qquad (6.137)\\
&\quad \mu \int_v \vec{J}(r') \cdot [\mathbf{G}(r', r) + \frac{1}{k^2} \nabla' \nabla' \cdot \mathbf{G}(r', r)] dV' \\
&\quad - \int_S [\nabla' \cdot \vec{A}(r') + \frac{1}{k^2} \nabla' \cdot \vec{J}(r')] \vec{n}' \cdot \mathbf{G}(r', r) dS' \\
&\quad + \int_{S_\infty} [\nabla' \cdot \vec{A}(r') + \frac{1}{k^2} \nabla' \cdot \vec{J}(r')] \vec{n}' \cdot \mathbf{G}(r', r) dS' \\
&\quad - \int_S [\vec{n}' \cdot \vec{A}(r') + \frac{1}{k^2} \vec{n}' \cdot \vec{J}] \nabla' \cdot \mathbf{G}(r', r) dS' \\
&\quad + \int_{S_\infty} [\vec{n}' \cdot \vec{A}(r') + \frac{1}{k^2} \vec{n}' \cdot \vec{J}(r')] \nabla' \cdot \mathbf{G}(r', r) dS' \\
&\quad - \int_S [(\nabla' \times \vec{A}(r')) \cdot (\vec{n}' \times \mathbf{G}(r', r)) - (\vec{n}' \times \vec{A}(r')) \cdot (\nabla' \times \mathbf{G}(r', r))] dS'
\end{aligned}$$

$$+\int_{S_\infty}[(\nabla'\times\vec{A}(r'))\cdot(\vec{n}'\times\mathbf{G})-(\vec{n}'\times\vec{A}(r'))\cdot(\nabla'\times\mathbf{G})]dS', \qquad (6.138)$$

where ($'$) denotes prime variables. It is assumed that the surface integrals at infinity vanish and the use of boundary conditions of eqs (6.135) and (6.136) eliminates other terms. The resultant equation is

$$\vec{A}(r,\omega)=\mu\int_v\vec{J}(r')\cdot[\mathbf{G}(r',r)+\frac{1}{k^2}\nabla'\nabla'\cdot\mathbf{G}(r',r)]dV' + \int_s[(\vec{n}'\times\vec{A}(r'))\cdot(\nabla'\times\mathbf{G}(r',r))]dS'. \qquad (6.139)$$

Examination of eq (6.139) indicates that it is necessary to specify the tangential components of the vector potential on the boundaries or equivalently, the tangential component of the electric field. In order to evaluate eq (6.139), it is necessary to solve the related Green's function boundary value problem. We begin by introducing three vector eigenfunctions: $\vec{L}, \vec{M}$, and $\vec{N}$, where

$$\vec{L}=A\nabla'\psi, \qquad (6.140)$$

$$\vec{M}=B\nabla'\times(q\phi\vec{a}), \qquad (6.141)$$

$$\vec{N}=C\nabla'\times(\nabla'\times(q\chi\vec{a})). \qquad (6.142)$$

The q term is a scalar weighting function [30], which depends on the coordinate system used. In cylindrical coordinates, $q=1$ with z the preferred direction. In cartesian coordinates the preferred direction could be $\vec{x}, \vec{y}$, or $\vec{z}$ with weighting factor $q=1$. All of the vector eigenfunctions (denoted by $\vec{Q}$) must satisfy on conductors a relation of the form: $\vec{n}\times\vec{Q}(r)=0$. The function $\vec{L}$ has zero curl and is called *longitudinal*, while $\vec{M}, \vec{N}$ have zero divergence and thus are called *transverse*.

The vector eigenfunction $\vec{L}$ is formed from:

$$(\nabla^2+k_\ell^2)\psi=0, \qquad (6.143)$$

where we require

$$\psi|_S=0, \qquad (6.144)$$

on surfaces. In most electromagnetic problems $\vec{L}$ is not required since the fields are transverse. However, in order to keep the analysis very general, the $\vec{L}$ vector eigenfunction will be included.

The vector eigenfunction $\vec{M}$ is formed from the scalar function:

$$(\nabla^2 + k_m^2)\phi = 0. \tag{6.145}$$

If $\vec{n} \cdot \vec{a} = \pm 1$, then

$$\phi|_S = 0, \tag{6.146}$$

on surfaces, and if $\vec{n} \cdot \vec{a} = 0$ then

$$\vec{n} \cdot (\nabla(q\phi))_s = 0. \tag{6.147}$$

The vector eigenfunction $\vec{N}$ is formed from

$$(\nabla^2 + k_j^2)\chi = 0. \tag{6.148}$$

If $\vec{n} \cdot \vec{a} = \pm 1$ then the boundary condition is

$$\vec{n} \cdot (\nabla q\chi)_s = 0, \tag{6.149}$$

whereas if $\vec{n} \cdot \vec{a} = 0$ then

$$\chi_s = 0, \tag{6.150}$$

on the surface. The normalization constants A, B, and C are determined by requiring all vector eigenfunctions to satisfy a relation of the form $\int \vec{Q}_n \cdot \vec{Q}_n d\vec{r} = \delta(\alpha_n - \alpha'_n)$; where α are eigenvalues

$$\delta(\alpha_\ell - \alpha'_\ell) = |A|^2 k_\ell^2 \int_v \psi^*(\alpha'_\ell, \vec{r})\psi(\alpha_\ell, \vec{r})d\vec{r} = |A|^2 k_\ell^2 \delta(\alpha_\ell - \alpha'_\ell), \tag{6.151}$$

$$\delta(\alpha_m - \alpha'_m) = |B|^2 \gamma_m^2 \int_v \phi^*(\alpha'_m, \vec{r})\phi(\alpha_m, \vec{r})d\vec{r} = |B|^2 \gamma_m^2 \delta(\alpha_m - \alpha'_m), \tag{6.152}$$

$$\delta(\alpha_n - \alpha'_n) = |C|^2 \gamma_n^2 k_n^2 \int_v \chi^*(\alpha'_n, \vec{r})\chi(\alpha_n, \vec{r})d\vec{r} = |C|^2 \gamma_n^2 k_n^2 \delta(\alpha_n - \alpha'_n), \tag{6.153}$$

where

$$[k_m^2 + \frac{\partial^2}{\partial \xi_a^2}](q\phi(r)) = \gamma_m^2 \phi(r), \tag{6.154}$$

$$[k_n^2 + \frac{\partial^2}{\partial \xi_a^2}](q\chi(r)) = \gamma_n^2 \chi(r), \tag{6.155}$$

and ξ is the coordinate in the preferred direction and γ_m^2 is the longitudinal part of the eigenvalue.

Thus, the constants are given by

$$|A| = \frac{1}{k_\ell}, \tag{6.156}$$

$$|B| = \frac{1}{\gamma_m}, \tag{6.157}$$

$$|C| = \frac{1}{k_n \gamma_n}. \tag{6.158}$$

Green's dyadic function can then be formed from the basis vector eigenfunctions,

$$\mathbf{G}(r', r) = \left[\sum_l \frac{\vec{L}\vec{L}^*}{k_\ell^2 - k^2} + \sum_m \frac{\vec{M}\vec{M}^*}{k_m^2 - k^2} + \sum_n \frac{\vec{N}\vec{N}^*}{k_n^2 - k^2} \right]. \tag{6.159}$$

The eigenvalue spectrum on a finite domain is discrete; on the infinite domain the spectrum may be continuous, discrete or banded. Therefore, the sum in eq (6.159) goes over to an integral for a continuous eigenvalue spectrum.

6.4.4 Fields of a Coaxial Line

As an example we consider an arbitrary sample in a coaxial line with the principle direction $\vec{z}(q = 1)$, of length L, outer radius b and inner radius a. In this example the boundary conditions are

$$\psi(\vec{r})|_{z=0,L} = 0, \tag{6.160}$$

$$\psi(\vec{r})|_{r=a,b} = 0, \tag{6.161}$$

$$\phi(\vec{r})|_{z=0,L} = 0, \tag{6.162}$$

$$\vec{n} \cdot (\nabla[q\phi(\vec{r})])|_{r=a,b} = 0, \tag{6.163}$$

$$\vec{z} \cdot \nabla[\chi(\vec{r})]|_{z=0,L} = 0, \tag{6.164}$$

$$\chi(\vec{r})|_{r=a,b} = 0. \tag{6.165}$$

Green's Function

The functions ψ, χ and ϕ that satisfy eqs (6.160)–(6.165) are the building blocks of the Green's function in eqs (6.140)–(6.142), (6.159)

$$\psi(r') = [J_p(\lambda r') + R_p N_p(\lambda r')] \sin(\frac{\pi n}{L} z') \exp(-jp\theta'), \tag{6.166}$$

$$\phi(r') = [J_p(\beta r') + S_p N_p(\beta r')] \sin(\frac{\pi n}{L} z') \exp(-jp\theta'), \tag{6.167}$$

$$\chi(r') = [J_p(\lambda r') + T_p N_p(\lambda r')] \cos(\frac{\pi n}{L} z') \exp(-jp\theta'), \tag{6.168}$$

where the constants $\lambda, \beta, R_p, S_p, T_p$ are determined from the boundary conditions

$$J_p(\lambda a) + R_p N_p(\lambda a) = 0, \tag{6.169}$$

$$J_p(\lambda b) + R_p N_p(\lambda b) = 0, \tag{6.170}$$

$$J'_p(\beta a) + S_p N'_p(\beta a) = 0, \tag{6.171}$$

$$J'_p(\beta b) + S_p N'_p(\beta b) = 0, \tag{6.172}$$

and

$$T_p = R_p. \tag{6.173}$$

The propagation constants are

$$k_\ell^2 = \lambda^2 + (\frac{n\pi}{L})^2, \tag{6.174}$$

$$k_m^2 = \beta^2 + (\frac{n\pi}{L})^2, \tag{6.175}$$

$$k_s^2 = \lambda^2 + (\frac{n\pi}{L})^2. \tag{6.176}$$

The vector eigenfunctions are formed from eqs (6.140-(6.142.

6.5 Appendix E: Numerical Methods

In the solution for permittivity (2.24) or (2.38) is solved for ϵ'_R and ϵ''_R using a Newton-Raphson root finding technique. It is easiest to treat real and imaginary components of (2.24) as independent real equations. The Newton-Raphson technique for a system of equations $\vec{F}(\vec{x}) = 0$ approximates the root by assuming a series expansion around a fixed point, x:

$$f(x) \approx f(\bar{x}) + (x - \bar{x})\frac{\partial f}{\partial x}(\bar{x}), \tag{6.177}$$

where $\bar{\bar{x}}$ is the approximate root. It is then assumed that $f(x) = 0$ and thus

$$\bar{x}_n \approx \bar{x}_{n-1} - \frac{f(\bar{x}_{n-1})}{f'(\bar{x}_{n-1})}. \tag{6.178}$$

The roots are then obtained by iteration. For systems of equations the method is generalized in terms of the Jacobian matrix,

$$\vec{x}_k = \vec{x}_{k-1} - \bar{\bar{J}}\,(\vec{x}_{k-1})\vec{F}(\vec{x}_{k-1}). \tag{6.179}$$

where the Jacobian matrix is given by

$$\bar{\bar{J}} = \begin{pmatrix} \frac{\partial f_1}{\partial x_1} & \frac{\partial f_1}{\partial x_2} & \frac{\partial f_1}{\partial x_3} & \frac{\partial f_1}{\partial x_4} \\ \frac{\partial f_2}{\partial x_1} & \frac{\partial f_2}{\partial x_2} & \frac{\partial f_2}{\partial x_3} & \frac{\partial f_2}{\partial x_4} \\ \frac{\partial f_3}{\partial x_1} & \frac{\partial f_3}{\partial x_2} & \frac{\partial f_3}{\partial x_3} & \frac{\partial f_3}{\partial x_4} \\ \frac{\partial f_4}{\partial x_1} & \frac{\partial f_4}{\partial x_2} & \frac{\partial f_4}{\partial x_3} & \frac{\partial f_4}{\partial x_4} \end{pmatrix} \tag{6.180}$$

The roots then are iteratively refined until desired convergence is obtained. The derivatives in the Jacobian can either be calculated analytically or calculated numerically. In our present software the derivatives are calculated numerically.

Equation (2.24) does not require the reference plane positions in the sample holder, but only the length of the waveguide and the sample length. equation (2.38) does require the reference plane positions and thus the scattering parameters must contain the rotation terms (eqs (2.15)- (2.16)). For short-circuited line measurements the reference planes must be rotated to the sample plane.

The cutoff frequency of the sample holder must be known very accurately.

6.6 Appendix F: Kramers-Kronig Relations

The real and imaginary components of any causal function are related by a dispersion relation. The complex permittivity is a causal function and whose real and imaginary components are related by the Hilbert transform [34]

$$\epsilon_r'(\omega) - \epsilon_{r\infty} = -\frac{2}{\pi}\int_0^\infty \frac{[\theta\epsilon_r''(\theta) - \omega\epsilon_r''(\omega)]}{\theta^2 - \omega^2}d\theta, \tag{6.181}$$

$$\epsilon_r''(\omega) = -\frac{2\omega}{\pi}\int_0^\infty \frac{[\epsilon_r'(\theta) - \epsilon_r'(\omega)]}{\theta^2 - \omega^2}d\theta. \tag{6.182}$$

The following summarizes some of the features of the Kramers-Kronig relations:

- The Hilbert transform relates real and imaginary components of a causal function.
- Direct solution requires complete data over full spectrum for one component.
- Equation (6.181) can be thought of as an integral equation for the unknown component when there exists some data for the other component.

The once-subtracted form of the dispersion relations are given by

$$\epsilon_r'(\omega) - \epsilon'(\omega_o) = -\frac{\omega - \omega_o}{\pi}P\int_{-\infty}^\infty \frac{\epsilon_r''(\theta)d\theta}{(\theta - \omega)(\theta - \omega_o)}, \tag{6.183}$$

$$\epsilon_r''(\omega) - \epsilon''(\omega_o) = \frac{\omega - \omega_o}{\pi}P\int_{-\infty}^\infty \frac{\epsilon_r'(\theta)d\theta}{(\theta - \omega)(\theta - \omega_o)}, \tag{6.184}$$

where P denotes principal value.

6.7 Appendix G: Data Smoothing

Due to the inherent noise in the calculated permittivity it is useful to find a curve that interpolates the data. The method of maximum entropy is particularly well suited for this type of problem and the procedure is summarized in this appendix.

In vector notation let the measured data be expressed as

$$\vec{\epsilon'} = [\epsilon'_r(\omega_1), \epsilon'_r(\omega_2), ...], \tag{6.185}$$

$$\vec{\epsilon''} = [\epsilon''_r(\omega_1), \epsilon''_r(\omega_2), ...]. \tag{6.186}$$

We define various moments of the data:

$$M_0 = 1, \tag{6.187}$$

$$M_n = \sum_{i=1}^{N} \epsilon'_i \omega_i^n, \tag{6.188}$$

for n=1,2, . . .,K. If we define

$$\alpha_{ki} = \omega_i^k, \tag{6.189}$$

and

$$\mathbf{A} = [\alpha_{ki}], \tag{6.190}$$

then the maximum entropy solution to this system is [35]:

$$\vec{\epsilon}'_s = \mathbf{A}^t[\mathbf{A}\mathbf{A}^\mathbf{t}]^{-1}\vec{\epsilon}'. \tag{6.191}$$

An analogous equation exists for ϵ''. This smoothing algorithm is essentially a k-power least squares fit of the data of the form

$$\epsilon(\omega)' = \sum_{i=0}^{K} a_i \omega^i, \tag{6.192}$$

where, i are the least-squares coefficients. When fitting an actual set of data the number of moments must be adjusted to obtain a fit that adequately represents the data trend.

Table 6.1: TR Software Variable Names

Type of Variable	Variable Name
sample length	samplelength
air line length	Lairline
TR method	newton=1
line 1	L_1
line 2	L_2
frequencies	freq(I)
initial guess	erguess, eiguess
cut off wavelength	lcut

6.8 Appendix H: Software

Software for data reduction of the scattering parameter data are given below. The routines use a Newton-Raphson iteration process which requires an initial guess. The program furnishes an initial guess from the solution of the Nicolson-Ross-Weir equations.

```
885         CALL Rot_ref_planes(L1,L2,Fco)
886     CASE ELSE
887         Beep(3)
888         DISP "Sample holder selected not available!"
889         PAUSE
890     END SELECT
891     RETURN
892   !
893   ! ////////////////////////////////////////////////////////
894   !
895 Use_tr_method: !
896     COM /Onee/ REAL Eps11i(801),REAL Eps11r(801)
898 !
903     FOR I=2 TO Datacount-1
904         DISP "Using S11 & S21 to calculate epsilon. I=";I
905         S11r=REAL(S11(I))
906         S11i=IMAG(S11(I))
907         S21r=REAL(S21(I))
908         S21i=IMAG(S21(I))
909         S22r=REAL(S22(I))
910         S22i=IMAG(S22(I))
911         S12r=REAL(S12(I))
912         S12i=IMAG(S12(I))
913         CALL Epnewton(Freq(I),Samplelength,E1guess,E2guess,Erf,Eif)
914         E1guess=Erf
915         E2guess=Eif
919         PRINT "UNCORRECTED EPSILON VALUES"
920         PRINT Erf,Eif
921         Eps1(I)=CMPLX(Erf,Eif)
922         Mu1(I)=1
923         Erf1=Erf
924         Eif1=Eif
925         IF Waveguide_type=1 THEN
926             CALL Gap_corr(Erf1,Eif1,Erf,Eif,D1,D2,D3,D4,Waveguide_type)
927         ELSE
928             CALL Gap_corr(Erf1,Eif1,Erf,Eif,0,0,Wd1,Wd2,Waveguide_type)
929         END IF
930 !   PRINT EPSILON VALUES
931         PRINT "UNSMOOTHED, GAP CORRECTED EPSILON VALUES",Erf,Eif
932         Eps2(I)=CMPLX(Erf,Eif)
933         CALL Uncerts21_real(Erf,Eif,Mur,Mui,Samplelength,Freq(I),Uncertrs21(I
),Uncertis21(I),Lcut,Lairline)
934   !     CALL Uncerts11_real(Erf,Eif,Mur,Mui,Samplelength,Freq(I),Uncertrs11(I
),Uncertis11(I),Lcut,L1)
936         Eps5(I)=CMPLX(Uncertrs21(I),Uncertis21(I))
937        PRINT Uncertainties
938      PRINT "FREQ=",Freq(I),"UNCERT=",Uncertrs21(I),Uncertis21(I)
939     NEXT I
940     Npts=Datacount
941   !
942         IF Method=1 THEN
943         Method=2
944         GOSUB Rotate_sparms
945         END IF
946    !    USE NICOLSON-ROSS TO CALCULATE EPSILON
947         CALL Weir(Er(*),Ei(*),Lcut,Npts)
948   !   PRINT WEIR-NICOLSON-ROSS RESULTS
949      PRINT "NICOLSON-ROSS EPSILON VALUES"
950     FOR I=1 TO Datacount
951     PRINT "FREQUENCY=",Freq(I),"EPSILON=",Er(I),Ei(I)
```

```
952     Eps3(I)=CMPLX(Er(I),-Ei(I))
953     Mu1(I)=1
954     NEXT I
955   !
956     Nmom=3
957 ! THERE ARE TWO SMOOTHING OPTIONS: 1) "SMOOTH" USES MAXIMUM ENTROPY TO SMOOT
H, IN THIS ROUTINE IT IS NECESSARY TO INPUT NUMBER OF MOMENTS (Nmom). 2) A RUNNI
958 ! AVERAGE TECHNIQUE (WIND=NUMBER OF POINTS AVERAGED OVER)
959      Wind=10
960      Npts=Datacount
961      PRINT "ENTERING SMOOTHING ROUTINE for GAP CORRECTED VALUES "
962   ! CALL Smooth(Datacount,Freq(*),Nmom,Eps4(*))
963     CALL Smooth1(Npts,Freq(*),Wind,Eps2(*),Eps4(*))
964     PRINT "SMOOTHED VALUES"
965     FOR I=2 TO Datacount-1
966         Mu4(I)=1
967         PRINT Eps4(I)
968     NEXT I
969     RETURN
970 !
971 ! ////////////////////////////////////////////////////////////
972 !
973 Use_scl_method: !
974     FOR I=2 TO Datacount-1
975         Reflr=REAL(S11(I))
976         Refli=IMAG(S11(I))
977         DISP "Using S11 & S21 to calculate epsilon. I=";I
978         CALL Epshort(Freq(I),Samplelength,E1guess,E2guess,Erf,Eif)
979         E1guess=Erf
980         E2guess=Eif
981         Eps1r(I)=Erf
982         Eps1i(I)=Eif
983         Eps1(I)=CMPLX(Erf,Eif)
984         PRINT "epsilon without gap correction=",Erf,Eif
985         IF Waveguide_type=1 THEN
986             CALL Gap_corr(Eps1r(I),Eps1i(I),Erf,Eif,D1,D2,D3,D4,Waveguide_typ
e)
987         ELSE
988             CALL Gap_corr(Eps1r(I),Eps1i(I),Erf,Eif,0,0,Wd1,Wd2,Waveguide_typ
e)
989         END IF
990   !
991         Eps2(I)=CMPLX(Erf,Eif)
992         Mu2(I)=CMPLX(1,0)
993         PRINT "uncorrected values="
994         PRINT USING "3D,2X,2D.5D,2X,MD.5D";I,REAL(Eps1(I)),IMAG(Eps1(I))
995         PRINT "GAP CORRECTED VALUES"
996         PRINT Erf,Eif
997       !
998         CALL Uncerts21_real(Erf,Eif,Mur,Mui,Samplelength,Freq(I),Uncertrs21(I
),Uncertis21(I),Lcut)
999   !     CALL Uncerts11_real(Erf,Eif,Mur,Mui,Samplelength,Freq(I),Uncertrs11(I
),Uncertis11(I),Lcut)
1000        Eps5(I)=CMPLX(Uncertrs21(I),Uncertis21(I))
1001       PRINT Uncertainties
1002       PRINT "FREQ=",Freq(I),"UNCERT=",Uncertrs21(I),Uncertis21(I)
1003      NEXT I
1004      !
1005        Wind=10
1006        Npts=Datacount
```

```
2435            DISP " ....CONTINUE to try again."
2436            PAUSE
2437            Diskdrive$=""
2438        CASE 55,64
2439            DISP " This disk is full, insert new floppy and/or";
2440            DISP " select new drive ...CONTINUE "
2441            PAUSE
2442            Diskdrive$=""
2443        CASE ELSE
2444            CALL Errortrap
2445            IF LEN(Filename$)>0 THEN GOTO Send_to_disk
2446        END SELECT
2447        GOTO Selectdrive
2448        !
2449    SUBEND
2450    !
2451    ! ************************************************************
2452    !
2453    DEF FNRs21(F,L,E11,E22)
2454        COM /Two/ M,Eps0,Mu0
2455        COM /Three/ Lcut,Shdis
2456        COM /Test_info4/ REAL Samplelength,L1,L2,Lairline,Fco
2457        COM /Meth/ Method
2458        COM /S/ S11r,S11i,S21r,S21i,S22r,S22i,S12r,S12i
2459        COM /Environment/ Temperature,Pressure,Humidity,C
2460        COMPLEX Gam,J,Epsol,Trans,S21t,S11t,S12t,S22t,G1,G2,R0,R
2461        S21t=CMPLX(S21r,S21i)
2462        S11t=CMPLX(S11r,S11i)
2463        S12t=CMPLX(S12r,S12i)
2464        S22t=CMPLX(S22r,S22i)
2465        J=CMPLX(0,1)
2466        Omeg=2*PI*F
2467        Epsol=CMPLX(E11,-E22)
2468        Omegcut=2*PI/Lcut/SQRT(Eps0*Mu0)
2469        Delta=SQRT(1-Omegcut^2/Omeg^2)
2470        K0=Omeg*SQRT(Eps0*Mu0)*Delta
2471        R0=SQRT((1/C^2)*Omeg^2-(2*PI/Lcut)^2)
2472        R=SQRT(Epsol*Eps0*Mu0*Omeg^2-(2*PI/Lcut)^2)
2473        Gam=(R0-R)/(R0+R)
2474        Trans=EXP(-J*(SQRT(Omeg^2*Epsol*Eps0*Mu0-(2*PI/Lcut)^2))*L)
2475        !
2476        IF Method=1 THEN
2477            RETURN REAL(S21t*S12t-S11t*S22t-(Trans^2-Gam^2)/(1-Trans^2*Gam^2)
*EXP(-2*J*K0*(Lairline-L)))
2478        END IF
2479        !
2480        IF Method=2 THEN
2481            RETURN REAL((S21t+S12t)/2*(1-Trans^2*Gam^2)-Trans*(1-Gam^2)*EXP(-
J*K0*(Lairline-L)))
2482        END IF
2483    FNEND
2484 !
2485 ! ************************************************************
2486 !
2487    DEF FNIs21(F,L,E11,E22)
2488        COM /Two/ M,Eps0,Mu0
2489        COM /Three/ Lcut,Shdis
2490        COM /Test_info4/ REAL Samplelength,L1,L2,Lairline,Fco
2491        COM /Meth/ Method
2492        COMPLEX Gam,J,Epsol,Trans,S21t,S11t,S22t,S12t,G1,G2,R0,R
```

```
2493        COM /S/ S11r,S11i,S21r,S21i,S22r,S22i,S12r,S12i
2494        COM /Environment/ Temperature,Pressure,Humidity,C
2495        S21t=CMPLX(S21r,S21i)
2496        S11t=CMPLX(S11r,S11i)
2497        S12t=CMPLX(S12r,S12i)
2498        S22t=CMPLX(S22r,S22i)
2499        Omeg=2*PI*F
2500        J=CMPLX(0,1)
2501        Omeg=2*PI*F
2502        Epsol=CMPLX(E11,-E22)
2503        Omegcut=2*PI/Lcut/SQRT(Eps0*Mu0)
2504        Delta=SQRT(1-Omegcut^2/Omeg^2)
2505        K0=Omeg*SQRT(Eps0*Mu0)*Delta
2506        R0=SQRT((1/C^2)*Omeg^2-(2*PI/Lcut)^2)
2507        R=SQRT(Epsol*Eps0*Mu0*Omeg^2-(2*PI/Lcut)^2)
2508        Gam=(R0-R)/(R0+R)
2509        Trans=EXP(-J*(SQRT(Omeg^2*Epsol*Eps0*Mu0-(2*PI/Lcut)^2))*L)
2510        !
2511        IF Method=1 THEN
2512            RETURN IMAG(S21t*S12t-(S11t*S22t)-(Trans^2-Gam^2)/(1-Gam^2*Trans^
2)*EXP(-2*J*K0*(Lairline-L)))
2513        END IF
2514    !   !
2515        IF Method=2 THEN
2516            RETURN IMAG((S21t+S12t)/2*(1-Trans^2*Gam^2)-(Trans*(1-Gam^2))*EXP
(-J*K0*(Lairline-L)))
2517        END IF
2518    FNEND
2519 !!
2520 ! ************************************************************
2521 !
2522    DEF FNDrs21e1(F,L,E11,E22,Delta)
2523        X1=FNRs21(F,L,E11+Delta,E22)
2524        X2=FNRs21(F,L,E11-Delta,E22)
2525        RETURN (X1-X2)/Delta/2
2526    FNEND
2527 !!
2528 ! ************************************************************
2529 !
2530    DEF FNDrs21e2(F,L,E1,E2,Delta)
2531        X1=FNRs21(F,L,E1,E2+Delta)
2532        X2=FNRs21(F,L,E1,E2-Delta)
2533        RETURN (X1-X2)/Delta/2
2534    FNEND
2535 !
2536 ! ************************************************************
2537 !
2538    DEF FNDis21e1(F,L,E1,E2,Delta)
2539        X1=FNIs21(F,L,E1+Delta,E2)
2540        X2=FNIs21(F,L,E1-Delta,E2)
2541        RETURN (X1-X2)/Delta/2
2542    FNEND
2543 !
2544 ! ************************************************************
2545 !
2546    DEF FNDis21e2(F,L,E1,E2,Delta)
2547        X1=FNIs21(F,L,E1,E2+Delta)
2548        X2=FNIs21(F,L,E1,E2-Delta)
2549        RETURN (X1-X2)/Delta/2
2550    FNEND
```

```
!
! ************************************************************
!
  SUB Epnewton(F,L,E1,E2,Erf,Eif)
!
! This sub-program calls all the functions needed to calculate
! the permittivity of the sample when the transmission/reflection
! method is used.
!
      OPTION BASE 1
      COM /Two/ M,Eps0,Mu0
      COM /S/ S11r,S11i,S21r,S21i,S22r,S22i,S12r,S12i
      DIM Alp(2,2),Injab(2,2),Beta(2),X(2),Deltx(2)
      Delta=1.E-8
      Ntrial=50
      Tolf=1.E-8
      Tolx=1.E-8
Epnewton:!
      X(1)=E1
      X(2)=E2
      FOR K=1 TO Ntrial
          Alp(1,1)=FNDrs21e1(F,L,X(1),X(2),Delta)
          Alp(1,2)=FNDrs21e2(F,L,X(1),X(2),Delta)
          Alp(2,1)=FNDis21e1(F,L,X(1),X(2),Delta)
          Alp(2,2)=FNDis21e2(F,L,X(1),X(2),Delta)
          Beta(1)=-FNRs21(F,L,X(1),X(2))
          Beta(2)=-FNIs21(F,L,X(1),X(2))
          Errf=0
          FOR I=1 TO 2
              Errf=Errf+ABS(Beta(I))
          NEXT I
          IF Errf<Tolf THEN GOTO Converged
          MAT Injab= INV(Alp)
          MAT Deltx= Injab*Beta
          FOR J=1 TO 2
              X(J)=X(J)+Deltx(J)
          NEXT J
          IF Errf<Tolx THEN GOTO Converged
      NEXT K
Converged:!
!     IF K=Ntrial THEN PRINT "TOOK NTRIAL INTERATIONS"
!     PRINT "NUMBER ITERATIONS=";K;"FREQUENCY=",F
!     PRINT "REAL EPSILON=";X(1)
!     PRINT "IMAGINARY EPSILON=";X(2)
      Erf=X(1)
      Eif=X(2)
  SUBEND
!
! ************************************************************
!
  DEF FNShrs21(F,L,E11,E22)
      COM /Two/ M,Eps0,Mu0
      COM /Three/ Lcut,Shdis
      COM /Refl/ Reflr,Refli
      COMPLEX Gam,J,Epsol,Trans,Refl,R0,R,X1,Delt,Bet
      COM /Environment/ Temperature,Pressure,Humidity,C
      Refl=CMPLX(Reflr,Refli)
      J=CMPLX(0,1)
      Omeg=2*PI*F
      Epsol=CMPLX(E11,-E22)
```

```
2611        R0=SQRT((1/C^2)*Omeg^2-(2*PI/Lcut)^2)*J
2612        R=SQRT(Epsol*Eps0*Mu0*Omeg^2-(2*PI/Lcut)^2)*J
2613        X1=TANH(R*L)
2614        Delt=EXP(-2*R0*(Shdis))
2615        Bet=R/R0
2616        X1=TANH(R*L)
2617        X2=REAL(Refl*(-2*Bet+((Delt-1)*Bet^2-(1+Delt))*X1)+(-2*Bet*Delt+((Del
t-1)*Bet^2+(1+Delt))*X1))
2618        RETURN X2
2619     FNEND
2620 !
2621 ! ************************************************************
2622 !
2623     DEF FNShis21(F,L,E1gues,E2gues)
2624        COMPLEX Gam,J,Epsol,Trans,Refl,R0,R,X1,Bet,Delt
2625        COM /Two/ M,Eps0,Mu0
2626        COM /Three/ Lcut,Shdis
2627        COM /Refl/ Reflr,Refli
2628        COM /Environment/ Temperature,Pressure,Humidity,C
2629        Refl=CMPLX(Reflr,Refli)
2630        Omeg=2*PI*F
2631        J=CMPLX(0,1)
2632        Epsol=CMPLX(E1gues,-E2gues)
2633        R0=SQRT((1/C^2)*Omeg^2-(2*PI/Lcut)^2)*J
2634        R=SQRT(Epsol*Eps0*Mu0*Omeg^2-(2*PI/Lcut)^2)*J
2635        Delt=EXP(-2*R0*Shdis)
2636        Bet=R/R0
2637        X1=TANH(R*L)
2638        X2=IMAG(Refl*(-2*Bet+((Delt-1)*Bet^2-(1+Delt))*X1)+(-2*Bet*Delt+((Del
t-1)*Bet^2+(1+Delt))*X1))
2639        RETURN X2
2640     FNEND
2641 !!
2642 ! ************************************************************
2643 !
2644     DEF FNShdrs21e1(F,L,E11,E22,Delta)
2645        X1=FNShrs21(F,L,E11+Delta,E22)
2646        X2=FNShrs21(F,L,E11-Delta,E22)
2647        RETURN (X1-X2)/Delta/2
2648     FNEND
2649 !!
2650 ! ************************************************************
2651 !
2652     DEF FNShdrs21e2(F,L,E1,E2,Delta)
2653        X1=FNShrs21(F,L,E1,E2+Delta)
2654        X2=FNShrs21(F,L,E1,E2-Delta)
2655        RETURN (X1-X2)/Delta/2
2656     FNEND
2657 !
2658 ! ************************************************************
2659 !
2660     DEF FNShdis21e1(F,L,E1,E2,Delta)
2661        X1=FNShis21(F,L,E1+Delta,E2)
2662        X2=FNShis21(F,L,E1-Delta,E2)
2663        RETURN (X1-X2)/Delta/2
2664     FNEND
2665 !
2666 ! ************************************************************
2667 !
2668     DEF FNShdis21e2(F,L,E1,E2,Delta)
```

```
2669        X1=FNShis21(F,L,E1,E2+Delta)
2670        X2=FNShis21(F,L,E1,E2-Delta)
2671        RETURN (X1-X2)/Delta/2
2672     FNEND
2673 !
2674 ! ************************************************************
2675 !
2676     SUB Epshort(F,L,E1,E2,Erf,Eif)
2677!
2678! This sub-program calls all the functions needed to calculate
2679! the permittivity of the sample when the short-circuit line
2680! method is employed.
2681!
2682        OPTION BASE 1
2683        COM /Refl/ Reflr,Refli
2684        DIM Alp(2,2),Injab(2,2),Beta(2),X(2),Deltx(2)
2685        Delta=1.E-8
2686        Ntrial=50
2687        Tolf=1.E-8
2688        Tolx=1.E-8
2689 Epshort: !
2690        X(1)=E1
2691        X(2)=E2
2692        FOR K=1 TO Ntrial
2693            Alp(1,1)=FNShdrs21e1(F,L,X(1),X(2),Delta)
2694            Alp(1,2)=FNShdrs21e2(F,L,X(1),X(2),Delta)
2695            Alp(2,1)=FNShdis21e1(F,L,X(1),X(2),Delta)
2696            Alp(2,2)=FNShdis21e2(F,L,X(1),X(2),Delta)
2697            Beta(1)=-FNShrs21(F,L,X(1),X(2))
2698            Beta(2)=-FNShis21(F,L,X(1),X(2))
2699            Errf=0
2700            FOR I=1 TO 2
2701                Errf=Errf+ABS(Beta(I))
2702            NEXT I
2703            IF Errf<Tolf THEN GOTO Converged
2704            MAT Injab= INV(Alp)
2705            MAT Deltx= Injab*Beta
2706            FOR J=1 TO 2
2707                X(J)=X(J)+Deltx(J)
2708            NEXT J
2709            IF Errf<Tolx THEN GOTO Converged
2710        NEXT K
2711 Converged:!
2712        Erf=X(1)
2713        Eif=X(2)
2714        IF K>10 THEN PRINT "CAUTION! NTRIALS, NOT CONVERGED",K
2715     SUBEND
2716 !
2717 ! ************************************************************
2718 !
2719     SUB Smooth(Npts,Freq(*),Nmom,COMPLEX Eps2(*))
2720!
2721        REAL Alp(8,401),Delta(8),Atran(401,8),C(8,8),D(8,8),E(8),Epsi(401),Ep
sr(401),Epslr(401),Epsli(401)
2722        COM /Onee/ Epslli(*),Epsllr(*)
2723        PRINT "NPTS",Npts,"NMOM",Nmom
2724        FOR I=1 TO Npts
2725           Epslr(I)=REAL(Eps2(I))
2726           Epsli(I)=IMAG(Eps2(I))
2727            FOR K=1 TO Nmom
```

```
2728              Alp(K,I)=(Freq(I)/1.E+9)^(K-1)
2729           NEXT K
2730        NEXT I
2731        FOR K=1 TO Nmom
2732           FOR I=1 TO Npts
2733              Delta(K)=Delta(K)+Alp(K,I)*Eps1r(I)
2734           NEXT I
2735        NEXT K
2736   ! !
2737        MAT Atran= TRN(Alp)
2738        MAT C= Alp*Atran
2739        MAT D= INV(C)
2740        MAT E= D*Delta
2741        MAT Epsr= Atran*E
2742   !
2743        FOR K=1 TO Nmom
2744           Delta(K)=0
2745           FOR I=1 TO Npts
2746              Delta(K)=Delta(K)+Alp(K,I)*Eps1i(I)
2747           NEXT I
2748        NEXT K
2749   ! !
2750        MAT Atran= TRN(Alp)
2751        MAT C= Alp*Atran
2752        MAT D= INV(C)
2753        MAT E= D*Delta
2754        MAT Epsi= Atran*E
2755   !
2756        FOR I=1 TO 401
2757           Eps11r(I)=Epsr(I)
2758           Eps11i(I)=Epsi(I)
2759        NEXT I
2760    SUBEND
2761 !
2762 ! ************************************************************
2763 !
2764    SUB Gap_corr(Er_uncor,Ei_uncor,Er_cor,Ei_cor,D1,D2,D3,D4,Guidetyp)
2765!
2766! In the routine, the real and imaginary parts of epsilon are
2767! corrected due to the airgap between the sample and the sample holder.
2768! If the guidetyp equals one, then an airgap correction for a coaxial
2769! sample holder is done, else a airgap correction is done for a waveguide
2770! sample holder.
2771!
2772 Gap_corr:    !
2773        IF Guidetyp=1 THEN
2774           L1=LGT(D2/D1)+LGT(D4/D3)
2775           L2=LGT(D3/D2)
2776           L3=LGT(D4/D1)
2777           Er_cor=L2/(L3-Er_uncor*L1)*Er_uncor
2778           IF Ei_uncor<=0 THEN
2779              Ei_cor=0
2780           ELSE
2781              Ei_cor=Er_cor*Ei_uncor/Er_uncor*L3/(L3-L1*(Er_uncor*(1+(Ei_un
cor/Er_uncor)^2)))
2782           END IF
2783        !
2784        ELSE
2785           Samplethick=D3
2786           Guidethick=D4
```

```
2787            Er_cor=Er_uncor*(Samplethick/(Guidethick-(Guidethick-Samplethick)
*Er_uncor))
2788            IF Ei_uncor>0 THEN
2789                Ei_cor=Er_cor*Ei_uncor/Er_uncor*Guidethick/(Guidethick-(Guide
thick-Samplethick)*Er_uncor)
2790            ELSE
2791                Ei_cor=0
2792            END IF
2793        !
2794         END IF
2795     SUBEND
2796    !
2797    ! ************************************************************
2798    !
2799     SUB Edit_data(Prompt$,Variable,OPTIONAL Multiplier,Uvariable)
2800!
2801! Edit_data is a 'boiler plate' routine which allows easy
2802! editing of variables throughout the program.
2803!
2804 Edit_data:OFF KEY
2805         IF NPAR>2 THEN
2806             Test=Variable*Multiplier
2807             IF NPAR=4 THEN Uvariable=Uvariable*Multiplier
2808         ELSE
2809             Test=Variable
2810         END IF
2811         ON ERROR GOTO Test_again
2812 Test_again:!
2813         OUTPUT 2 USING "K,#";Test
2814         DISP "Please enter the value of ";Prompt$;
2815         INPUT Variable
2816         OFF ERROR
2817         IF NPAR=4 THEN
2818             Utest=Uvariable
2819             ON ERROR GOTO Utest_again
2820 Utest_again:!
2821             OUTPUT 2 USING "K,#";Utest
2822             DISP "Enter the uncertainty in ";Prompt$;
2823             INPUT Uvariable
2824             OFF ERROR
2825         END IF
2826         IF NPAR>2 THEN
2827             Variable=Variable/Multiplier
2828             IF NPAR=4 THEN Uvariable=Uvariable/Multiplier
2829         END IF
2830     SUBEND
2831    !
2832    ! ************************************************************
2833    !
2834     SUB Speed_of_light
2835!
2836! This sub-program calculates the speed of light in the laboratory
2837! given the temperature, relative humidity, and pressure.
2838!
2839 Init_com:     !
2840         COM /Environment/ Temperature,Pressure,Humdity,C
2841 Speed_of_light: !
2842         Theta=300/(273.15+Temperature)
2843         Esaturated=Theta^5/(.4151*10^(9.834*Theta-10))
2844         E=Humidity*Esaturated/100
```

```
2845        Kpa=Pressure/10
2846        Pdryair=Kpa-E
2847        N=1+((((41.6*Theta)+2.39)*E*Theta)+(2.588*Pdryair*Theta))*10^(-6)
2848        C=2.99792458*10^8/N
2849     SUBEND
2850  !
2851  ! ************************************************************
2852  !
2853     ! NICOLSON-ROSS-WEIR SOLUTION TECHNIQUE FOR NON-MAGNETIC MATERIALS
2854     SUB Weir(Er(*),Ei(*),Lcut,Npts)
2855     COMPLEX Gg,Xg,Results
2856     COM /Sparms/ REAL Freq(*),COMPLEX S11(*),S21(*),S12(*),S22(*)
2857     COM /Sparms/ Mag_s11_id$,Ang_s11_id$,Mag_s21_id$,Ang_s21_id$
2858     COM /Sparms/ Mag_s22_id$,Ang_s22_id$,Mag_s12_id$,Ang_s12_id$
2859     COM /Test_info4/ REAL Samplelength,L1,L2,Lairline,Fco
2860     !
2861     FOR Ii=1 TO Npts
2862         Xg=(S11(Ii)^2-S21(Ii)^2+1)/2/S11(Ii)
2863         Gg=Xg+SQRT(Xg^2-1)
2864         IF ABS(Gg)>1 THEN
2865         Gg=Xg-SQRT(Xg^2-1)
2866         END IF
2867         Lam=2.9972E+8/Freq(Ii)
2868         Results=(1-Lam^2/Lcut^2)*(1-Gg)^2/(1+Gg)^2+Lam^2/Lcut^2
2869         Er(Ii)=REAL(Results)
2870         Ei(Ii)=-IMAG(Results)
2871         NEXT Ii
2872     SUBEND
2873     !
2874     ! RUNNING AVERAGE SMOOTHING
2875     ! WIND = NUMBER OF POINTS AVERGED OVER
2876         SUB Smooth1(Npts,REAL Freq(*),Wind,COMPLEX Eps2(*),Eps4(*))
2879         !
2880         FOR I=2 TO Npts-1
2881          Remp=0
2882          Itemp=0
2883          IF I<8 THEN
2884          FOR N=I TO I+5
2886           Remp=Remp+REAL(Eps2(N))
2887           Itemp=Itemp+IMAG(Eps2(N))
2888          NEXT N
2890          Eps4(I)=CMPLX(Remp/6,Itemp/6)
2891          GOTO 2907
2892          END IF
2894          IF I>Npts-6 THEN
2895          FOR N=I-5 TO I
2896          Remp=Remp+REAL(Eps2(N))
2897          Itemp=Itemp+IMAG(Eps2(N))
2898          NEXT N
2899          Eps4(I)=CMPLX(Remp/6,Itemp/6)
2900          GOTO 2907
2901          END IF
2902          FOR N=I-5 TO I+5
2903          Remp=Remp+REAL(Eps2(N))
2904          Itemp=Itemp+IMAG(Eps2(N))
2905          NEXT N
2906          Eps4(I)=CMPLX(Remp/11,Itemp/11)
2907          NEXT I
2908          !
2909          SUBEND
```

```
2910        !
2911    SUB Uncerts21_real(Epsolr,Epsoli,Mur,Mui,Length,Freq,Uncertr,Uncerti,Lcut
,Lairline)
2912        COMPLEX J,A,B,C,Z,X1,X2,Gamma,Gammaa
2913        COMPLEX Epsol,Mu,S,Ders
2914    !
2915    PRINT "LCUT=",Lcut
2916  Uncerts_real:  !
2917        RAD
2918        Eps0=1/36/PI*1.E-9
2919        Mu0=4*PI*1.E-7
2920        Epsol=CMPLX(Epsolr,-Epsoli)
2921        Mu=CMPLX(1,0)
2922        Omega=2*PI*Freq
2923        Cv=2.9972E+8
2924        J=CMPLX(0,1)
2925        Gamma=J*SQRT(Omega^2*Epsol/Cv^2-(2*PI/Lcut)^2)
2926        Gammaa=J*SQRT(Omega^2/Cv^2-(2*PI/Lcut)^2)
2927        X1=FNGam(Epsolr,Epsoli,Mur,Mui,Omega,Lcut)
2928        Z=EXP(-Gamma*Length)
2929        S=(1-X1^2)*Z/(1-X1^2*Z^2)
2930        Ang=ARG(S)
2931        Mag=ABS(S)
2932        A=Omega^2/2/Gamma/Cv^2/Gammaa/(1+Gamma/Gammaa)*(1+(1-Gamma/Gammaa)/(1
+Gamma/Gammaa))
2933        B=Length*Omega^2*Z/2/Cv^2/Gamma
2934        C=-Gamma*Z
2935        Ders=EXP(J*Ang)*(1-X1^2*Z^2)/(2*A*(S*X1*Z^2-X1*Z)+B*((1-X1^2)+2*S*X1^
2*Z))
2936        Sreal=REAL(Ders)
2937        Simag=IMAG(Ders)
2938        Agreal=REAL(Ders*J*Mag)
2939        Agimag=IMAG(Ders*J*Mag)
2940            Deltth=FNDelths21(Freq/1.E+9,ABS(S))
2941            Delts21=FNDelts21(ABS(S))
2942            Deltlen=5.E-6
2943        Ltimag=IMAG((-C*(1-X1^2)-2*S*C*X1^2*Z)/(2*A*(S*X1*Z^2-X1*Z)+B*((1-X1^
2)+2*S*X1^2*Z)))
2944        Ltreal=REAL((-C*(1-X1^2)-2*S*C*X1^2*Z)/(2*A*(S*X1*Z^2-X1*Z)+B*((1-X1^
2)+2*S*X1^2*Z)))
2945    !
2946                Uncertr=(SQRT((Sreal*Delts21)^2+(Agreal*Deltth)^2+(Ltreal*Del
tlen)^2))
2947                Uncerti=(SQRT((Simag*Delts21)^2+(Agimag*Deltth)^2+(Ltimag*Del
tlen)^2))
2948    !
2949    SUBEND
2950    ! ************************************************************
2951    SUB Uncerts11_real(Epsolr,Epsoli,Mur,Mui,Length,Freq,Uncertr,Uncerti,Lcut
,L1)
2952        COMPLEX J,A,B,C,Z,X1,X2,Devl,Devs,Gamma,Gammaa
2953        COMPLEX Epsol,Mu,S,Gam
2954    !
2955  Uncerts_real:  !
2956        RAD
2957        Epsol=CMPLX(Epsolr,-Epsoli)
2958        Mu=CMPLX(Mur,-Mui)
2959        Omega=2*PI*Freq
2960        Cv=2.9972E+8
2961        J=CMPLX(0,1)
```

```
2962        Gamma=J*SQRT(Omega^2*Epsol/Cv^2-(2*PI/Lcut)^2)
2963        Gammaa=J*SQRT(Omega^2/Cv^2-(2*PI/Lcut)^2)
2964        X1=FNGam(Epsolr,Epsoli,1,0,Omega,Lcut)
2965        Z=EXP(-Gamma*Length)
2966        A=Omega^2/2/Gamma/Cv^2/Gammaa/(1+Gamma/Gammaa)*(1+(1-Gamma/Gammaa)/(1
+Gamma/Gammaa))
2967        B=Length*Omega^2*Z/2/Cv^2/Gamma
2968        C=-Gamma*Z
2969        J=CMPLX(0,1)
2970        S=(1-Z^2)*X1/(1-X1^2*Z^2)*EXP(-2*L1*Gammaa)
2971        Ang=ARG(S)
2972        Mag=ABS(S)
2973        !
2974        Devs=EXP(J*Ang)*(1-X1^2*Z^2)/(A*(2*S*X1*Z^2+(1-Z^2))+B*(2*S*X1^2*Z-2*
Z*X1))
2975        Sreal=REAL(Devs)
2976        Simag=IMAG(Devs)
2977        Agreal=REAL(Devs*Mag*J)
2978        Agimag=IMAG(Devs*Mag*J)
2979        Devl=2*C*(Z*X1-S*X1^2*Z)/(A*(1-Z^2+2*S*X1*Z^2)+2*B*(S*X1^2*Z-Z*X1))
2980        Ltreal=REAL(Devl)
2981        Ltimag=IMAG(Devl)
2982     !
2983             Deltlen=5.E-6
2984             Deltts11=FNDelths11(Freq/1.E+9,ABS(S))*.5
2985             Delts11=(.008*ABS(S)+.002)*(1/17*Freq/1.E+9+16/17)
2986    !
2987                 Uncertr=(SQRT((Sreal*Delts11)^2+(Agreal*Deltts11)^2+(Ltreal*D
eltlen)^2))
2988                 Uncerti=(SQRT((Simag*Delts11)^2+(Agimag*Deltts11)^2+(Ltimag*D
eltlen)^2))
2989    !
2990    SUBEND
2991    ! ************************************************************
2992    SUB Uncertsh_real(Epsolr,Epsoli,Mur,Mui,L,Freq,Uncertr,Uncerti)
2993        COMPLEX J,A,B,C,Z,X1,X2,Th,Sh,G,G0,Dedl,Dedr,Dedth,Dfdl,Dfdg,Dgde,Rh0
2994        COMPLEX Epsol,Mu,S11
2995        COM /Two/ Mmx,Eps0,Mu0
2996        COM /Three/ Lcut,Shdis
2997    !
2998 Uncerts_real:  !
2999        RAD
3000        Epsol=CMPLX(Epsolr,-Epsoli)
3001        Mu=CMPLX(Mur,-Mui)
3002        Omega=2*PI*Freq
3003        J=CMPLX(0,1)
3004        G0=SQRT(Omega^2*Eps0*Mu0-(2*PI/Lcut)^2)*J
3005        G=J*SQRT(Omega^2*Eps0*Epsol*Mu*Mu0-(2*PI/Lcut)^2)
3006        !
3007        Th=TANH(G*L)
3008        Sh=1./COSH(G*L)
3009        !
3010        Rh0=(G0*Th-G)/(G0*Th+G)
3011        Mag=ABS(Rh0)
3012        Ang=ARG(Rh0)
3013        !
3014        Dfdl=(1./(G0*Th+G))*(G0*G*Sh^2-(G0*Th-G)/(G0*Th+G)*G0*G*Sh^2)
3015        Dfdg=(1./(G0*Th+G))*((G0*L*Sh^2-1)-(G0*Th-G)/(G0*Th+G)*(G0*L*Sh^2+1))
3016        Dgde=-(Mu0*Omega^2*Eps0)/G/2
3017        !
```

```
3018        Dedl=-Dfdl/Dfdg/Dgde
3019        Dedr=EXP(J*Ang)/Dfdg/Dgde
3020        Dedth=J*EXP(J*Ang)*Mag/Dfdg/Dgde
3021        !
3022        Rdedl=REAL(Dedl)
3023        Idedl=IMAG(Dedl)
3024        Rdedr=REAL(Dedr)
3025        Idedr=IMAG(Dedr)
3026        Rdedth=REAL(Dedth)
3027        Idedth=IMAG(Dedth)
3028   !
3029        S11=(G0*TANH(G*L)-G)/(G0*TANH(G*L)+G)
3030        Deltlen=5.E-6
3031        Deltth=FNDelths11(Freq/1.E+9,ABS(S11))
3032        Delts11=(.008*ABS(S11)+.002)*(1/17*Freq/1.E+9+16/17)
3033    !
3034        Uncertr=(((Rdedr*Delts11)^2+(Rdedth*Deltth)^2+(Rdedl*Deltlen)^2)^.5)
3035        Uncerti=(((Idedr*Delts11)^2+(Idedth*Deltth)^2+(Idedl*Deltlen)^2)^.5)
3036        !
3037        !
3038    SUBEND
3039   !****************************************************************
3040    DEF FNDelths11(F,S11)
3041   !
3042        IF F<18.1 THEN
3043            IF S11<.1 THEN
3044                RETURN MIN(6.28,.029*EXP(.0246/S11)*(.11138*F+.9949))
3045            ELSE
3046                RETURN MIN(6.28,(-.01938*S11+.03683)*(.11138*F+.9949))
3047            END IF
3048        ELSE
3049        PRINT "OUT OF RANGE IN FNDELTTH"
3050        END IF
3051        !
3052    FNEND
3053    !
3054    DEF FNGam(Epsolr,Epsoli,Mur,Mui,Omega,Lcut)
3055        COMPLEX Epsol,Mu,Gamma,Gammaa
3056    !
3057        Eps0=1/36/PI*1.E-9
3058        Mu0=4*PI*1.E-7
3059  Gam:  !
3060        Epsol=CMPLX(Epsolr,-Epsoli)
3061        Mu=CMPLX(Mur,-Mui)
3062        Cv=2.9972E+8
3063        Gamma=SQRT(Omega^2*Epsol/Cv^2-(2*PI/Lcut)^2)
3064        Gammaa=SQRT(Omega^2/Cv^2-(2*PI/Lcut)^2)
3065    !
3066        RETURN (1-Gamma/Gammaa)/(1+Gamma/Gammaa)
3067    !
3068    FNEND
3069    ! ************************************************************
3160    DEF FNDelts21(S21)
3161        Db=20*LGT(S21)
3162     ! ASSUME 0.03 DB UNCERT
3163        IF 20*LGT(S21)>-40 THEN
3164        RETURN .0034
3165        ELSE
3166        A=-.01113
3167        B=.56+A*90
```

```
3168        RETURN A*Db+B
3169        END IF
3170     FNEND
3190     DEF FNDelths21(F,Mag)
3191    !
3192        Db=20*LGT(Mag)
3193        IF Db>-40 THEN
3194            RETURN .00205*F+.00113
3195        ELSE
3196        Ds1=2.552E-4*EXP(-.0828*Db)
3197        Ds2=.00437*EXP(-.0575*Db)
3198        A=(Ds2-Ds1)/16.
3199        B=Ds1-2*A
3200        RETURN A*F+B
3201        END IF
3202     FNEND
3203    !
3204    ! ************************************************************
```